ISSN 1810-0384

ADVANCES IN ELECTROMETALLURGY

No. 2 Volume 8 2010

CAMBRIDGE INTERNATIONAL SCIENCE PUBLISHING

Advances in Electrometallurgy is a cover-to-cover English translation of *Sovremennaya Elektrometallurgiya*, published four times a year by International Association 'Welding' at the E.O. Paton Electric Welding Institute, National Academy of Sciences of Ukraine, 11 Bozhenko Street, 03680 Kyiv, Ukraine

Published by

Cambridge International Science Publishing Ltd
7 Meadow Walk, Great Abington, Cambridge CB21 6AZ, England
Tel: +44 (0) 1223 893295; Fax: +44 (0) 1223 894539
email: cisp@cisp-publishing.com; http://www.cisp-publishing.com

Advances in Electrometallurgy 2010 **8** *(2) 81–86*
Translated from Sovremennaya Elektrometallurgiya 2010 **8** *(2) 3–7*

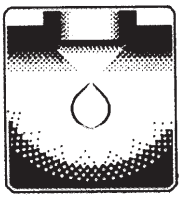

ELECTROSLAG TECHNOLOGY

Development and investigation of technology for electroslag melting of 800 mm diameter ingots without surface defects

S.V. Davidchenko, I.N. Logozinskii, I.M. Bilonik, A.S. Sal'nikov, S.S. Kazakov, M.I. Gasik and A.Yu. Kuz'menko

Elektrometallurgicheskii Zavod Dneprospetsstal', Zaporozh'e

The results of experimental investigations of the effect of different electric parameters of ESR melting on the quality of surface of ERS ingots are presented. The electric condition for melting of ESR ingots without surface defects are determined.

Elektrometallurgicheskii Zavod Dneprospetsstal', Zaporozh'e is one of the largest plants in Ukraine producing special steels and alloys by special electrometallurgy methods. The steelmelting shop of the plant has a large amount of experience with melting of ingots by electroslag melting of different profile and mass for the production of sections and sheet metal products. The currently available park of the solidification moulds greatly differs so that it is possible to produce ESR ingots with the weight and cross-section in a wide range: profiled ingots weighing from 1.0 to 4.3 t, sheet ingots weighing 9–20 t (Table 1). Consequently, the plant can satisfy the requirements of users of metal products for important applications, mainly as regards rolled sections and sheets.

To produce large dies, it is necessary to forge large sections produced from tool steels. Therefore, the development of the technology for producing new billets by ESR for the production of forgings has been one of the priority directions. However, the production of these forgings requires ESR ingots with the mass of no less than 5.8 t. In the determination of the mass of the ingot and the solidification mould for the ESR process it was necessary to take into account the production conditions and the possibilities of

Table 1. Cross-section and weight of ESR ingots

Ingot type	Ingot diameter, mm	Ingot mass (maximum), t	Solidification mould cross section, mm	Ingot mass (maximum), t
Profiled	300	1,0	350×350	1,5
	460	1,8	415×415	2,2
	800	He	500×500	3,8
		Not determined	565×565	4 3
Sheet	–	–	650×1100	9,0
	–	–	650×350	11 5
	–	–	650×1480	12,5
	–	–	700×1450	20,0

available equipment. The following problems were solved simultaneously:

– melting of initial metal and manufacture of consumable electrodes with the required mass and sections;

– development of ESR technology for the selected consumable electrode and heat treatment of the ingot;

– development of the technology for forging ESR ingots in a forging-press shop;

– modernisation of the ESR furnace.

Taking these requirements into account, a solidification mould with a diameter of 800 mm with a maximum mass of the melted ingots of 6 t was selected. The steel melting shop has at its disposal various modifications of the ESR furnaces: OKB-905, OKB-1065, ESR-20-VG. Previously, investigations were carried out to master the forging of metal products of the required range produced from sheet ingots with the weight of 9 t. Melting in the ESR-20-VG furnace and the forging of these ingots, designed for the production of sheets, did not give the required results.

The most suitable equipment from the viewpoint of organisation of melting of the given ingot was the ESR OKB-1065 single-column furnace after modernisation. Therefore, the development of technology and investigation of the melting of ingots were carried out in the OKB-1065 furnace, fitted with an ARShMT regulator using the classic single-electrode remelting procedure.

The following investigations were carried out in the modernisation of equipment:

– additional watercooled cables were placed on the supporting part of the furnace and the baseplate;

– the truck was constructed for the baseplate specially developed and produced for melting ESR ingots with a diameter of 800 mm;

– a large baseplate with the water cooling system of the slit type was constructed and installed;

– the design of the mechanism for lifting the electrode holder in the furnace was modified because the length of the 370 × 370 mm required for melting 5.8 t ingots increased by 2 m.

In the determination of the production method of 800 mm diameter ingots, the entire technological cycle was investigated – from the melting of initial metal and manufacture of electrodes to melting of the ESR ingot, heated treatment and forging.

The economic efficiency of the ESR process and the quality of the metal and surface of the ingot depend strongly on the ratio of the dimensions of the electrode and the solidification mould. According to the recommendations published in [1], the optimum filling factor for the ingots weighing more than 4 t should be 0.60–0.75. To fulfil this requirement, the diameter of the electrode for melting the ingot with the diameter of 800 mm should be 500–600 mm. These electrodes can be produced in the conditions of the Dneprospettstal' plant only by casting into compound ingot moulds.

The manufacture of the electrode by forging includes another expensive processing treatment, increasing the production costs of the ESR metal.

The electrode, produced by the casting of the metal into the ingot mould producing the ingot–electrode is preferred both from the viewpoint of ESR technology and the method of production, dimensions, the geometrical parameters and mass (6.2–6.5 t). At the same time, in addition to the positive aspects of the application of the ingot with the diameter of 500–600 mm produced by casting into an ingot mould, the quality of the electrode for the ESR process includes the following factors delaying the application of the process;

–the need for the removal of the riser section with shrinkage prior to ESR leading to losses of the metal and the reduction of the yield of suitable metal;

–it is not possible to weld to the electrode a transition head with the cross-section of 370 × 370 mm;

–the expenditure for acquiring new or reconstructing the existing welding equipment;

–the expenditure for acquiring ingot moulds for casting of metal.

The accepted technology can be used to produce in equipment for continuous casting

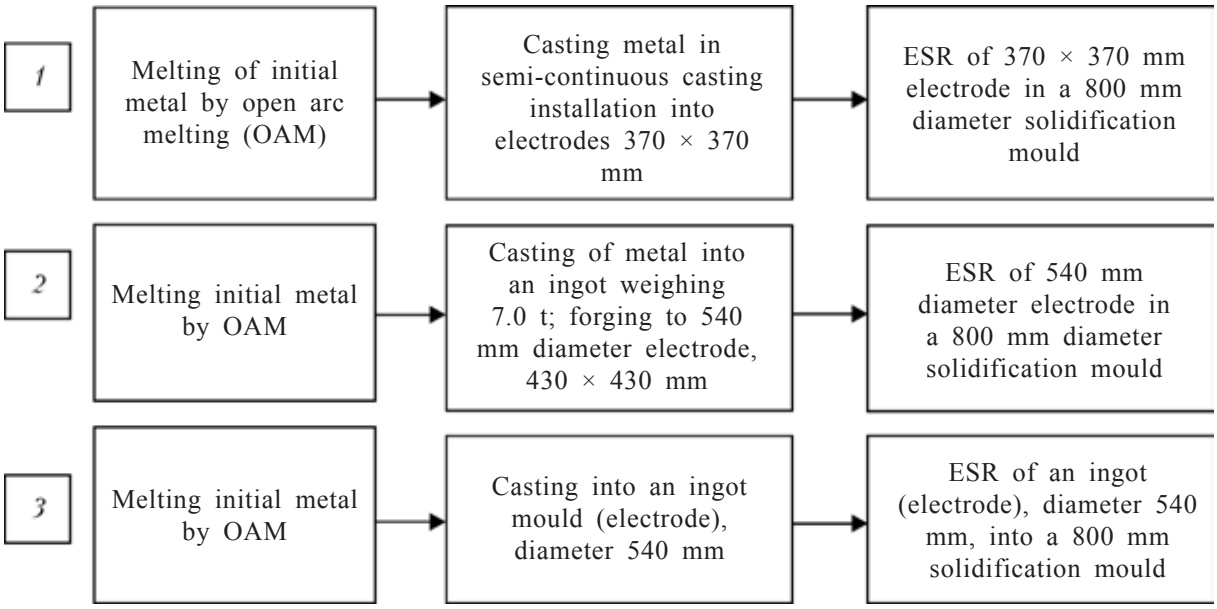

Fig. 1. Schemes (1–3) of production of electrodes in the period of adoption of technology of melting ESR ingots with a diameter of 800 mm.

of steel cast electrodes with the cross-section of 370 × 370 mm or with a diameter of 405 mm for melting 4.3 t ingots. In electroslag melting of these electrodes in a solidification mould with a diameter of 800 mm, the filling factor is 50–20% lower than in the case of the 580 mm diameter electrode.

One of the advantages of this method, in comparison with other variants, is that it is not required to invest in the development of technology and organisation of the production of new consumable electrodes. This variant of the method of production of ESR ingots was accepted for further development.

Thus, the development of the technology of production of initial metal for subsequent ESR for melting ingots with the damage of 800 mm continued in three directions (Fig. 1):

– melting of the initial metal in ODV furnaces followed by casting in semi–continuous casting installation into electrodes with the size of 370 × 370 mm;

– melting of the initial metal in the ODV furnaces by casting into compound ingot moulds producing 7 t ingots, forging of the produced ingot to electrodes with a diameter of 500 mm or the cross-section of 430 × 430 mm;

– melting of the initial metal in the ODV furnaces followed by pouring into an ingot mould with a diameter of 580 mm, producing ingots–electrodes.

The development of the new electrical erosion was based on the conventional differentiated melting regime [2] which proved to be highly successful in ESR into a solidification mould with a cross-section of 565×565 mm (Fig. 2). Using the method, described in [3], the conditions of the power is supplied in ESR were calculated for the three previously mentioned variants of remelting technology (Fig. 1).

However, to ensure that the technological requirements in melting of the ESR ingots with a diameter of 800 mm using 370×370 mm cross-section electrodes with a diameter of 500–600 mm are fulfilled, the calculated data show that the required electrical power is 50–40% higher than for the ingot with the cross-section of 565×565 mm.

The first experimental ESR ingots with a diameter of 800 mm were melted using ESR of cast electrodes 370×770 mm and steels 4Kh5MFS, 4Kh5MF1S and 4Kh5M3F in accordance with the classic differentiated regimes using ANF-6 flux. The amount of flux was determined on the basis of the resistance of the slag pool, sustained by the

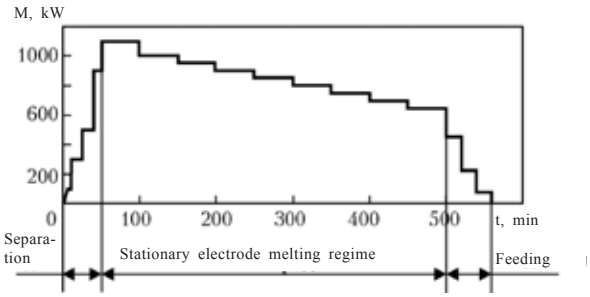

Fig. 2. Classic differentiated regime of ESR melting in a 565 × 565 mm solidification mould. M – supplied power, t – time elapsed from activating the furnace.

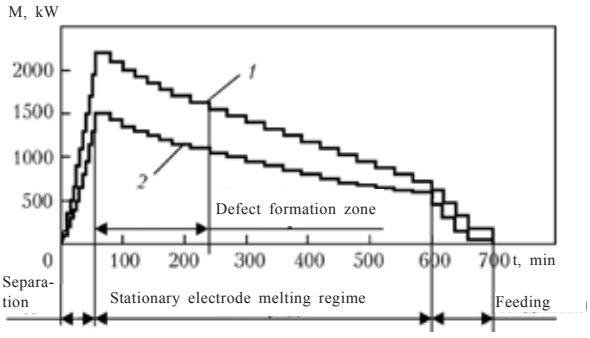

Fig. 3. Graphs of the experimental ESR conditions in a solidification mould with a diameter of 800 mm: 1, 2) the maximum and minimum supplied power, respectively.

ARShMT regulator to ensure stable melting with respect to current. The calculated regime of the power supply (Fig. 3, curve 2) was applied to the first 10 experimental melts.

After extracting the ingots from the solidification mould, notches and corrugation were found on the surface of the ingots (Fig. 4). The corrugation was in the form of a wavy surface with slags found in the depressions at a depth of up to 60 mm. The defect was distributed along the height of the ingot in the same zone.

The part of the ingot starting from the end of the bottom part (150–300 mm) did not contain defects and this was followed by constrictions with corrugation along the length of 250–600 mm. No surface defects were found in the upper part of the ingot.

At the ingot length of 1700 mm, the surface with the defects equal to 30% or more. In most cases, the defects were found in the ingots produced from ledeburitic tool steels Kh12-SH, Kh12V-Sh, Kh12MF-Sh. As shown by further investigations, the more extensive occurrence of constrictions and corrugation in the ledeburitic steel in comparison with other steels is determined by the thermophysical properties of these materials.

To eliminate defects, investigations were carried out into the effect on the formation of defects by melting at a higher power which was initially increased by 10–15% and then increased to the maximum possible power for the OKB 1065 furnace, i.e., increase by 30–40% in relation to the initial level (Fig. 3, curve 1). This was carried out in the regime with holding time of up to 3 h at the maximum power in the initial melting period after reaching the melting regime.

The electrical regime was corrected to optimise the temperature of the slag pool and prevent the formation of constrictions and corrugation in the ingot. The middle phase of melting and its completion, as indicated by the power diagrams, was characterised by moderate values.

Tests were carried out of ESR of different steel grades Kh12, Kh12v, Kh12MF, 95Kh5GM, 4Kh5MFS, 4Kh5MF1S, 5Kh-N2MF, etc. Constrictions and corrugation formed in the melted experimental melts in the same section. This was determined by the temperature conditions in the melting space [4].

Long-term experience with the production of ESR ingots with smaller mass, for example 4.3 t, of the steels of the same grade indicates the absence of the same surface defects formed in differentiated remelting conditions at different supplied power levels.

The ingots with the low quality surface are not suitable for forging, and the deformation of these ingot is accompanied by the propagation of the phase with the formation of a large cavities in the forgings. The removal of the defects in the ingot by dressing of machine prior to deformation does not solve the problem.

The removal of the surface defects in abrasive dressing machines results in the formation of stresses and cracks; ledeburitic and die steels are especially susceptible to the formation of these defects. This operation

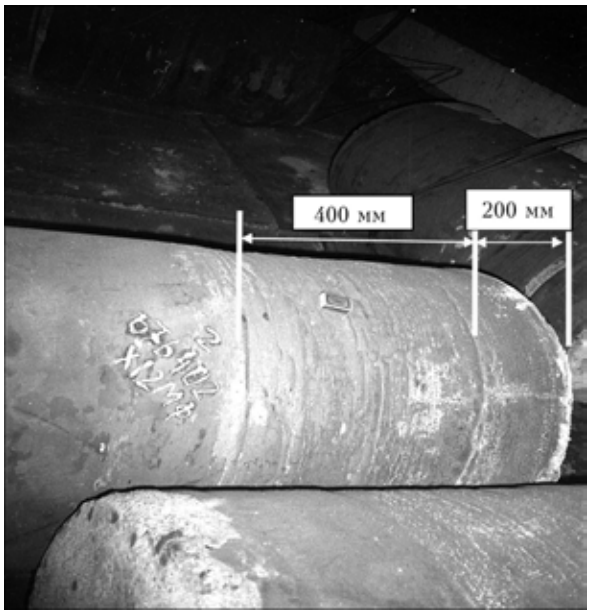

Fig. 4. Constriction and corrugation in the first ESR ingots with a diameter of 800 mm, melted in the experimental conditions.

should be followed by repeated annealing.

In machining by turning, the surface layer of the ingot metal is removed and this is highly undesirable because this has a negative effect in forging and leads to the formation of surface defects. Additional consumption of metal greatly increases the production costs of ESR metal. This method of production of ingots is not capable of competition.

Thus, the selected electrical conditions of ESR of the electrode with a cross-section of 370×370 mm in melting at a high power do not result in the removal of defects in melting ingots with the diameter of 800 mm. The variation of the power in the initial melting period of the electrode influences the start of formation of constrictions and corrugation, i.e., the zone in which they are located is displaced upwards or downwards in the direction of ingot height.

To determine more correctly the tested technological conditions of remelting and the effect of these conditions on the surface quality of ESR ingots with a diameter of 800 mm, a series of melts was produced using a consumable electrode with a larger cross section (430×430 mm) which were cast into an ingot mould with a diameter of 580 mm in accordance with the calculation conditions. Even larger constrictions and corrugation formed on the surface of the ingot in the same zone in the steels of all grains, and by the deepest defects were detected as previously in the ingots of the Kh12-Sh ledeburitic steels.

The formation of large defects in the ingots in ESR with the higher cooling coefficient is determined by the conditions of formation of the ingot and ESR of the consumable electrode. To solve the problem of melting with the higher filling coefficient in the OKB-1065 furnace, with the ARShMT automatic control system and in the absence of the power reserve of the furnace transformers, it is necessary to apply other technical solutions and methods.

Analysis of the technological features of the variants of electroslag remelting in an 800 mm diameter solidification mould by the single-electrode method of remelting in OKB 1065 furnaces shows that to obtain the ESR ingots without defects it is necessary to supply power in accordance with the different algorithm, i.e., in completely new electrical conditions. Therefore, the graph of supplied power was changed and the conditions were determined in such a manner as to ensure sufficient heating of the slag pool and of the consumable electrode directly in the zone of formation of constriction and corrugation. Calculations were carried out to determine the melting period with respect to time characterised by the formation of defects in the ingot, and a new graph of variation of power during melting was constructed.

The new regime differs from the standard classic differentiated regime by the fact that instead of reducing the power in the initial melting period of the power is in fact increase by 30% or more (Fig. 5) [5]. The first experimental melts in the solidification mould with a diameter of 800 mm, produced in the special conditions with higher supplied power in ESR of the electrode with a cross-section of 370 × 370 mm, yielded positive results. The melted ingots did not contain any constrictions or corrugation, the surface

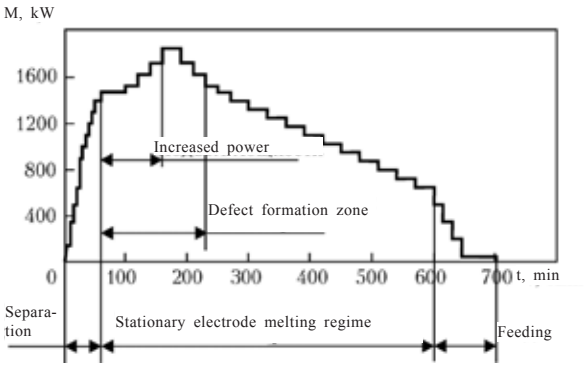

Fig. 5. Graph of the ESR conditions with the increase of the power supplied into the solidification mould with a diameter of 800 mm in the initial period.

quality corresponding to the standard level for the ingots with a cross-section of 565 × 565 mm weighing 4.3 t (Fig. 6).

Deformation of the ingots took place without any problems. The forgings were free from defects associated with the surface quality of the ingots, and all the parameters of the quality of the metal corresponded to the requirements of standard documents. Therefore, the metal was transported to the customer.

Since the application of the new electrical melting conditions resulted in positive data for both the quality of the surface of the ingot with a diameter of 800 mm and ESR metal as a whole, it has been decided to apply this technology in production.

Conclusions

1. The variation of the power from minimum and maximum in the initial melting period of the consumable electrode with a cross-section of 370×370 mm in the OKB 1065 furnace using the ANF-6 flux and a solidification mould with a diameter of 800 mm does not produce the ingot without surface defects in the form of constrictions and corrugation.

2. The stepped increase of the power after reaching the stationary melting regime of the electrode in the 10–30% period of melting up to 25% in relation to the initial value produces the ESR ingots with a diameter of 800 mm without surface defects.

3. The lowest losses and most acceptable technology of the three investigated variants (Fig. 1) of the production of ESR ingots with a diameter of 800 mm from the viewpoint of organisation of production have been obtained for the technology of ASR using the electrodes with a cross-section of 370×370 mm.

4. The proposed technology of melting was used in the period 2007–2008 for melting more than 4000 t of ESR ingots with a diameter of 800 mm using steels of different grades (Kh12MF-Sh, Kh12(V)-Sh, 4Kh5MF(1) S-Sh, EP609-Sh, EI691-Sh, 95Kh5GM-Sh, etc) have been used to produce more than 2500 t of forgings of different cross-section with a diameter of up to 600 mm and strips up to 300×800×2000 mm in size whose quality satisfies the standard requirements. The metal has been tested and supplied to the customer.

5. The original nature of the proposed technology of the electrical conditions of ESR has been confirmed by the State Department of Intellectual Property and The state company The Ukrainian Institute of Industrial Property [5].

Fig. 6. ESR ingots with a diameter of 800 mm in Kh12MF-Sh steel, produced in ESR of the electrode with a cross-section of 370 × 370 mm with increased supplied power.

References

1. Bocharnikov I.V., et al.,Probl. Spets. Elektrometall., 1990, No. 2, 22–26.
2. Glebov A.G. and Moshkevich E.I., Electroslag remelting, Metallurgiya, Moscow, 1985.
3. Mironov Yu.M. and Tarasov V.A., Spets. Vopr. Elektrotermii, 1975, No. 3, 35–53.
4. Medovar B.I., et al., Thermal processes in electroslag remelting, Naukova Dumka, Kiev, 1978.
5. Davidenko S.V., et al., Ukrainian patent 21520, MPC S22V 9/18,

Advances in Electrometallurgy 2010 **8** *(2) 87–92*
Translated from Sovremennaya Elektrometallurgiya 2010 **8** *(2) 8–2*

Alloying titanium with oxygen from the gas phase in chamber electroslag remelting of titanium sponge

S.N. Ratiev, O.A. Ryabtseva, A.A. Troyanskii, A.D. Ryabtsev, S.I. Davydov and L.Ya. Shvartsman

Donetsk National Technical University, Donetsk ZTMK Company, Zaporozh'e

The possibility of application of gaseous oxygen as an of alloying component in the process of chamber-type electroslag remelting of titanium sponge is considered. It was experimentally shown that remelting in argon–oxygen atmospheres allows uniform adding of considerable amounts of oxygen into titanium leading to changes of the structure and properties of the latter.

In the group of promising structural materials, adopted in recent years by industry, a special position is occupied by titanium and its alloys [1, 2]. The continuous expansion of the area of application of these materials in different branches of technology is explained by the favourable combination of the physical–chemical properties.

In addition to the increase of the volume of production of titanium, the quality of the material has also been improved. The decrease of the content of harmful impurities increases the plasticity and toughness of the material and reduces sensitivity to notches and other defects. On the other hand, the improvement of the purity of titanium reduces the level of the strength characteristics of the material and, consequently, complicates the production of commercial alloys.

The main impurities in commercial purity titanium, having a strong effect on the properties of titanium, included gases (oxygen, nitrogen and hydrogen). It is necessary to mention oxygen in which, in contrast to nitrogen and hydrogen, has not only a positive but also a negative effect on the properties of titanium [3–5]. Having the small atomic radius, oxygen forms wide regions of interstitial solutions with α- and β-modifications of titanium.

The region of the α-solutions includes the concentration from 0 to 34 at.% of oxygen without any phase transformations and disruption of the homogeneity of the structure of these solutions. The limiting solubility of oxygen in β-titanium at the peritectic temperature of 1740°C is only 6 at.%. The different solubility of oxygen in the two titanium modifications is explained by the fact that the implantation of the oxygen atoms into the cavities of the BCC lattices of β-titanium results in a considerably larger number of disruptions in comparison with the introduction of the same atoms into the octahedral cavities of the HCP lattice of β-Ti.

Oxygen increases the temperature of the $\alpha \rightarrow \beta$ transformation and widens the temperature range of the α-phase, i.e., it is a α-stabiliser. Within the limits of the concentration range of the solid solutions, oxygen and titanium form compounds with the ordered structure, the so-called suboxides.

The formation of a solid solution of oxygen in Ti is associated with the extensive disruption of the crystal lattice reducing greatly the mechanical properties of the metal. The

increase of the oxygen content increases the strength and hardness and reduces the plasticity of titanium. Controlling the oxygen content of the metal, it is possible to obtain the optimum ratio of the plasticity and strength characteristics of the titanium alloys.

Thus, oxygen may be regarded as a promising alloying element to produce new titanium alloys. This is especially important for medical components because in addition to the mechanical properties, corrosion resistance and biocompatibility are also important in this case. In contrast to other alloying components, for example, vanadium, oxygen is 'safer' [6].

The sources of oxygen as the alloying element may include titanium scrap [7–9], tailings from the cover of the systems for producing titanium sponge [10, 11], titanium oxides [12, 13], and also gaseous oxygen [14].

The application of gaseous oxygen for alloying titanium is economically most efficient. In the group of the metallurgical processes of melting titanium, the most suitable method for using this source of oxygen is chamber electroslag remelting (CESR) because alloying of titanium with oxygen from the gas phase during vacuum-arc and electron-beam remelting is very difficult as a result of the presence of vacuum in the melting space. CESR in contrast to canonic ESR can be used to produce almost any atmosphere in the melting space and efficiently refine and additionally alloy the metal [15–19].

In this article, special attention is given to investigating the possibilities of alloying titanium with oxygen directly from the gas phase during chamber electroslag remelting of titanium sponge with different initial oxygen content.

Consumable electrodes for CESR were produced by pressing titanium sponge produced at the ZTMK company. Both the standard sponge of grade TG100 with the oxygen content of 0.0 35% (melts 3–6) and the sponge alloyed in advance with oxygen [14] to 0.11% (melts 1, 2, 7 and 8, Table 1) were used. The pressed electrodes with the diameter of 40 mm and 600 mm long were remelted in a solidification mould with the diameter of 60 mm (Fig. 1). Remelting was carried out in a chamber electroslag furnace, constructed on the basis of A-558 equipment (Fig. 2).

Equipment was also fitted with cylinders with an argon–oxygen mixture and also devices for controlling the flowrate and pressure

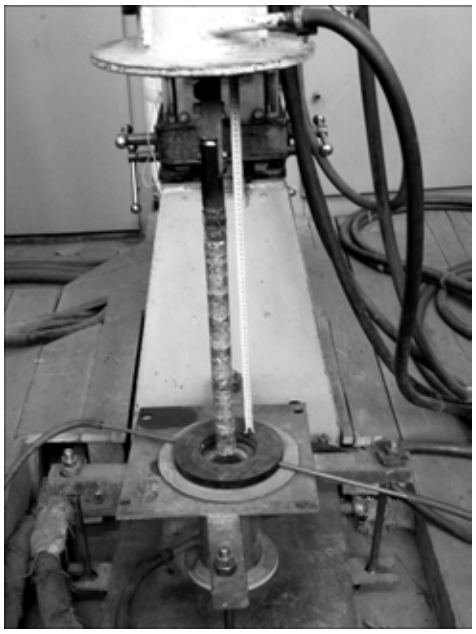

Fig. 1. A pressed consumable electrode produced from titanium sponge.

Fig. 2. General view of the chamber furnace for electroslag remelting with dosing devices and a power source.

Table 1. Oxygen content in the experimental ingots of various melts

Melt No.	Electrode	Slag	Furnace atmosphere	Mass fraction of oxygen %
1	Titanium sponge, alloyed with oxygen	CaF_2+Ca (2.5 %)	Argon ('still')	0.110 / 0.083
2	As above	CaF_2	As above	0.110 / 0.110
3	TG110 titanium sponge	CaF_2	As above	0.035 / 0.053
4	As above	CaF_2	Argon ('flowing')	0.035 / 0.075
5	As above	CaF_2	Argon + 30% oxygen mixture, minimum consumption, 'flowing'	0.035 / 0.110
6	As above	CaF_2	Argon + 30% oxygen mixture, maximum consumption, 'flowing'	0.035 / 0.230
7	Titanium sponge, alloyed with oxygen	CaF_2	Argon + 30% oxygen mixture, minimum consumption, 'flowing'	0.110 / 0.220
8	As above	CaF_2	Argon + 30% oxygen mixture, maximum consumption, 'flowing'	0.110 / 0.270

Comment. The numerator gives the initial oxygen content, the denominator the content after remelting.

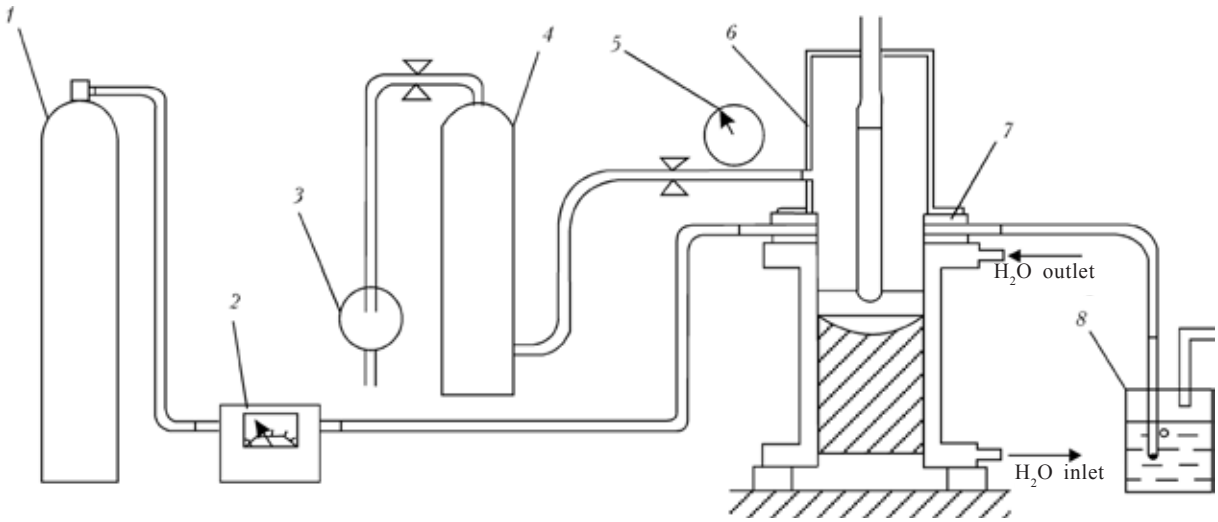

Fig. 3. Diagram of the supply of gases into the melting chamber of the chamber electroslag melting furnace: 1) gas cylinder with an argon-oxygen mixture; 2) gas flowrate meter; 3) vacuum pump; 4) intermediate chamber-filter; 5) vacuum gauge; 6) protective jacket; 7) sealing interlayer with orifices for the supply of gas into the working space; 8) water valve

of gases (Fig. 3).

During melting, the excess pressure of gases (up to 25 kPa) was maintained in the system to compensate possible losses of gases. The source of gaseous oxygen was the first grade argon, containing 0.002% oxygen (GOST 10157-79), and especially prepared argon–oxygen mixture (30% oxygen).

Remelting was carried out under a flux produced from pure CaF_2, grade Ch (TU 6-09-5335-88) and under a CaF_2+ Ca flux. The flux was melted directly in the solidification mould by the solid start method. The starting mixture was produced from titanium

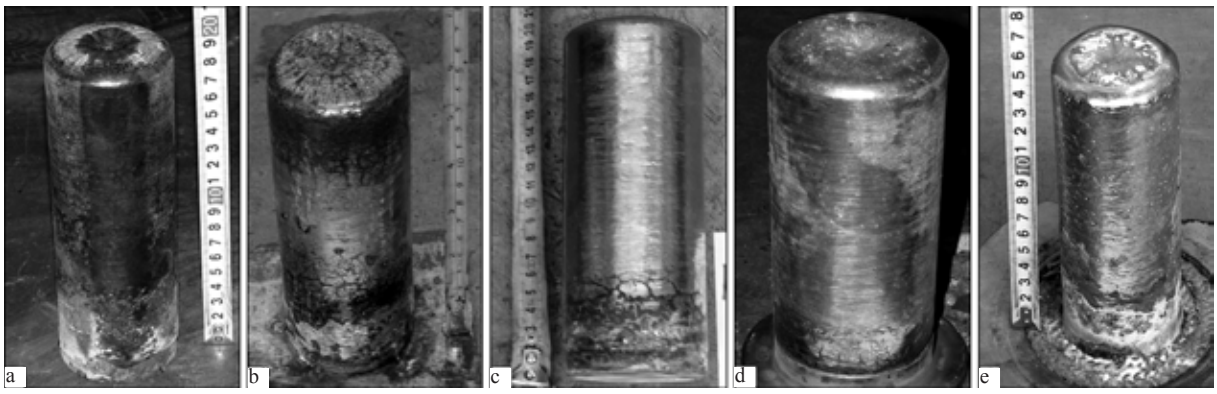

Fig. 4. Titanium ingots alloyed with oxygen in the chamber electroslag remelting: a) melt 6 (O = 0.23); b) melt 8 (O = 0.27%); c) melt 5 (O = 11%); d) melt 4 (O = 0.07%); e) melt 1 (O = 0.0 to 3%).

shavings and working flux.

The electrical parameters of remelting were maintained at: U = 40 V, I = 2.0–2.2 kA, ensuring high quality of the formation of the surface of the melted ingots. The argon-oxygen mixture was supplied through pipes in the sealing gasket of the upper flange of the water-cooled solidification mould (Fig. 1, 3).

Transverse templates were produced from the ingots (Fig. 4) and used for the preparation of specimens for the determination of the chemical composition and investigation of the structure of the metal in the cast conditioned. The structure was studied at a magnifications 50-500 on microscopes of Carl Zeiss, Axiovert 40 MAT, Neophot-21, a Neophot-2. The specimens were photographed with a digital camera and the digitised file was analysed using VideoTest Metall 1.0 computer program. Hardness was measured in a Rockwell device on the HRC scale and the results were transferred to the HB values, using tables. The gas content of the metal and the specimens was determined in LECO equipment.

The required amount of the argon and the argon–oxygen mixture blown into the working space for alloying titanium with oxygen was determined by the calculations. It was assumed that the mass in the melting rate is 6 g/s, and the pickup of oxygen is 100%. Consequently, to increase the oxygen content of the metal by 0.1% it is necessary to add 0.011 l/s of the argon–oxygen mixture (30% oxygen) and 15 l/s of commercial argon.

Taking into account the technical possibilities, remelting was carried out at the minimum (0.0 31 l/s, melts 5, 7) and maximum (0.32 l/s, melts 6 and 8) consumption of the argon–oxygen mixture. The comparison melts 2 and 3 were produced in the atmosphere of commercial purity argon and in the 'still' atmosphere (Table 1).

As indicated by the table, at all investigated variants of the CESR method, with the exception of the melt produced under CaF_2+ Ca flux (melt 1), the results show a large increase of the oxygen content of titanium and also in the remelting the sponge in commercial purity argon with a low fraction of oxygen (melts 3, 4).

Evidently, the latter is associated with the capacity of the titanium sponge characterised by the developed (from 0.1 to 20 m^2/g) specific surface with the magnesium chloride salt remaining on the surface after magnesium thermal reduction, to adsorb oxygen, nitrogen and atmospheric moisture even prior to remelting. For example, the surface of the sponge equal to $0.1 m^2/g$ contains no less than 0.005% oxygen, and 1 m^2 of the surface of titanium adsorbs up to 0.03 g of water vapour from the air [9]. In addition, the moisture, oxygen and nitrogen are also brought in by commercial purity argon. All these increases the content of not only oxygen but also nitrogen in the metal after remelting, including after CESR under the CaF_2 flux.

The 'flowing' atmosphere of technical purity argon, in comparison with the 'still' atmosphere, increases the oxygen content of titanium produced by CESR by a factor of 1.5 (melts 3 and 4). The application for alloying of the argon–oxygen mixture with 30% of oxygen increases the oxygen content 2–7 times (melts 5–8).

Attention should be given to the fact that the degree of pickup of oxygen does not increase with the increase of the gas flowrate. In fact, the degree of pickup decreases. For example, at the minimum flowrate (0.031 l/s), the degree of pickup is 27 (melt 5) and 39 (melt 7) and at the maximum flowrate (0.3 l/s) it is 6 (melt 8) and 7% (melt 6). Evidently, this is associated with the fact that the supply of oxygen to the oxidised metal is not the limiting member in the process of oxidation of the titanium electrode.

It should be mentioned that in alloying titanium with gaseous oxygen the nitrogen content of the metal was higher (up to 0.020–0.030%). However, the content was within the range of the requirements of GOST 19807–91 for titanium grades VT1-00 and VT1-0 (up to 0.04%of nitrogen) and ASTM B-337 for commercial purity titanium Grade 1–Grade 3 (0.03–0.05%).

The indirect indicator of the content and distribution of the impurity in titanium is the hardness of the metal. Figure 5 shows the hardness in the horizontal cross-section of the experimental ingots. As indicated by the graph, the hardness of the metal of the investigated specimens increases with increasing oxygen content. For example, the highest hardness is characteristic of the specimens with the oxygen content of 0.27 % (melt 8), and the lowest hardness for the specimens with the mass fraction of oxygen of 0.0 53% (melt 3). The hardness in the radial direction remains approximately constant, indicating the uniform distribution of the impurities in the horizontal cross-section of the ingots.

The microstructure of the specimens taken from the centre of the ingots is shown in Fig. 6. It may be seen that the oxygen content of titanium has a strong effect on the formation

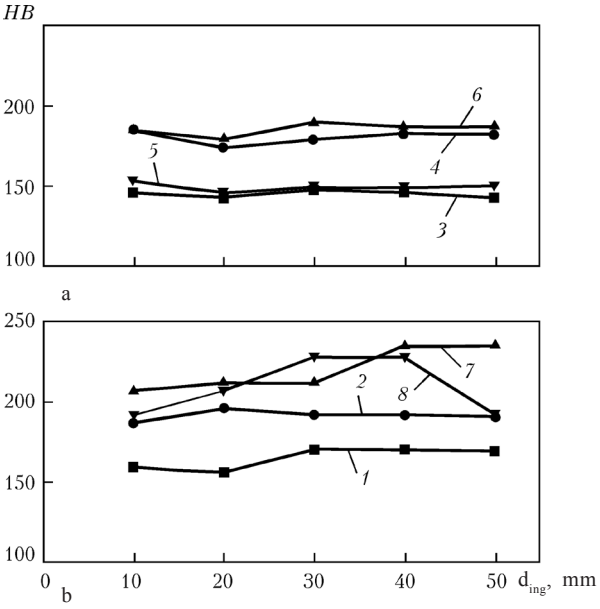

Fig. 5. Hardness distribution in the ingots melted from titanium sponge grade TG100 (a) and from titanium sponge, alloyed in advance with oxygen (up to 0.11%) (b): 1-4, 6-8) the numbers of melts (Table 1); d_{ing} is the ingot diameter.

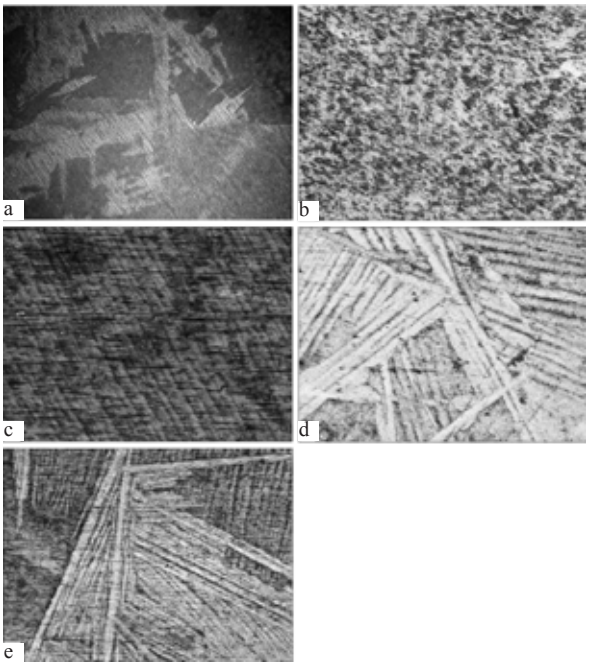

Fig. 6. Microstructure of the metal: a, b) [O] = 0.0 75%, melt 4; c) × 50; b)× 100; c) [O] = 0.0 53%, melt 3; d) [O] = 0.23%, melt 6, e) [O] = 0.27%, melt 8.

of the structure of the metal. For example, for titanium with the oxygen content in the range 0.0 53–0.110% (melts 1–5) the characteristic feature is the formation of the coarse dendritic structure in which the differences

between the individual areas are visible and a small magnification (Fig. 6a). The dendritic areas are etched uniformly without a distinctive substructure (Fig. 6b). In some cases, the areas inside dendrites showed a plate-shaped substructure with low intensity (Fig. 6c), typical of commercial purity titanium in the cast condition.

The increase of the oxygen content up to 0.2% and higher (Fig. 6d, e) results in the formation of the structure of shear transformation, supporting the increase of the strength characteristics. The formation of these structures in cast titanium can be explained by the larger mass fraction of oxygen which affects the kinetics of the phase polymorphous transformation in the metal during cooling of the ingot.

Conclusions

1. The chamber electroslag remelting methods, used for metallurgical processing, guarantees the supply of oxygen from the gas phase into titanium during remelting of the sponge.

2. The experiments have shown that it is possible to increase the oxygen content in the metal by a factor of 2–7 in comparison with the initial content.

3. The results of investigations of the structure and hardness measurements show that the process ensures high chemical and structural homogeneity of the titanium ingots.

References

1. Pol'kin I.S., Using titanium in different areas of industry, Ti-2006 v SNG, Proceedings, Suzdal' 21–24.5.2006, Naukova Dumka, Kiev, 2006.
2. Chervonyi I.F., et al., Titanium and areas of application, Ti-2007 v SNG, Yalta 15–18.4. 2007, Kiev, 2007, 314–325.
3. Lyakishev N.P. (editor), Equilibrium diagrams of binary metallic systems, in three volumes, Mashinostroenie, Moscow, 1999.
4. Gurevich S.M. (editor), Metallurgy and technology of welding titanium and its alloys, Naukova Dumka, Kiev, 1979.
5. Eremenko V.N., Titanium and its alloys, National Academy of Sciences of Ukraine, Kiev, 1960.
6. Nikolaev G.I., Titanium and its alloys, Publishing House of the Academy of Sciences of the Ukrainian SSR, Kiev, 1960.
7. Trubin A.N., et al., Titan, 2002, no. 1, 33–36.
8. Karasev E.A., et al., ibid, 2004, No. 1, 30–33.
9. Sergeev V.V. (edior), Metallurgy of titanium, Metallurgiya, 1971.
10. Ryabtsev A.D., et al., Sovremen. Elektrometall., 2007, No. 3, 3–6.
11. Davydov S.I., et al., Ti2006 v SNG, Suzdal', 21–24.5.2006. Naukova dumka, Kiev, 253–257.
12. Trubin A.N. and Puzanov I.Yu., Titan 2003, No. 1.
13. Reznichenko V.A., et al., Ti-2005 v SNG, 21–25.5.2005, Kiev, 151–156.
14. Ovchinnikov A.V., et al., Ti2--7 v SNG, Yalta, 15–18.4.2007, Kiev, 2007, 170–1673.
15. Ryabtsev A.D. and Troyanskii A.A., Elektrometallurgiya,
16. Troyanskii A.A. and Ryabtsev A.D., Titan, 2007, No. 1, 28–31.
17. Benz M.G., et al., Materials Research Innovationes, 1999, No. 6, 364–368.
18. Ryabtsev A.D., et al., Probl. Spets. Elektrometall., 2002, No. 3, 10–13.
19. Ryabtsev A.D., et al., Probl. Spets. Elektrometall., 2002, No. 4, 3–8.

Advances in Electrometallurgy 2010 **8** *(2) 93–97*
Translated from Sovremennaya Elektrometallurgiya 2010 **8** *(2) 13–16*

Production of ingots of KhN73MBTYu creep-resisting alloy by electroslag remelting of rolling production waste

S.V. Skripnik and D.F. Chernega

Titan Company, Kiev; Kiev Polytechnical Institute

The possibility of producing high-quality ingots of heat-resistant nickel-based alloy KhN73MBTYu using the method of ESR of consumable electrodes, pressed (welded) from rolling production waste is shown. The chemical composition, structure and mechanical properties of ingots with a diameter of 390 mm weighing 0.72 t are presented. The prospects for application of new resources-saving technology at engineering companies are shown.

The KhN73MBTYu (EI698) heat-resisting, dispersion-hardened alloy is used widely in the manufacture of working blades, turbine discs, wheels and other components for gas turbines working at temperatures up to 750°C. For the components for important applications, the alloy is produced from pure (with no impurity elements) charge materials by vacuum-induction melting (VIM). Therefore, the price of these alloys is very high and the coefficient of utilisation is relatively low as a result of a large number of metallurgical processing treatments.

In many cases, the discs and wheels for gas turbines are produced from bars by deformation methods, including upsetting, piercing and rolling. The piercing of the blanks in series production is associated with the formation of a large amount of waste metal characterised by the same geometry and standard chemical composition. This create suitable conditions for the electroslag processing of these valuable materials.

The present article is concerned with the examination of the possibilities of producing ingots by electroslag remelting from the waste of KhN73MBTYu creep-resisting nickel–chromium alloy in rolling production or rejected components with the same configuration with the standard composition of the given alloy in one of the engineering companies.

It was required to utilise pieces of the material of the same geometry, for example, the circular cross-section and different thickness of a standard composition. For assembling (welding) of the consumable electrodes it was required to select the welding materials with, if possible, the chemical composition similar to that of the parent alloy. The amount of the weld the material should be minimum but sufficient for reliable joining of the elements of the consumable electrode taking into account the nature of the electroslag remelting process, and also the safety of the melting process.

In melting high-quality electroslag remelted ingots it is necessary to ensure the optimum position of the consumable electrode in relation to the slag pool [1]. In this case, the electrode feed rate and, consequently, the current should be such as to ensure that the tip of the electrode, immersed in the slag, has the form of a regular cone and remains in this shape throughout the entire melting period. This means that the joining of the elements of the composite consumable elec-

Table 1. Chemical composition of the parent and deposited metal

Material	Mass fraction of elements,%										
	C	Si	Mn	Cr	Mo	Nb	W	Al	Ti	s	
	0.06	0.34	2.25	19.0	1.9	1.6	0.19	0.10	0.10	0.007	0.016
	0.05	0.025	1.90	21.3	2.4		0.2			0.010	0.010

Comment. Base – nickel

trode with a circular welded joint around the perimeter of the cross-section does not prevent the possible penetration into the metal pool of pieces of parent metal as a result of the initial melting of the welded joint.

There are two reliable and safe (with respect to melting) methods of assembling (welding) the composite consumable electrode with shortcomings and disadvantages. The first method is based on producing a welded joint throughout the entire cross-section of the consumable electrode, for example, by electroslag welding with a plate-shaped electrode ensuring high chemical homogeneity of the ingot.

However, this method requires plate-shaped electrodes with the composition identical to that of the parent metal, and also appropriate equipment.

The second method is based on the production of the welded joint by electric arc welding with compulsory welding of the upper part of each element to be welded to the produced composite electrode and ensures melting of the metal of the welded joint only after melting the connecting element made of the parent material.

Taking into account the configuration of the material pieces used in the process and characterised by different diameters (150–170 mm) and thickness (30–40 mm), experiments were carried out with the second variant of assembling (welding) of the composite consumable electrodes. The electrodes OZL-25B and OZL-44 appear to be the most suitable electrodes for manual arc welding as regards the composition (Table 1).

In accordance with the technical requirements on the composition of the KhN73MBTYu alloy (Table 2), the most suitable electrodes are OZL-25B, containing important alloying elements such as niobium which in combination with either alloying elements greatly increases the plasticity of the KhN73MBTYu alloy in long-term testing in the hot state. This is important in using the

Table 2. Chemical composition of samples of creep-resisting KhN73MBTYu alloy, taking in the direction of height of experimental ESR ingot

Sampling area in axial part of ingot	Mass fraction of elements, %										
	C	Si	Mn	Cr	Mo	Nb	Fe	Al	Ti	S	
	0.04	0.30	0.16	14.80	2.8	2.0	0.66	1.57	2.35	0.004	0.003
2/3 of height	0.04	0.31	0.17	14.70	2.7	2.0	0.68	1.57	2.35	0.004	0.004
1/3 of height	0.04	0.31	0.17	14.77	2.7	2.0	0.68	1.56	2.35	0.003	0.004
Hll 3	0.04	0.31	0.16	14.75	2.7	2.0	0.68	1.56	2.35	0.002	0.004
TU 14-1-5329-96	0.03... 0.07	≤0.50	≤0.40	13.0... 16.0	2.8. 3.2	1.90. 2.20	≤2.0	1.45. 1.80	2.35. 2.75	≤0.007	≤0.015

Comment. Base – nickel

component with notches [2]. This element also takes part in the formation of the hardening intermetallic phases of the Ni_3B type and also the carbides causing grain refining.

The absence of aluminium and titanium in the composition of the welding electrode has almost no effect on the final content of these elements in the ingot because the amount of these elements is very small. In the presence of a large amount of the welding material the shortage of these elements can be eliminated by dosed supply into the slag pool during melting. Since the slag contains unavoidably the oxides of metals with variable valence of the type of iron, manganese, titanium, etc, the oxidation–reduction processes taking place in electroslag remelting (this must be taken into account) should be accompanied by deoxidation of the slag pool during melting.

The distinguishing special feature of the composite consumable electrode is the higher electrical resistance as a result of the presence of a large number of welded joints between the welded elements. This must be taken into account in the determination of the technological parameters of electroslag melting and the voltage in the transformer should be increased. On one hand, to produce satisfactory surface and quality of the ingot, determined by the stability of the parameters of the electroslag process, and also ensure safety, it is necessary to produce the welded joints with a relatively large cross section and satisfactory quality. On the other hand, taking into account the economic considerations, it is essential to minimise the volume of labour-consuming welded joints produced from expensive and low weldability materials.

Taking these factors into account, a consumable electrode (Fig. 1), consisting of 146 waste pieces in the form of discs weighing 4.5–5.3 kg, was produced. The discs were welded by manual arc welding in several technological operations using OZL-25B electrodes with a diameter of 4 mm. The length of the composite electrode reached 3.2 m, and the cross-section was rectangular, 270–280 mm. The consumption of the welding materials in the form of the OZL-25B electrodes was

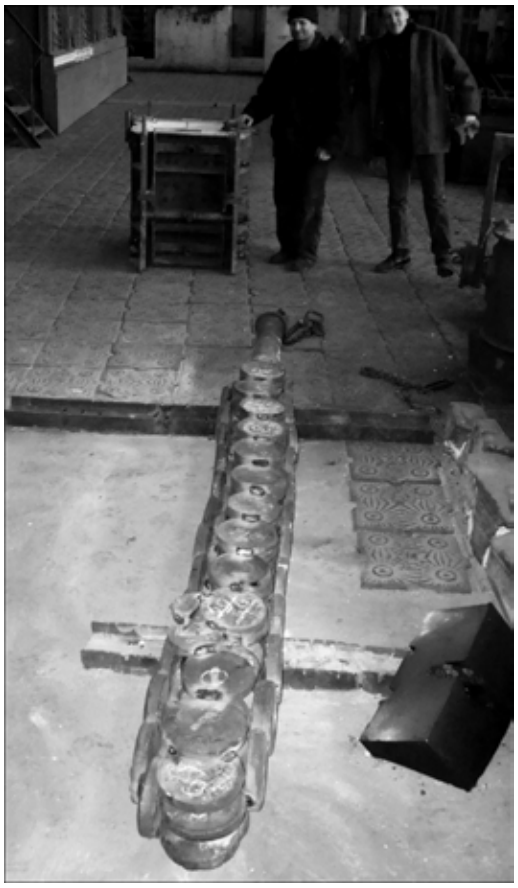

Fig. 1. A composite consumable electrode produced from the waste of KhN73MBTYu alloy.

10 kg. The total mass of the consumable electrode was 0.70 2t, and the fraction of the metal welding electrodes was only 1.4%, which have no effect on the composition of the parent metal.

The composite consumable electrodes were remelted under ANF-6 flux in a USh-116 electroslag furnace (Fig. 2). During melting, the slag pool was deoxidised with primary and aluminium, 3.5 kg per 1 t of alloy. The deoxidation of the slag with the aluminium powder resulted in the complete pickup of titanium and aluminium from the initial metal (Table 2). The attempts to carry out melting in the electrical regime usually used for the ingots of this diameter resulted in certain technological difficulties regarding the stability of the process, in particular, it was not possible to produce ingots with a high quality surface (Fig. 3a). The optimum parameters of the main period of melting the

Fig. 2. Fragment of melting an ingot of KhN73MBTYu alloy in the USh-116 equipment.

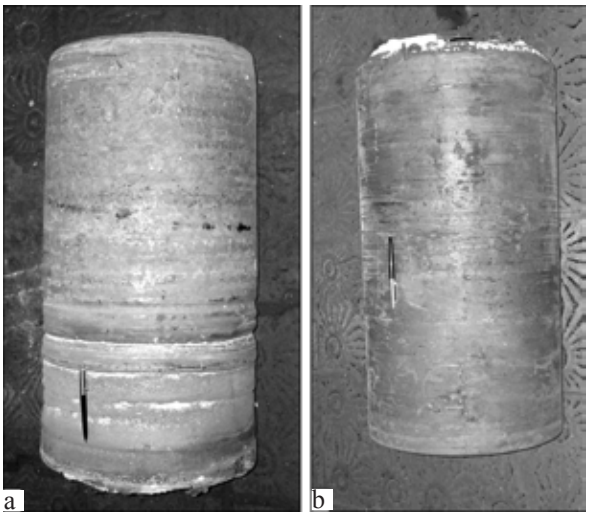

Fig. 3. Ingots of KhN73MBTYu alloy weighing 0.72 t, melted in the conditions accepted in the standard technology for the electrode with the solid cross-section (a) and in the optimum conditions, accepted for remelting the composite electrode of the given design (b).

composite consumable electrode of this design were as follows: the melting current 8.5... 9.0 kA, voltage 60 V; the depth of the slag pool 120–130 mm; the coefficient of filling the solidification mould 0.32...0.35; melting productivity 0.36 t/h.

The produced experimental ESR ingot with the diameter of 390 mm, 760 mm long, weighing 0.72 t was characterised by a flat smooth surface without burns (Fig. 3b). The macrostructure of the ingot was characterised by high density and by the absence of liquation, solidification and other defects (Fig. 4). The microstructure was uniform, fine-grained with the uniform distribution of the dispersed particles of the hardening intermetallic phases (Fig. 5). The mechanical properties of the cast alloy of the experimental ingots were considerably higher than those recommended by the technical conditions for the deformed alloy of this grade (Table 3). Evidently, this is caused by the fact that the metal is in fact subjected to the VIM+ESR duplex process.

The primary melting operation (vacuum-induction melting) of the nickel-based creep-resisting alloys resulta in high purity of the liquid metal: a decrease of the content of gases and nonmetallic inclusions and also harmful low-melting impurities, such as lead, tin, antimony, arsenic, bismuth, silver, etc [3, 4]. However, to produce the metal of the required quality in the final product this is not yet sufficient. The optimum process of secondary refining remelting (in the group of the processes VAR, PAR, EBR and ESR) for the nickel-based creep-resisting alloys of this composition is electroslag remelting ensuring gradual solidification of the relatively small volume of liquid metal which is constant in time. The solidification of this type ensures high physical and chemical homogeneity of the ingot, i.e., predetermines the stable high values of the physical and mechanical properties of the final product [5]. The VIM+ESR technological procedure, used in

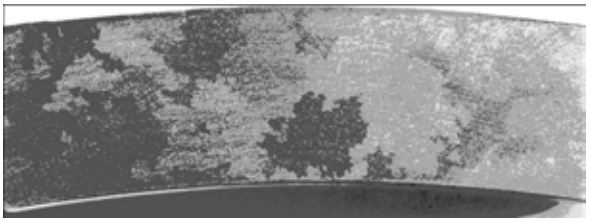

Fig. 4. Fragment of the macrostructure (×3) of an ingot of KhN73MBTYu alloy.

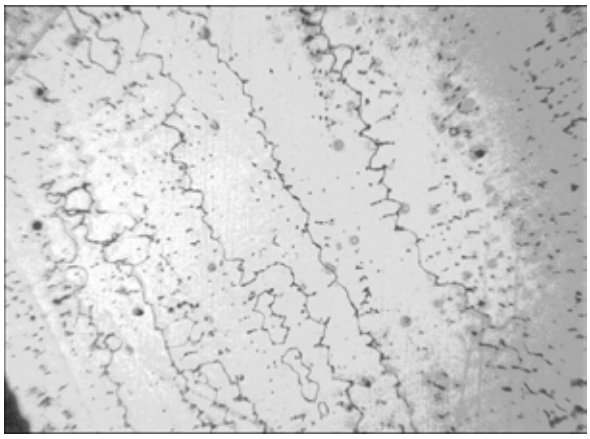

Fig. 5. Microstructure (× 40) of an ingot of KhN73MBTYu alloy.

the production of creep resisting alloys, has been accepted in all industrially developed countries of the world [5].

Recently, special attention has been paid to the problem of processing the waste of alloyed steels and alloys. Elements such as niobium, molybdenum, tungsten, nickel are very expensive, in short supply and should not be wasted. Electroslag technologies can be used to process the expensive metal waste into high-quality blanks for the components of gas turbine engines, reducing the price of the final product. This is especially important in the period of economic downturn and when increasing the volume of production.

References

1. Latash Yu.V. and Medovar B.I., Electroslag remelting, Metallurgiya, Moscow, 1970.
2. Khimushin F.F., Creep-resisting steels and alloys, Metallurgiya, Moscow, 1969.
3. Paton B.E. and Medovar B.I., Electroslag metal, Naukova Dumka, Kiev, 1981.
4. Gulyaev A.P., Clean steel, Metallurgiya, Moscow, 1975.
5. Paton B.E. and Medovar B.I.,In: Electroslag technologies, proceedings of the conference devoted to 30 years of electroslag remelting, Naukova Dumka, Kiev, 1988, 5–11.

Table 3. Short-term mechanical properties and long-term strength of ESR metal of KhN73MBTYu alloy

Heat treatment conditions	Sampling area	Test temperaure, °C	σ_B, MPa	σ_{02}, MPa	σ_5, %	ψ, %	KCU, J/cm²	HB, MPa	Long-term strength	
									σ, MPa	t, h
Quenching, 1120°C, 8 h, air	B		1243	873	22.3	27.3	66	3620	—	—
Tempering 1000°C, 4 h, air	C	20	1250	873	25.1	34.3	79	3621	—	–
	H		1256	846	23.0	30.1	68	3625		–
Ageing at 750°C, 20 h, air	B		—	—	—	—	—	—	400	91.0
	C	750	—	—	—	—	—	—	400	91.3
	H		—	—	—	—	—	—	400	89.2
Requirements of TU14-1-5329-96 (min)		20	1150	720	16	18	39	2860... 3400	—	–
		750	—	—	—	—	—	—	390	50.0

Comment. B – top, C – centre, H – bottom of ingot.

Advances in Electrometallurgy 2010 **8** *(2) 98–102*
Translated from Sovremennaya Elektrometallurgiya 2010 **8** *(2) 17–20*

Mathematical modelling of heat generation in the slag pool in electroslag casting with melting on of flange stop valves

A.F. Muzhichenko, M.A. Poleshchuk and V.L. Shevtsov

E.O. Paton Electric Welding Institute, Kiev

Using mathematic modeling, the distribution of volume heat sources in the slag pool in electroslag casting with melting-on is determined. The task is considered in the three-dimensional version. The boundary conditions are determined. Good correlation is found between the experimental and calculated values of electric current passing through the elements.

The stop valves with flanges at the end of nipples are used for the extraction of oil and natural gas by the fountain method. In many Ukrainian deposits, these systems work at the pressure of the extracted product of up to 70 MPa. The E.O. Paton Electric Welding Institute, Kiev, developed a technology for producing the blanks for bodies of these stop valves by the methods of electroslag casting with melting-on (ESCM) based on electroslag melting of only the central part of the body of the valve with simultaneous melting-on of the pre-produced nipples with flanges [1, 2].

The ESCM process consists of three stages (Fig. 1). The first (Fig. 1a) and third (Fig. 1c) stages are based on the electroslag casting of a solid section cylindrical ingot by the monofilar method. The process of melting-on of nipples takes place in the second stage (Fig. 1n). In this stage, during melting of the consumable electrode, the slag and metal pools travel upwards along the ends of the nipples. They are melted to the cast part of the blank.

In developing ESCM technology, special attention was given to high-quality melting-

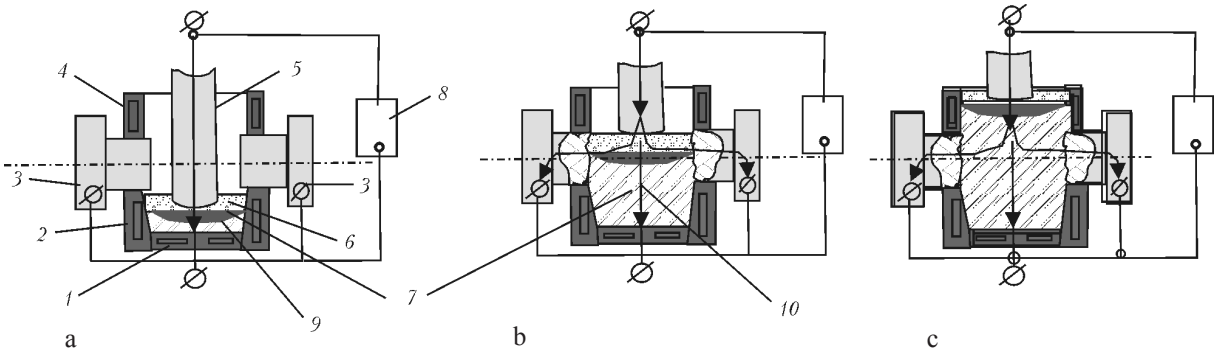

Figure 1. Diagram of the process of ESCM of flange stop valves: a) initial stage; b) melting-on stage; c) final stage; 1) baseplate; 2) solidification mould (lower part); 3) nipples with the flanges; 4) the solidification mould (upper part); 5) the consumable electrode; 6, 7) the slag and metal pools, respectively; 8) power source; 9) the melted part of the blank.

on the nipples without formation of cracks and lack of fusion defects and to obtaining the required properties of the metal in the melting-on zone [3]. The special feature of ESCM is that the stage of melting-on is characterised by the formation, in the slag pool, of additional routes of passage of current from the consumable electrode to the nipples (Fig. 1b) which affects the distribution of heat in the slag and, consequently, the quality of melting-on.

The special features of heat generation in the slag pool were investigated by mathematical modelling. Similar problems have been studied by many investigators from the very beginning of the application of mathematical modelling methods for investigating electroslag processes [4–7]. However, all these methods were two-dimensional, axisymmetric, or were produced to this condition. At the same time, the problem in the investigated in this work in the area of melting-on of the metal is three-dimensional.

The blank of the body of the flange stop valve is a complicated spatial figure (Fig. 2). The problem of the distribution of the density of heat generation in the slag pool in ESCM of the blanks of this type was solved in the cylindrical coordinate system (z, r,) with the origin situated at the intersection of the longitudinal axes of the body and the nipples. The blank has two planes of symmetry: at θ = 0 and 180° (S_{C1} – along the axis of the metal) and θ = 90 and 270° (S_{C2} – across the axis of the nipple). Therefore, the mathematical modelling of the processes is carried out only in a quarter of the blank.

The mathematical model of the electrical and thermal processes in the slag pool in ESCM consists of solving the following problems:

– construction of a three-dimensional finite-element model of the melting space. For this purpose, the geometrical model of the blank is included in the calculation programme in the three-dimensional IGS format using AutoCAD software. This format makes it possible to transfer both the volumes of the blank and the slag pool and the restricting surfaces, lines and key points. In solving the given problem, it is possible to examine in detail only the central part of the blank restricted by the melting space of the solidification mould with the ends of the melted-on nozzles oriented in the direction into the blank. The remaining parts will be investigated in lesser detail;

– calculation of the fields of the electrical potential and the density of current in the slag pool in the three-dimensional formulation;

– the calculation of the distribution of specific volume heat sources in the slag pool in the three-dimensional formulation.

In addition to this, in order to verify the adequacy of the proposed model with respect

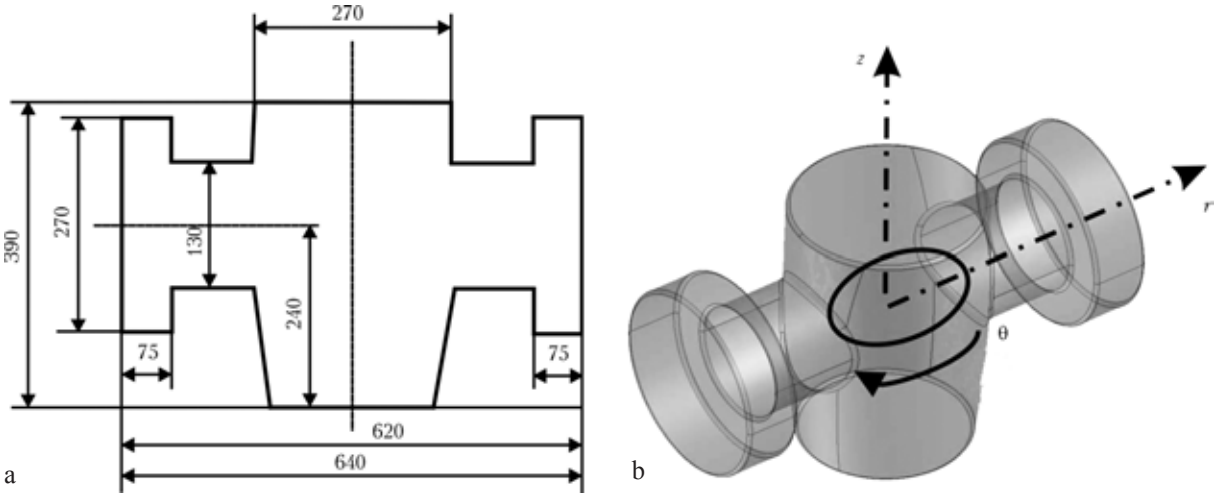

Fig. 2. The blank for the body of a flange stop valves with the efficient passage section of 80 mm: a) sketch; b) isometry.

to the actual process, calculations are carried out of the integral values of the current at the boundaries of the nipples, the consumable electrode and the metallic pool for individual moments of ESCM. The calculation values of the current were compared with the experimental data, obtained at the appropriate moment of ESCM.

The current density in the slag wool was calculated using the model of the electrical processes formulated in the form of the field of potentials [6, 8]:

$$div(\sigma\, grad\, \varphi) = 0 \qquad (1)$$

The results of the calculation of the current density are used to determine the volume density of the heat sources, generated in the slag pool:

$$q = \sigma |grad\, \varphi|^2, \qquad (2)$$

where $\sigma = \sigma(t)$ is the specific electrical conductivity of the slag i.e., the value which depends on temperature and is reciprocal to the specific electrical resistance, ohm^{-1} mm^{-1}; φ is the potential of the electrical field, V.

The values of the variation of the specific electrical resistance of the ANF-6 slag in the temperature range 1200–1600°C were taken from [7, 8]. The initial conditions were represented by the results of distribution of temperature in the slag pool, determined in [9].

The solution of the equations (1) and (2) will be found in the area of the slag pool a restricted at the top by the end of the consumable electrode S_E; at the bottom – by the surface of the molten metal S_M; at the sides by the wall of the solidification mould, covered with the skull S_K and the melted end of the nipple S_N, and also by two symmetric planes (S_{C1} and S_{C2} – along and across the axis of the nipple, respectively) (Fig. 3).

The problem is solved in the quasi-stationary formulation for different positions of the surface of the metal pool in relation to the longitudinal axis of the melted-on nipple. The boundary conditions are presented in Table 1.

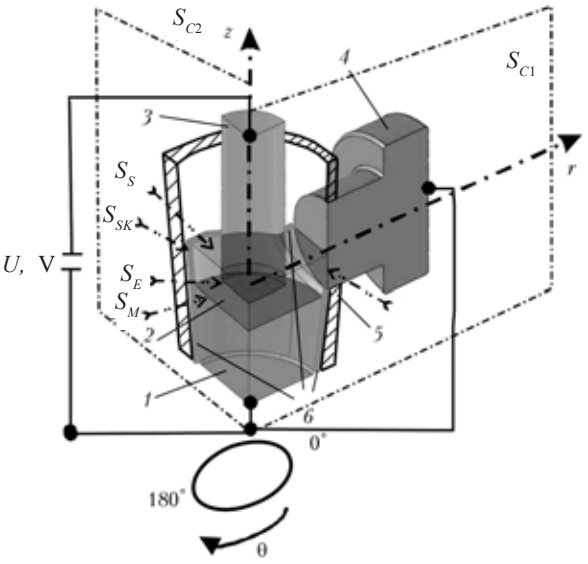

Fig. 3. Diagram of the boundary conditions, used in solving the problem: 1) the melted part of the blank; 2) the slag pool; 3) the consumable electrode; 4) the melted-on nipple; 5) solidification mould; 6) the skull.

The geometrical model is divided into network of finite elements. The highest gradient of the variation of the potential in the slag pool is recorded in the region below the electrode and, consequently, the network at the ends of the electrode and the nipples is several times denser [5, 6].

Table 1. The boundary conditions for calculating the distribution of volume heat sources

Notation of the boundary	Parameters at boundary		
	φ, V	σ, ohm^{-1} mm^{-1}	T_c, °C
S_E	$\varphi = U$	$s_M(T)$	1510
S_S	$\frac{\partial \varphi}{\partial Y} = 0$	$\sigma_{sl}(T)$	1600
S_M	$\varphi = U_0$	$\sigma_M(T)$	1550
S_{SK}		$\sigma = \infty$	1200
S_S	$\varphi = U_0$	$\sigma_M(T)$	1510
S_{C1},S_{C2}	$\frac{\partial I}{\partial n} = 0$	$\sigma_M(T)$	T_S
	$\frac{\partial \varphi}{\partial n} = 0$	$\sigma_M(T)$	T_M

Comment. Here σ_M, σ_S, is the specific conductivity of metal and slag, respectively; T_M, T_S is the temperature of metal and slag, respectively, n is the normal to the symmetry plane.

To to verify the correctness of formulation of the boundary conditions and the accepted assumptions, experimental melting trials were carried out on a blank of a body of a stop flow of with the conventional passage of 80 mm. A multichannel automatic recording device and current transformers, placed in the appropriate circuits, were used for the continuous recording of the current passing through the consumable electrode, the melted blank and the melted-on nozzles throughout the entire melting period. The current of the consumable electrode and the voltage of the power source were maintained constant (3.2 kA and 57 V, respectively) at the depth of the ANF-6 slag pool of 75 mm. The position of the surface of the metal pool in relation to the baseplate was calculated on the basis of the melting time of the marks on the consumable electrode.

The measurement results are presented in Fig. 4 in the form of curves. The graph also gives the current passing through these elements are determined by calculations using the mathematical model on different levels of the metal pool surface.

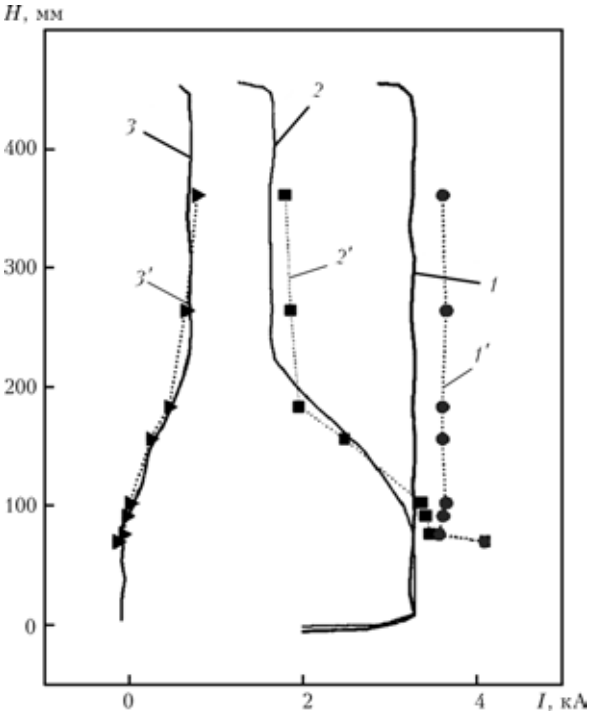

Fig. 4. Distribution of current in elation to the height of the blank of the body of the stop valve *H*: 1) the current in the consumable electrode (1' – calculated); 2) the current in the baseplate (2' – calculated); 3) the nipple (3'– calculated).

Figure 4 shows the satisfactory correlation between the calculated and experimental data. This confirms that the proposed mathematical model of distribution of the volume heat sources in the slag pool corresponds to the actual process in ESCM.

Figure 5 shows the distribution of the current density and the volume density of the heat sources in the slag pool in different moments of the ESCM process of the blanks of the bodies of the flange stop valves with the efficient cross-section of 80 mm. In the calculations, the depth of the slag pool (ANF-6) was assumed to be equal to 75 mm, the diameter of the consumable electrode 130 mm, the diameter of melted-on nipples 160 mm, working current 3.2 kA, the voltage in the consumable electrode U = 40 V, the voltage on the surface of the metal bath and the end of the nozzle was assumed equal to U_0 = 0.

The distribution of current in the volume heat sources was determined for four different positions of the surface of the metal pool in relation to the axis of the nipple.

The distribution of current density corresponds to the scale (*a*) and that of the density of the volume heat sources to the scale (*b*).

As indicated by the Fig. 5, until the surface of the slag reaches the nipple (position I), the distribution of the current in the volume heat sources is identical with that in melting of the cylindrical ingot [4, 5]. The pattern of current distribution and the release of heat in the volume of the slag change greatly after the surface of the slag pool reaches the end of the melted-on nipple (position *II*). A new zone of high-intensity heat release, and differing from the zone at the wall of the solidification mould, appears in the vicinity of the end of the nipple. The position of the new heat release zone is shown clearly in Fig. 5. The heat generation pattern become similar to that in bifilar melting [6]. An additional quasi-consumable electrode appears to have formed in the slag pool. When the surface of the metal pool reaches the end of the melted-on nipple, the intensity of the additional heat

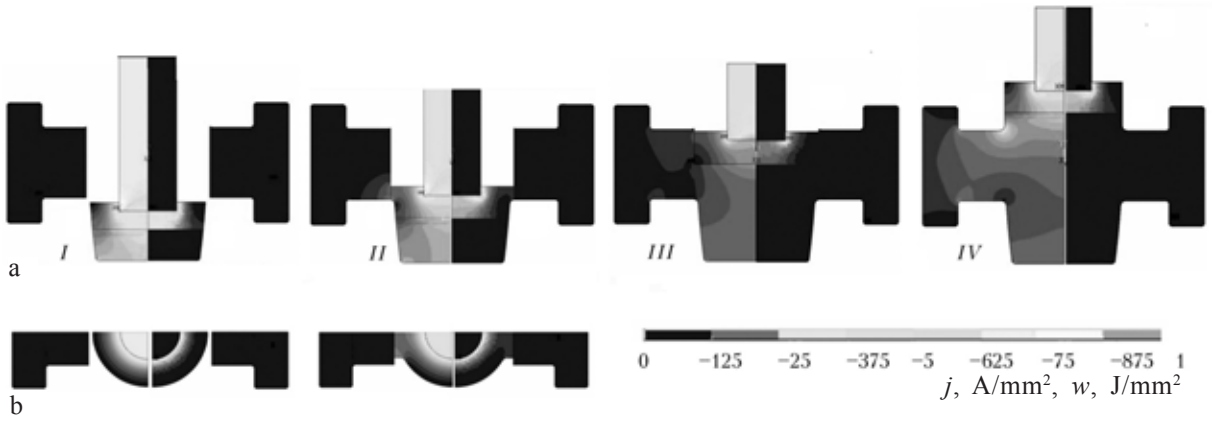

Fig. 5. Distribution of the current density j (a) and the density of the heat sources w in the cross-section in the plane $_C$ and on the surface of the slag pool (b) for different distances of the surface of the metal pool from the axis of the nipple: I) 170; II) 80; III) 0; IV) 120 mm.

sources in the slag decreases (position *III*), and after completing the melting-on process (position *IV*) the pattern of current distribution and 80° becomes identical with that in position I.

Thus, Fig. 5 shows that if the nipples are electrically connected using conductors with a baseplate, the slag pool in the vicinity of the nipples is characterised by the formation of a zone of high-intensity heat release and, consequently, the end of the nipple is heated at a higher rate, melts and a high quality joint forms with the melted part of the blank.

Conclusions

1. The investigation results have been used to develop a three-dimensional mathematical model of the distribution of current and volume heat sources in the slag pool in ESCM.

2. The adequacy of the model has been confirmed by experimental data.

3. The model can be used in selecting the technological parameters of melting of the blanks for the bodies of the stop valves of different standard dimensions prior to melting.

References

1. Poleshchuk M.A., et al., Sovremen. Elektrometall., 2009, No. 2, 13–17.
2. Poleshchuk M.A., et al., 2009, No. 4, 49–54.
3. Poleshchuk M.A., et al., Sovremen. Elektrometall., 2009, No. 4, 8–12.
4. Shevtsov V.L., Probl. Spets. Elektrometall., 1975, No. 2, 26–31.
5. Makara .M., et al., Probl. Spets. Elektrometall., 1975, No. 2, 6–10.
6. Medovar B.I., et al., In: Mathematical methods in the investigation of the processes in special electrometallurgy, Naukova Dumka, Kiev, 1976.
7. Makhnenko V.I., et al., Sovremen. Elektrometall., 2008, No. 4, 30–37.
8. Eric R.H., Slag properties and design issues pertinent to matte smelting electric furnaces, in: Seventh International conference on molten slags, fluxes and salts, South African Institute of Mining and Metallurgy, Cape Town, 2004, 531–541.
9 Hara S., et al., Transaction ISIJ, 1983, volume 23, 1053–1058.

Advances in Electrometallurgy 2010 **8** *(2) 103–108*
Translated from Sovremennaya Elektrometallurgiya 2010 **8** *(2) 21–24*

ELECTRON BEAM PROCESSES

Dissipative properties of Fe–Cu nanocomposites

A.I. Ustinov, V.S. Skorodzievskii, V.N. Taranenko and V.A. Telichko

E.O. Paton Electric Welding Institute, Kiev
G.V. Kurdyumov Institute of Physics of Metals, Kiev

The mechanical and dissipative properties of Fe–Cu nanostructured vacuum condensates with 19 and 40 wt.% of copper in their initial state (deposition at T_c = 270°C) and after isothermal annealing at T = 650°C are studied. Microhardness HV of both condensates in initial state was 5.5 GPa and did not change after annealing, whereas the scatter of mechanical energy in annealed condensates increased, the level of the logarithmic decrement for the Fe–Cu condensate increased 2.0...2.5 times in relation to its values for the Fe–19 % Cu condensate. The relatively high stability of values of the logarithmical decrement for condensates of both compositions in cyclic deformation in the temperature range 20...300°C is also noted.

The Fe–Cu composite alloys are characterised by the combination of high mechanical properties and high damping capacity at temperatures up to 450°C [1, 2]. The low mutual solubility of copper and iron [3] improves the stability of the structure and, consequently, the thermal stability of the mechanical properties which are determined, in addition to the composition of the composite, by the dimensions of structural elements which depend strongly on the technology of production of the material.

It was shown in [4] that the vacuum condensates of the Fe–Cu system, deposited at substrate temperatures lower than 400°C, are characterised by the formation of grains with the size of 0.3–0.5 μm. The dependence of microhardness HV on composition of these materials is described by a wide maximum (5.5 GPa), and the deposition corresponds to the copper content of 30 wt.%.[1] It was also shown that the initial condensates based on iron (copper content 20–40%) are in the non-equilibrium condition: examination by x-ray diffraction analysis and electron microscopic showed only reflections of BCC iron. Annealing of the condensates of these compositions at T = 420°C resulted in the precipitation of the nanosized copper particles with the FCC lattice in the matrix BCC grains [4].

It was shown in [6] that the Cu–Fe vacuum condensates based on copper (iron content up to 7%) are characterised by the high level of scattering of mechanical energy, but the HV microhardness of these condensates is 2.0–2.2 GPa, i.e., 2.0–2.5 times lower than that of the Fe–(20...40) % Cu condensates.

[1]VT1-0 alloy is characterised by high elasticity and a low level of scattering of the mechanical energy in the range T = 20–400°C [1], essential in investigating the dissipative properties of the condensates, deposited on the substrate as coatings.

In this work, investigations were carried out into the effect of the copper content on the dissipative properties of the Fe–19% Cu and Fe–40% Cu condensates in the initial condition (after deposition) and after heat treatment.

The experimental procedure

The Fe–19% Cu and Fe–40% Cu condensates with the thickness of 60 μm were produced by vacuum electron beam deposition of the vapour phases of the components in joint evaporation from two independent evaporators. The condensates were deposited at a temperature of 270°C on the substrate with a thickness of 1.8 mm, produced from the sheets of VT1-0 titanium alloy. At a two-fold difference in the copper content, the resultant condensates were characterised by approximately the same *HV* microhardness, *HV* ≈ 5.2 GPa.

The dissipative properties of the condensates were investigated in laboratory equipment [7] in cantilever fixing of the specimens with the condensates, deposited in the form of coatings (Fig. 1). The initial data and the amplitude dependences of the logarithmic decrement (LD) $\delta_1(A)$ for the specimens with the coatings were determined using the oscillograms of attenuating bending oscillations with a frequency of 130–140 Hz.

The amplitude dependences $\delta_1(A)$ were measured in heating of the condensates in the temperature range 20–450°C. The amplitude dependences of LD, relating to the material of the condensates $\delta(\varepsilon)$, where ε is the strain amplitude of the uniformly deformed coating, were calculated [8] on the basis of experimental data for $\delta_1(A)$.

The microhardness of the condensate was measured on cross sections by the Vickers method using a Polyvar Met optical microscope with the constant load on the indentor of 49 mN with the duration of 10 s. The error of the measurements did not exceed ±10%.

The condensates were investigated in the initial condition and after heat treatment, isothermal annealing in vacuum at T = 650°C, for 2 h. In order to take into account the contribution of the substrate and the total scattering of energy by the specimens with the coating, measurements were taken of the amplitude dependences of LD for the specimens without a coating in the initial condition and after isothermal annealing.

Experimental results

The scattering of energy for the Fe–19% Cu condensates in the initial condition is characterised by the amplitude dependences of LD. The increase of temperature to 450°C resulted in approximately the same increase of the degree of scattering in the entire strain amplitude range (Fig. 2). At room temperature, the values of LD did not exceed $2\cdot10^{-3}$. With increase of temperature, the value is slightly increased, starting at T = 250°C, and subsequently increased to $6.5\cdot10^{-2}$ at T = 450°C

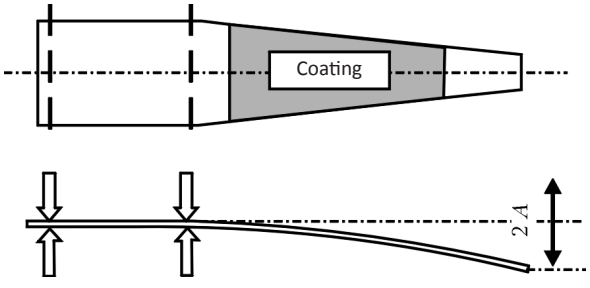

Fig. 1. Schematic representation of the shape and alternating deformation of the specimen with a coating: A) the amplitude of oscillations of the free end of the specimen.

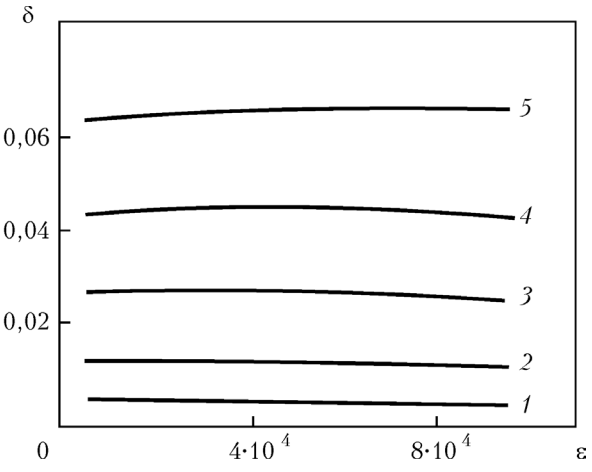

Fig. 2. Effect of temperature on the amplitude dependences of LD of the Fe–19% Cu condensates in the initial condition: curves 1–5 correspond to the temperatures of 20, 250, 350, 400 and 450°C.

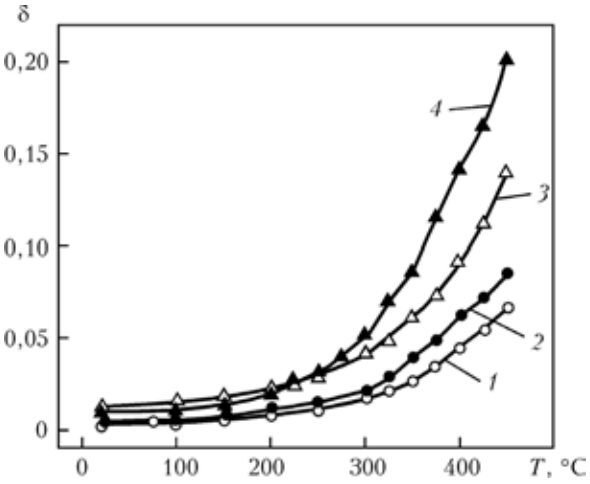

Fig. 3. Temperature dependence of LD of the Fe–19% Cu (1, 2) and Fe–40% Cu (3, 4) condensate in the initial condition (1, 3) and after annealing at T = 650°C (2, 4); the section of the curves $\delta_1(\varepsilon)|_T$ on the level $\varepsilon = 6 \cdot 10^{-4}$.

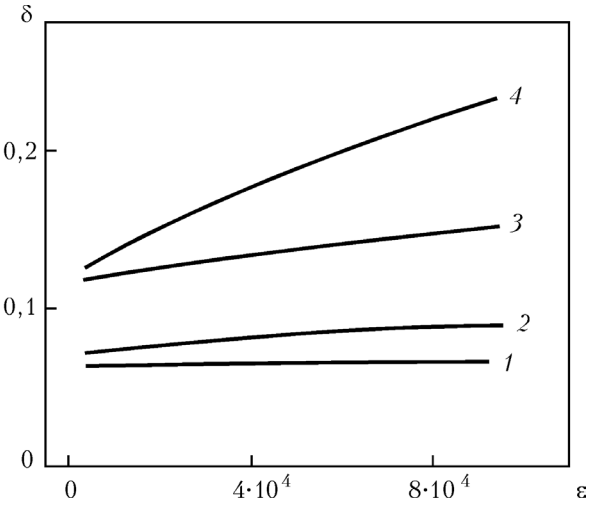

Fig. 4. Amplitude dependences of LD of the Fe–19% Cu (1, 2) and Fe–40% Cu (3, 4) condensates at T = 450°C; 1, 3) initial condition; 2, 4) after annealing at T = 650°C.

(Fig. 3, curve 1).

For the Fe–40% Cu condensates in the initial condition, the values of LD were 2.0–2.5 times higher than the appropriate values, obtained for the Fe–19% Cu condensates. In addition to this, the scattering of energy in the Fe–40% Cu condensates was characterised by the amplitude–dependent form at elevated temperatures (Fig. 4, curve 3). As for the Fe–19% Cu condensates, heating of this condensate was characterised by a rapid increase of LD, starting at T = 250°C (Fig. 3, curve 3).

The effect of isothermal annealing of the Fe–19% Cu and Fe–40% Cu condensates on the scattering characteristics of mechanical energy is shown in Fig. 3 and 4. It may be seen that for both condensates, the values of LD are higher than the values obtained for the initial condition, in particular, in the area of high strain amplitude. For these values, as in the initial condition, the values of LD rapidly increased at T >250°C (Fig. 3, curves 2 and 4).

It should be mentioned that the microhardness of both condensates was practically constant during heat treatment. For the annealed condensates, the microhardness values (5.2 and 5.15 GPa for Fe–19% Cu and Fe–40% Cu respectively) did not differ within the range of the measurement error $\Delta HV = \pm$ 0.5 MPa in comparison with the microhardness in the initial condition (respectively 5.3 and 5.2 GPa for Fe–19% Cu and Fe–40% Cu).

Stability of energy scattering characteristics

Investigations were carried out into the effect of heating–cooling thermal cycles and the duration of alternating the formation of the specimens with the coatings on the scattering of mechanical energy in the specimens. The thermal stability of the energy scattering characteristics of the condensates was determined by comparing the intermediate relationships $\delta_1(A)|_T$, measured for the same temperatures during heating of the specimens to 450°C followed by cooling.

For the specimens with the condensates of the two compositions in the initial condition and after isothermal annealing, the results show almost complete agreement of the $\delta_1(A)|_T$, curves, as shown on the example of the specimen with the Fe–19% Cu coating (Fig. 5).

The tests of the cyclic stability of the energy scattering characteristics of the condensates were carried out in heating the specimens to 200 and 300°C and this was followed by alternating deformation with the amplitude of $\varepsilon_m = 7 \cdot 10^{-4}$ and the duration of

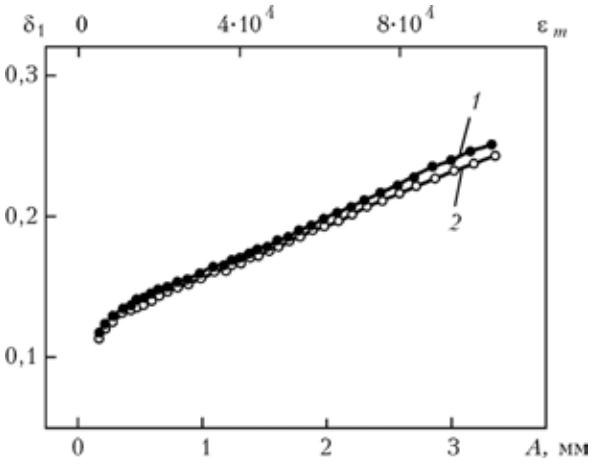

Fig. 5. Amplitude dependences of LD for the specimen with the non-annealed coating Fe–19% Cu measured at the intermediate temperature of 250°C during heating of the specimen to 450°C (1) followed by cooling (2).

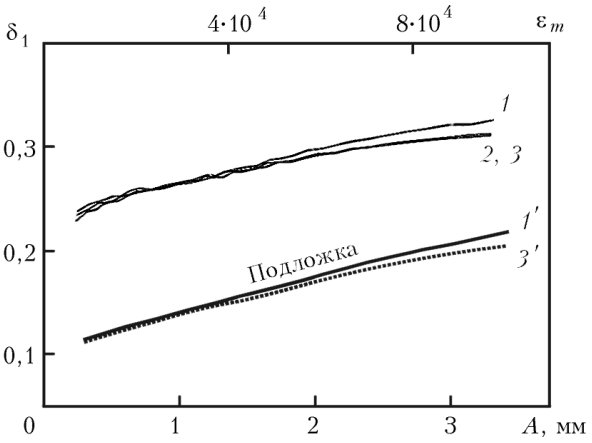

Fig. 6. Amplitude dependences of LD of the specimens without a coating and with the Fe–40% Cu coating, annealed at T = 650°C, on the duration of cyclic deformation at T = 250°C: 1, 1') the initial condition of the specimen with and without the coating, respectively; 2) the specimen after $N = 1 \cdot 10^5$ cycles; 3, 3') the specimen with and without the coating after $N = 3 \cdot 10^3$ cycles; the maximum strain amplitude of the coating $\varepsilon_m = 7.5 \cdot 10^{-4}$.

up to $N = 5 \cdot 10^5$ cycles (ε_m is the maximum strain amplitude of the coating in the vicinity of the root section of the specimen).

The resultant dependences $\delta_1(A)$ obtain prior to and during cyclic deformation of the specimens were in complete agreement in the strain amplitude range $5 \cdot 10^{-5} < \varepsilon_m < 5 \cdot 10^{-4}$ (Fig. 6, curves 1–3). Partial decrease of LD at the amplitude of $\varepsilon_m > 6 \cdot 10^{-4}$ is explained by the decrease of the contribution of the substrate and the total scattering of energy of the specimen with a coating as a result of cold working of the substrate in the clamping area (Fig. 6, curves 1', 3').

Analysis of the experimental data

The weak linear amplitude dependence of LD is characteristic of the hardened metals, in which the acting stresses are not sufficient for release and displacement of the dislocations [2] or the displacement of the dislocation is not possible in the medium of the high density dislocation network [9]. The similar characteristics of energy scattering in the investigated Fe–Cu condensates may also indicate the restricted effect of the energy scattering centres in space.

The hardening of the metals with the decrease of the grain size is associated with the reduction of the number of dislocations capable of moving in the body of the grains [10], consequently the mechanical properties of the metals with the submicron or smaller grains become dependent also on the deformation resistance at the grain boundaries [11]. In these materials, the scattering of mechanical energy, associated with the rearrangement of the atomic configurations at the grain boundaries, may become comparable with the scattering determined by the movement of dislocations inside the grains or may even be stronger [12].

In the investigated condensates with the mean grain size of 0.3–0.5 μm of the grain boundary factor intensifies by the presence of nanosized particles of copper associated with the BCC matrix or with the particles precipitated in the matrix during isothermal annealing. Fracturing of the coherent bond of the particles and results in the formation of additional structural disruptions of the iron–copper boundary and, consequently, in the increase of the degree of scattering of energy in the annealed condensates.

Comparison of the amplitude dependences $\delta(\varepsilon)$ for the condensates of the two compositions (Fig. 4) shows that the scattering of energy depends strongly on the copper content of the condensates; a large increase of LD is detected at temperatures higher than 250°C,

indicating the thermally activated nature of the processes of rearrangement of the atomic structure.

It should be be mentioned that the extensive scattering of energy at T = 230–250°C, determined by grain boundary diffusion, typical of pure copper was recorded both in the specimens with the large grains [13] and in the films on the specimens [14]. On the basis of the experimental results it may be assumed that the low melting point of copper (in comparison with iron) is an important factor determining the contribution of the copper component of the scattering of the energy of the Fe–Cu condensates.

It should also be noted that with the increase of the temperature of the condensates, the values of LD of the condensates increase in the entire range of strain amplitude, starting with the lowest values, approximately $\varepsilon \approx 5 \cdot 10^{-5}$ (Fig. 2, 4), indicating the initiation of grain boundary processes in the fields of low external stresses with the amplitude $\sigma \approx 7...10$ MPa, where $\sigma = \varepsilon \cdot E$; E is the elasticity modulus of the condensate (Table 1).

Nevertheless, it may be assumed that the further increase of the applied stress is, up to σ = 200 MPa ($\varepsilon \approx 1 \cdot 10^{-3}$), does not lead to the failure of the condensates through the grain boundaries. This assumption is justified if the cyclic stability of the amplitude dependences of δ_1 (Fig. 6) is taken into account, together with the relatively large difference between the maximum amplitude of the applied stresses and the yield limit (σ = 200 MPa, σ_T = 1.8 GPa)[1].

Table 1. Elasticity modulus of Fe–Cu condensates and the amplitude of acting alternating stresses in testing in the temperature range 20–450°C

T, °C	Fe–19 % Cu			Fe–40 % Cu		
	E, GPa	σ, MPa		E, GPa	σ, MPa	
		min	max		min	max
20	200	10,0	200	180	9,0	180
250	185	9,0	185	170	8,0	170
450	170	8,0	170	150	7,5	150

Comment. The elasticity modulus condensates were estimated in the approximation of the rule of mixing, $E(T) = (1 - v) E_{Fe}(T) + vE_{Cu}(T)$, where v is the volume fraction of copper in the condensate, and also using the literature data for the elasticity modulus of copper [2] and iron [15] in the temperature range 20...450°C.

The nanosized scale of the segregation is precipitated copper particles indicates that the Fe–Cu condensates can be regarded as the dispersion–hardened systems. Other same time, the absence of a large difference of microhardness in the non-annealed and annealed conditions shows that the strength properties of these materials are controlled by the size of the structural elements.

Conclusions

1. The experimental results show that the increase of the copper content in the Fe–Cu vacuum condensates, deposited at the substrate temperature of 270°C, from 19 to 40% results in doubling of the scattering characteristics of mechanical energy in the temperature range 250... 450°C.

2. It is shown that the precipitation of the nanosized copper particles in the iron grain in annealing of the Fe–19% and Fe–40% condensates increases the energy scattering characteristics by 50–25% without any large decrease of the hardness.

References

1. Pisarenko G.S., et al., Vibration-absorbing properties of structural materials, Naukova Dumka, Kiev, 1971.
2. Golovin S.A., et al., Elastic and damping properties of structural metallic materials, Metallurgiya, Moscow, 1987.
3. Elliot R.P., Constitution of binary alloys, the first supplement, McGraw-Hill, New York, 1965.
4. Ustinov A.I., et al., Structure and mechanical properties of the Fe–Cu nanocomposite produced by deposition of the vapour phases, HighMatTech-2009, Kiev, 2009, 295.
5. Filippov N.I., Production and properties of superfine-grained iron–copper pseudoalloys, Institute of Powder Metallurgy, National Academy of Sciences of Ukraine, Kiev, 2002.
6. Ustinov A.I., et al., Materials Engineering, to be published.
7. Ustinov A.I., et al., Probl. Prochn., 2001, No. 4, 55 –61.
8. Ustinov A.I., et al., Probl. Prochn., 2007, No. 6, 134–143.
9. Valiev R.Z., et al., Fiz. Met. Metalloved., 1992, No. 4, 70–86.

[1]The yield limit of metals can be estimated on the basis of the microhardness values, using the approximation $\sigma_T \approx HV/3$ (for example, in copper in [14]). In this approach, for the investigated Fe–Cu condensates we obtain $\sigma_T \approx$ 1.8 GPa at T = 20°C, which is an order of magnitude lower than the maximum amplitude of the applied alternating stress.

10. Andrievskii R.A. and Glezer A.M., ibid, 1999, No. 1, 50–73.
11. Firstov S.A., Special features of the deformation and failure of micro- and nanocrystalline materials, in: Advanced materials and technologies, volume 2, Kiev, 2003, 610–630.
12. Ke T., In: Elasticity and inelasticity of metals, IL, Moscow, 1954, 271–306.
13. Choi D.H. and Nix W.D., Acta Materialia, 2006, No. 54, 679–687.
14. Warner D.H., et al., Int. J. Plasticity, 2006, No. 22, 754–774.
15. Bozort R., Ferromagnetism, IL, Moscow, 1956.

Advances in Electrometallurgy 2010 **8** *(2) 109–113*
Translated from Sovremennaya Elektrometallurgiya 2010 **8** *(2) 25–29*

Investigation of the metal of ingots produced from reduced molybdenum concentrate by electron beam remelting

V.O. Mushegyan

Paton-Armeniya National Technical Centre, E.O. Paton Electric Welding Institute, Kiev

The metal of molybdenum ingots produced from briquettes of reduced Mo powder using electron beam remelting is studied. The statistic parameters, configuration and spatial position of non-metallic inclusions are defined. The comparative analysis of inclusions in ingots produced by electron beam remelting and vacuum arc remelting is carried out.

Metallic molybdenum is usually produced by reduction of pure molybdenum trioxide or pure ammonium molybdate with hydrogen [1]. Depending on the production conditions, powders with different grain size and sets of the grains are produced. The solid and gaseous impurities, present in the powder in the form of soluble and insoluble impurities, strongly affect the behaviour of the powder during processing and also the final properties of compacted metal.

The properties of the powder are to a certain extent inter-dependent. For example, the large specific surface of the fine dispersion powder is the reason for the increase of surface adsorption of gases which in turn influences the subsequent processes of treatment of metallic powder. Consequently, the content of, for example, oxygen, is 0.05–0.020% [2] which is satisfactory only when the fine dispersion structure of the powder metal is taken into account.

Thus, powder metallurgy ensures that molybdenum is pure as regards impurities and this purity is essential for a limited number of component (mainly for heating elements).

To use the molybdenum in conditions requiring a specific level of the ductility properties, it is necessary to carry out additional purification to remove impurities. This purification is conducted by vacuum remelting methods – electric arc and electron beam [3].

A source of advanced industrial arc melting of molybdenum includes the individual experiments carried out in 1943 to explain the possibilities of arc vacuum melting of molybdenum using alternating current [4] which laid foundations to the development of the process of production of molybdenum in the form of larger blanks than those produced at that time by powder metallurgy processes thus expanding the area of application of molybdenum as the structural material.

Regardless of the fact that the structure of the metal in conventional metallographic investigations was satisfactory and contained only a small number of nonmetallic inclusions, the metal could not be forged. The impact of a hammer on an ingot, heated to 1100°C, transformed latter to a pile of individual crystals.

It was shown that it is necessary to deoxidise the metal in vacuum arc remelting (VAR). Melting of bars with the controlled addition of carbon produced ingots which could be forged. Previously, in melting molybdenum in

vacuum and deoxidation with carbon it was necessary to maintain the carbon content in the metal at approximately 0.06% to produce a malleable ingot.

Improvement of equipment and technology resulted in a reduction of the carbon content. In the present time, the ingots produced by electric arc melting contain approximately 0.001% oxygen and 0.02% carbon. These values are higher than the limiting solubility of these elements at moderate temperatures (up to 600°C). Therefore, the volume of the grain, especially the boundaries of the grains, are characterised by the precipitation of molybdenum oxides and carbides (Fig. 1) with the size of 5–10 μm of the irregular elongated shape (the elongation coefficient is in the range 3–6) making them probable crack nuclei.

One of the main problems of restricting the application of molybdenum as a structural material is cold brittleness, i.e., the transition of the metal from the ductile state of the brittle state with a decrease of temperature [5]. This is characteristic of all metals and alloys with the body-centred cubic lattice.

In practice, the transition temperature is determined as a 'jump' which takes place as a result of narrowing of the cross-section of the specimen at fracture with a decrease of test temperature. The relative reduction in area of the specimen rapidly decreases. The transition temperature is influenced by mechanical, chemical and metallurgical factors.

The effect of chemical composition on transition temperature has been studied in more detail than the effect of other factors. Nonmetallic impurities (nitrogen, carbon and, in particular, oxygen) determine the nature of failure. The most important factor is the transition from failure by separation to failure at the grain boundaries.

According to the data in [2], an increase of the oxygen content from 0.002 to 0.010% increases the transition temperature by 150°C. This is the consequence of the fact that at the mass fraction of oxygen greater than 0.008 wt.%, the fracture characteristics are highly sensitive to deformation as a result of the precipitation of oxides at the grain boundaries.

Nitrogen increases the transition temperature at a lower rate. Carbon in small concentrations weakens the detrimental effect of oxygen but at a high content has the same effect as oxygen. Thus, to improve the ductility properties of molybdenum, it is necessary to reduce the amount of the impurities, especially those mentioned previously.

Electron beam melting with an intermediate container (EBMIC) is an efficient method of reducing the impurity content [6]. In comparison with vacuum arc remelting, this method has a number of advantages. Whilst in vacuum arc remelting the removal of the impurity-saturated vapour phase from the refined surface of the ingot is screened by

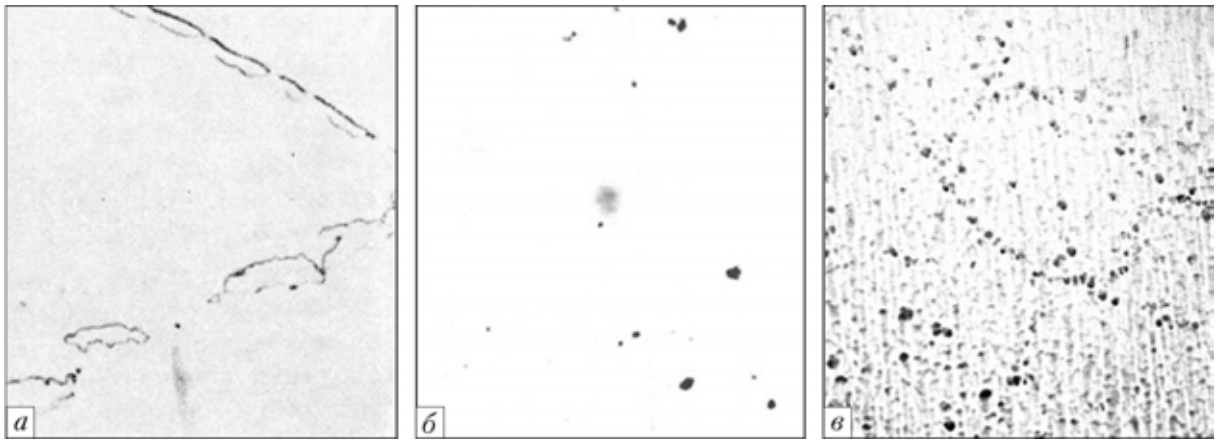

Fig. 1. Oxide and carbide inclusions in molybdenum ingots: a) vacuum arc remelting [4], × 2000; b) EBMIC, × 1000; c) EBMIC ,electrolytic etching, × 500.

the consumable electrode, the intermediate container not only increases the evaporation surface of the impurities and also increases the efficiency of evaporation as a result of free pumping of the vapour phase from this surface.

In addition, EBMIC makes it possible to keep the molybdenum the melt in the intermediate container for almost unlimited time at a temperature 50–100°C higher than the melting point. This cannot be achieved in vacuum arc remelting because of the rigid connection of the holding time in the liquid phase and the melt temperature in relation to the productivity of melting.

The experimental data in [7] show that even in the case of direct electron beam remelting (double remelting) the impurity content of molybdenum is lower than in vacuum arc remelting (0.0006% of oxygen and 0.002% carbon).

The application of the intermediate container permits the use of a mechanism for the removal of nonmetallic inclusions from the molten metal in which the inclusions float on the surface of liquid metal in the intermediate container and breakup under the effect of the electron beam [8].

To investigate the effect of EBMIC on the content of impurities in inclusions in the metal of the molybdenum ingots, investigations were carried out on ingots produced by including in the melting production process the reduced molybdenum concentrate produced by Chistoe Zhelezo Company (Yerevan, Armenia) in the form of briquettes [9]. The content of the impurities in the briquettes was relatively high (0.2% oxygen, 0.005% carbon and 0.03% nitrogen), considerably higher than in the molybdenum bar is produced by conventional technology for melting of ingots [2]. This created additional difficulties in electron beam remelting.

To increase the intensity of refining, prior to melting in the intermediate container, the briquettes were placed on a watercooled bottom plate for heating and gas removal.

Efficient refining of molybdenum was ensured as a result of the high pumping rate and the residual pressure in the melting chamber (approximately $1\cdot10^{-1}...1\cdot10^{-2}$ Pa).

Molybdenum ingots with the diameter of 70 and 100 mm were produced electron beam remelting. Metallographic examination of the structure of the specimens taken from the ingot was carried out in a Neophot-32 optical microscope, magnification 100–1000. The polished surfaces of the sections, treated by electrolytic etching, showed inclusions with the size of 0.15–2.0 μm, uniformly distributed on the surface of the section, including at the grain boundaries (Fig. 1, 2, Table 1). The inclusions had a regular circular shape, the elongation coefficient did not exceed 2.

These special features of the structure were accompanied by a decrease of HV hardness of the ingot (1400...1550, in comparison with 1760...1800 MPa for the metal of the ingots produced by vacuum arc remelting).

The impact toughness of the specimens of the ingots was determined at the Ya.E. Osada Scientific and Research Tube Institute. The dependence of Mesnager-type specimens on the test temperature showed that the cold brittleness threshold for the molybdenum produced by EBMIC is in the range 100–200°C (Fig. 3).

Preliminary tests of hot-deformed tubular blanks carried out on the microspecimens with the diameter of 1 mm showed a large increase of the ductility of the paste metal in comparison with the extruded molybdenum bar is produced from the metal prepared by conventional powder technology [10]

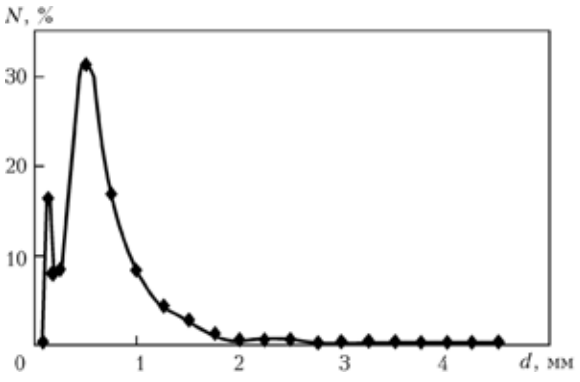

Fig. 2. The curve of the size distribution of the inclusions (in percent of the total number N).

Table 1. The size distribution of nonmetallic inclusions

Size of inclusions, μm	Number of inclusions	Mass fraction of inclusions,%
0.10	0	0
0.15	76	15.96639
0.20	38	7.983193
0.25	40	8.403361
0.50	151	31.72269
0.75	80	16.80672
1.00	39	8.193277
1.25	20	4.201681
1.50	13	2.731092
1.75	5	1.050420
2.00	2	0.420168
2.25	3	0.630252
2.50	3	0.630252
2.75	0	0
3.00	0	0
3.25	2	0.420168
3.50	0	0
3.75	0	0
4.00	0	0
4.25	0	0

(Fig. 4). The figure shows that the EBMIC method reduced the temperature of transition to the ductile state.

It is promising to increase the carbon content of the EBMIC ingots whilst maintaining the resultant dimensions and the shape of the inclusions for the application of the mechanism of high temperature heterogenisation [11].

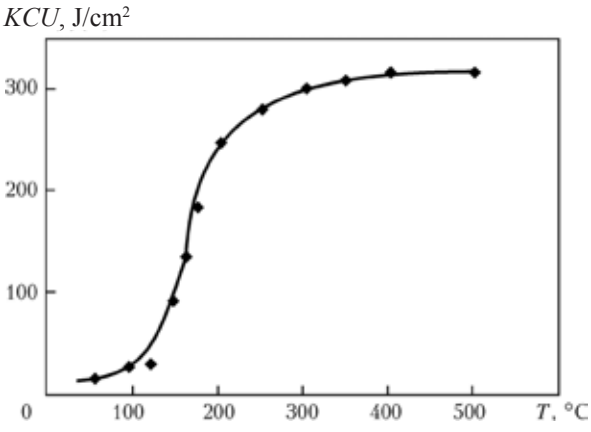

Fig. 3. Dependence of the impact toughness of EBMIC molybdenum on test temperature.

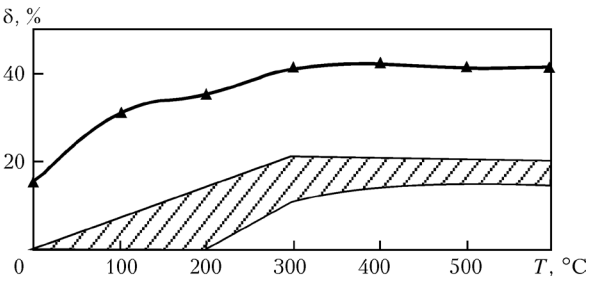

Fig. 4. Dependence of the relative elongation of the molybdenum specimens on test temperature *T* (crosshatched region – molybdenum powder bars [10]; solid line – sleeves produced from EBMIC molybdenum).

Conclusions

1. The experimental results show that EBMIC is an efficient method of refining molybdenum to remove harmful impurities. The mass fraction of oxygen and carbon is respectively 0.0006 and 0.002%.

2. The carbide and oxide inclusions in the molybdenum ingots, prepared by EBMIC, are characterised by the size which is approximately 10 times smaller than the size of the inclusions in the ingots produced by vacuum arc remelting, and also the configuration similar to the spherical, with the uniform distribution in the body of the grain.

3. It has been established that after EBMIC molybdenum shows high plasticity in comparison with the molybdenum produced by conventional methods.

References

1. Tawsing S.H., Molybdenum powder, IL, Moscow, 1962.
2. Zelikman A.N., Molybdenum, Metallurgiya, Moscow, 1970.
3. Smelyanskii M.Ya., et al., Arc vacuum furnaces and the electron melting systems, Metallurgizdat, Moscow, 1962.
4. Timmons G.A. and Neynlingr.G., Arc melting of molybdenum, in: Molybdenum, IL, Moscow, 1962, 28–42.
5. Trefilov V.I., et al., Physical fundamentals of the strength of refractory metals, Naukova Dumka, Kiev, 1975.
6. Paton B.E., et al., Electron beam melting, Naukova Dumka, Kiev, 1997.
7. Zaboronok G.F., et al., Electron beam melting of metals, Metallurgiya, Moscow, 1965.
8. Paton B.E., et al., Electron beam melting of titanium,

Naukova Dumka, Kiev, 2006.
9. Paton B.E., et al., Sovremen. Elektrometall., 2006. No. 4, 26–28.
10. Ershov I.O. and Manegin Yu.A., Metalloved. Term. Obrab. Met., 1999, No. 2, 106–109.
11. Movchan B.A., et al., Electron beam melting and refining of metals and alloys, Naukova Dumka, Kiev, 1972.

Advances in Electrometallurgy 2010 **8** *(2) 114–119*
Translated from Sovremennaya Elektrometallurgiya 2010 **8** *(2) 29–33*

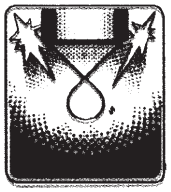

PLASMA ARC TECHNOLOGY

Preliminary deoxidation of chromium steels melted in plasma arc furnace with accumulative hearth

V.R. Burnashev and V.A. Shapovalov

E.O. Paton Electric Welding Institute, Kiev

The optimal addition of aluminium in the period of preliminary deoxidization of the studied steels is defined. It is recommended for 05Kh12N2M and 07Kh12NMFBR steels to add 2 kg/t of lumpy aluminium, while for 05Kh14N15M3Ts steel – 3 kg/t. It was established that the increase of consumption of aluminium in the period of preliminary deoxidization higher than the specified one leads to deterioration of the service characteristics of the investigated steels.

The corrosion-resisting steels 05Kh12N2M, 07Kh12NMFBR (with the chromium content of 12%) and 05Kh14N15M3Ts (the chromium content 14%), Table 1, are designed for the manufacture of tubular systems of boilers, valves and other closing equipment, working at high temperatures.

The most suitable deoxidation element for the investigated steels is aluminium. The residual amount of aluminium in 05Kh12N2M and 07Kh12NMFBR steels should not exceed 0.15%. A higher aluminium content of the finished metal may result in the formation of thermal brittleness and cracking in welding. In deoxidation with aluminium, the alumina inclusions are removed from the steel to a sufficiently high extent [1–4]. For example, at mass fractions of 0.05...0.2% oxygen and 0.02...0.8% of aluminium, the amount of alumina in the completed steel was on aver-

Table 1. Chemical composition of the investigated materials

Material	Mass fraction of elements, %											
	Mn	Cr	Ni	Mo	Nb	V	Si	C	S	P	N	
							No more than					
05Kh14N15MZTs	1.4–1.7	13.0–15.0	14.0–16.0	2.0–3.0	—	—	0.30	0.05	0.02	0.025	0.03	
07Kh12NMFBR	0.3–0.8	11.5–13.0	0.8–1.3	0.8–1.0	0.1–0.2	0.1–0.2	0.20	0.05–0.08	0.02	0.020	0.03	0.1
05Kh12N2M	0.3–0.8	11.5–13.0	1.4–2.0	0.8–1.0	—	—	0.17–0.37	0.05	0.02	0.020	0.03	0.1

Comment. Iron – balance

age 0.01, and 60–90% was removed.

At the excess of oxygen in the steel and insufficient amount of aluminium as a result of the exothermic nature of the oxidation reaction of aluminium and local superheating of the metal, liquid nonmetallic inclusions may form in the steel. In the solidified metal, the inclusions are detected in the form of globules, containing iron oxide and alumina. In the presence of an excess amount of aluminium, fine solid inclusions form in the metal and it is difficult to remove these inclusions from the still bath. It is therefore very important to know the optimum amount of aluminium, introduced in the preliminary deoxidation period [1].

The most favourable period for the preliminary deoxidation of metal with aluminium melted in the plasma furnaces with the ceramic crucible is the end of melting.

Approximate thermodynamic calculations were carried out to determine the optimum consumption of aluminium in the process of preliminary deoxidation of chromium steels. Calculations were carried out using the procedure described in [5]. An iron alloy, containing 12–14% of chromium, was investigated.

The equilibrium constant of the deoxidation reaction of the steels was determined using the following equation:

$$\lg k_{[O],\,Al_2O_3} = -\frac{21114}{T} + 6.836 - \lg f_O^{Cr} - \frac{2}{3}\lg f_{Al}^{Cr}, \quad (1)$$

where $-\frac{21114}{T} + 6{,}836$ is the constant of the deoxidation reaction of iron with aluminium [5]; $\lg f_O^{Cr}\ \frac{2}{3}\lg f_{Al}^{Cr}$ are the terms taking into account the effect of chromium on the coefficient of activity of oxygen and aluminium, respectively.

The concept of the 'parameter of interaction' e_i^j was introduced to take into account quantitatively the effect of the content of the component *i* on the coefficient of activity of element in [6]

$$\lg f_O^{Cr} = e_O^{Cr}[Cr,\%],$$
$$\lg f_{Al}^{Cr} = e_{Al}^{Cr}[Cr,\%],$$

After substituting the interaction parameters into the equation (1) we obtain

$$\lg k_{[O],Al_2O_3} = -\frac{21114}{T} + 6.836 - \\ -e_O^{Cr}[Cr,\%] - \frac{2}{3}e_{Al}^{Cr}[Cr,\%]. \quad (2)$$

The parameters of interaction e_i^j of the first order for diluted solutions in iron were taken from [4, 6–8].

The minimum oxygen content and the optimum amount of the deoxidation element (aluminium) were determined using the equations presented in [5]:

$$\lg[O]_{min} = 0.713\lg k_{[O],R_2O_3} - \\ -\frac{1812}{T} + 1.065 - 0.475\lg A_R; \quad (3)$$

$$\lg[R]^* = 0.431\ \lg k_{[O],R_2O_3} + \\ +\frac{2718}{T} - 1.168 + 0.713\ \lg A_R, \quad (4)$$

where A_g is the atomic mass of the deoxidation element.

The expressions (2)–(4) were used to calculate the values of $\lg k_{[O],Al_2O_3}$ $[O]_{min}$ and [R]*. The calculated results are presented in Table 2.

The results of calculations were used for plotting the polytherms of the solubility of oxygen in the investigated steels and the graphs of the dependence of the minimum oxygen content on the chromium content of the steel.

Analysis of the solubility polytherms of oxygen (Fig. 1) shows that for the investigated chromium steels, the solubility of oxygen increases with increasing temperature. It was also found that an increase of the chromium content increases the mass fraction of oxygen (Fig. 2). This is in agreement with the experimental results published in [9].

The optimum addition of aluminium in the process of preliminary deoxidation according to the calculations for the chromium steels 05Kh12N2M and 07Kh12NMFBR is in the

Table 2. Thermodynamics of deoxidation of investigated steels with aluminium

Temperature	05Kh14N15MZTs			07Kh12NMFBR			05Kh12N2M		
	Deoxidation constant $\lg k_{[0].Al2O3}$	Optimum Al consumption [R]*. kg/t	Miximum oxygen content $[O]_{min}$. ppm	Deoxidation constant $\lg k_{[O].Al2O3}$	Optimum Al consumption [R]*. kg/t	Miximum oxygen content $[0]_{min}$. ppm	Deoxidation constant $\lg k_{[0].Al2O3}$	Optimum Al consumption [R]*. kg/t	Miximum oxygen content $[O]_{min}$. ppm
1723	–5.121	1.69	0.4809	–5.048	1.82	0.5425	–5.114	1.70	0.4867
1773	–4.784	2.13	0.8956	–4.713	2.29	1.007	–4.777	2.15	0.9062
1823	–4.465	2.65	1.612	–4.396	2.84	1.807	–4.458	2.67	1.6310
1873	–4.164	3.26	2.812	–4.096	3.49	3.142	–4.157	3.28	2.8440
1923	–3.878	3.97	4.765	–3.812	4.24	5.309	–3.871	3.99	4.8170

range 2–2.6 kg/t (Table 2). For the 05Kh-14N15M3Ts steel it is in the range 2–2 kg/t.

In the actual conditions of plasma arc skull melting it is not possible to reduce the oxygen concentration to the given calculated values because of the of interaction of the metal with the lining, the slags, and the metal jet in casting in air.

The results of calculations were taken into account in producing a series of experimental melts of chromium steels. The studies to determine the optimum conditions of the oxidation of the special steels were carried out in a plasma arc furnace with alternating current with a UPK-50 ceramic crucible [10, 11].

The melts of the investigated materials were produced in argon at an excess pressure of 290 Pa. Argon for the melts was of the A grade (GOST 10157–79). The mass fraction of the impurities in argon, according to this standard, is as follows: no more than 0.006% nitrogen; no more than 0.0007% of oxygen; the moisture content at a temperature of 290 K and a pressure of 101 kPa is 0.007 g/m^3.

In melting the steel in basic furnaces, the basic slag was produced using limestone and fluorspar. The most important component of the slag mixtures is limestone CaO. The freshly dehydrated limestone is also used to melt the high-quality steel. Fluorspar CaF_2 is used for diluted high-basicity slags. The application of CaF_2 makes it possible to dilute high-basicity slags without reducing their basicity. This is very important for the effective removal of sulphur. Al_2O_3 is used in the melting stainless steels to diluted high-density magnesial slags.

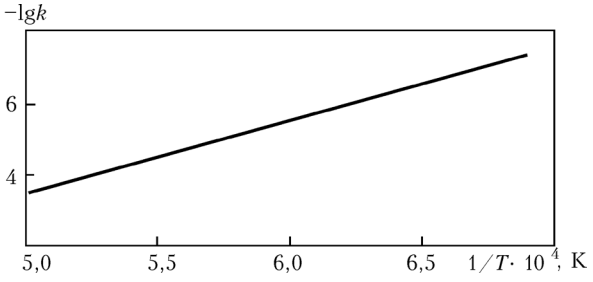

Fig. 1. Polytherms of solubility of oxygen in the investigated steels.

Thus, the charge was supplied starting with loading of the flux on the baseplate in the amount of 2 wt.% of the mass of the charge. In melting 05Kh15N15M3Ts and 05Kh12N2M steel, the flux contained 75% CaO and 25% CaF_2, and when melting 07Kh12NMFBR steel it was 45% CaO, 30% Al_2O_3 and 25% CaF_2. The mass of the charge was 10–25 kg.

During melting, after forming the pool, aluminium pieces were introduced in the amount of 0–3 kg/t. Samples of metal were taken in 5 minutes intervals by sucking into quartz tubes. This was accompanied by measurement of the temperature of the metal by the contact method using VR20/5 thermocouple (tungsten–rhenium) with a diameter of 0.35 mm with the protection of the junction by a boron carbide sheath. The pool temperature was maintained on the level of the optimum calculated temperature (1530–1550°C).

In measuring the temperature to protect the metal against contact with the external atmosphere, argon was blown through an orifice. KSP-4 recording device was used as a secondary device and the readings of the device were converted using the calibration tables [12]. The measurement error was ±20°C.

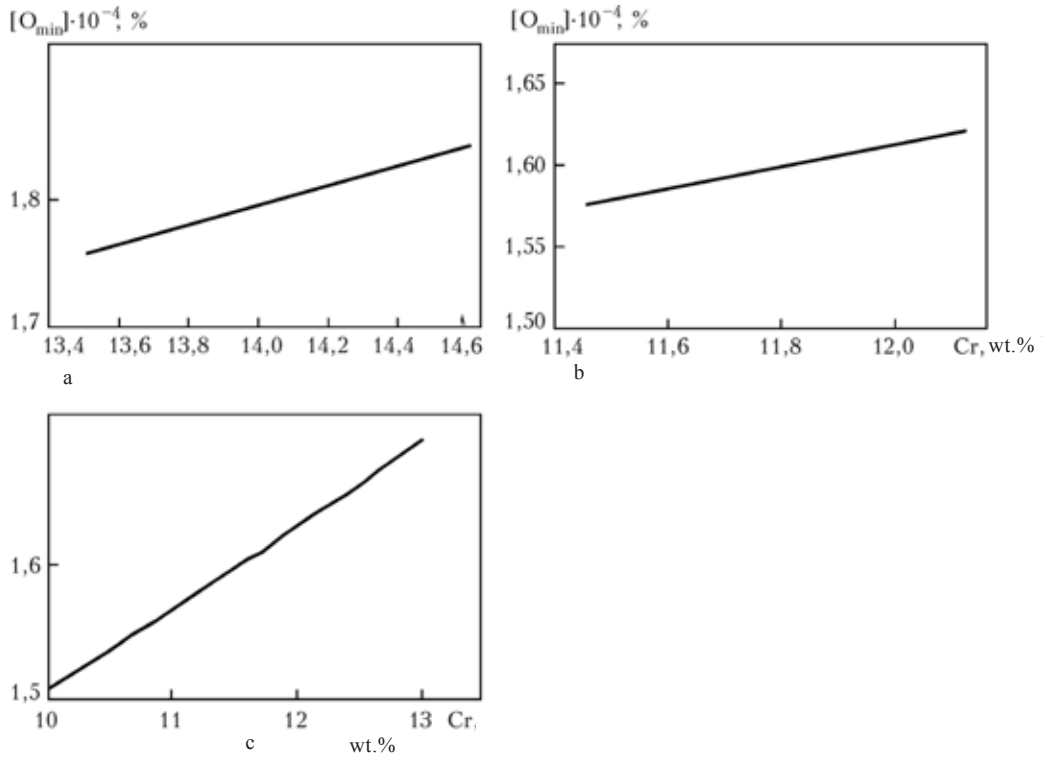

Fig. 2. Variation of the mass fraction of oxygen in relation to the chromium content of the investigated steels: a) 05Kh-14N15M3Ts; b) 05Kh12N2M; c) 07Kh12NMFBR.

The metal was poured by tilting the furnace. The metal was discharged through the discharge orifice into a copper mould. Argon was used for protecting the metal stream in pouring against secondary oxidation.

The produced ingots were forged into sheets and bars, heat treated, and specimens were produced for the determination of the oxygen content, and the microsections and specimens for the electrochemical precipitation of non-metallic inclusions.

The experimental results (Fig. 3, 4) shows that the variation of the consumption of aluminium in the period of preliminary deoxidation of the investigated steels in the range 1–3 kg/t increases the rate of removal of oxygen and also the degree of refining of metal to remove oxygen. The degree of contamination of the metal with the oxide inclusions decreases, as indicated by the results of metallographic analysis (Table 3).

It should be mentioned that the decrease of the mass fraction of oxygen takes place mainly in the initial melting period. The further decrease of the oxygen content with time is very small.

When the consumption of aluminium in the preliminary deoxidation period is increased above 3 kg/t the degree of refining of the melt tends to decrease. This is associated with the effect of aluminium on the oxygen activity coefficient.

Metallographic evaluation of the quality of the produced metal shows that the minimum contamination with the oxide inclusions (Table 3) for the 05Kh12N2M and 07Kh12NMFBR steels was detected after adding 2 kg/t of aluminium in the preliminary deoxidation period. In the case of the 05Kh14N15M3Ts steel this minimum is obtained at a consumption of 3 kg/t. The residual aluminium content in the completed metal is in the range 0.08–0.15 and 0.24%. The contamination of the non-metallic inclusions did not exceed number 3 on the contamination scale. The deformation properties of the steel were satisfactory [13].

With the increase of the consumption of aluminium to 2 kg/t the mechanical properties of

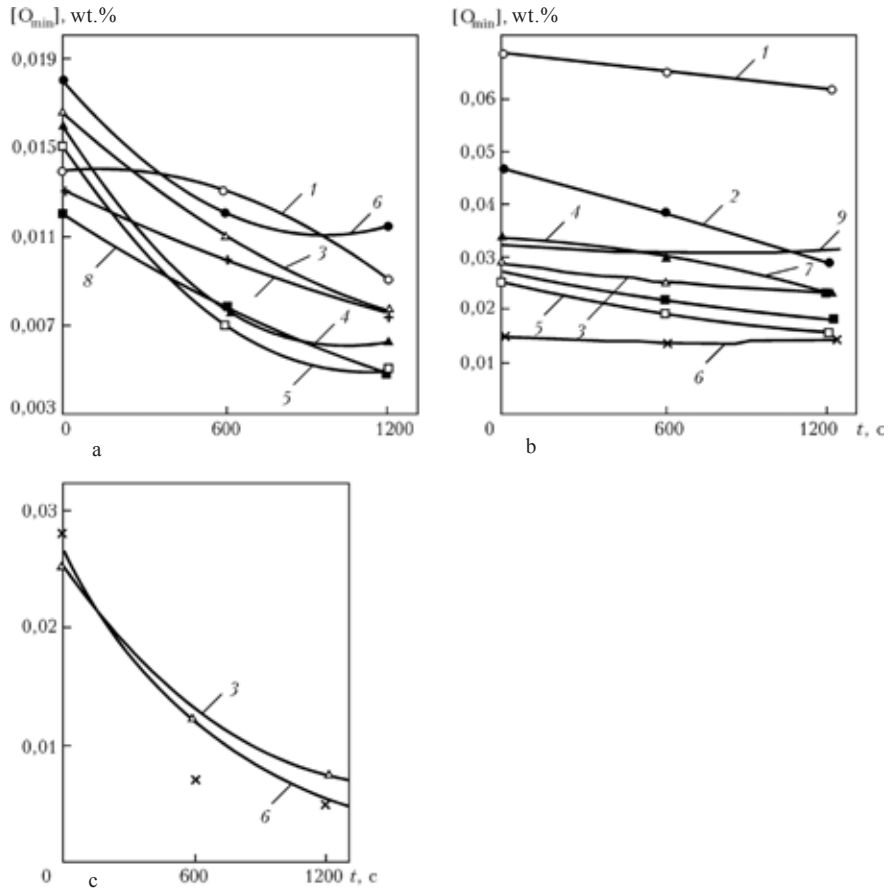

Fig. 3. Variation of the oxygen content with time in relation to the consumption of aluminium in the heat of preliminary deoxidation of the investigated steels, kg/t; a) 07Kh12NMFBR; b) 05Kh12N2M; c) 05Kh14N15M3Ts; 1) 0; 2) 0.5; 3) 1; 4) 1.5; 5) 2; 6) 3; 7) 3.5; 8) 4; 9) basic technology.

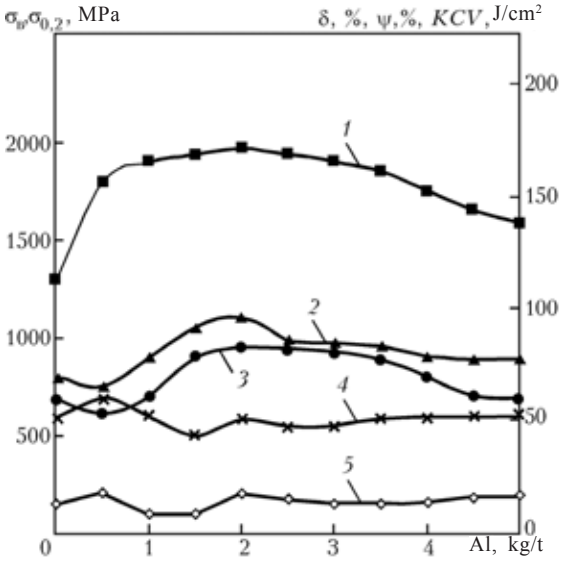

Fig. 4. Dependence of the mechanical properties of 05Kh12N2M steel on the consumption of aluminium in the preliminary deoxidation period: 1) KCV; 2) σ_B; 3) $\sigma_{0.2}$, 4) ψ; 5) δ.

05Kh12N2M steel improved. A further increase of the consumption of aluminium to 5 kg/t reduces the mechanical properties by 20–30%.

It should be mentioned that the results of approximate calculations and experiments carried out to determine the optimum conditions of aluminium are quite similar.

On the basis of the experimental results it is possible to, and the following optimum deoxidation conditions with aluminium: for the 05Kh12N2M and 07Kh12NMFBR steels preliminary 2 kg/t, final 0.5 kg/t; for 05Kh14N15M3Ts steel preliminary 3 kg t, final 0.5 kg/t.

References

1. Burnashev V.R., et al., Selection of the optimum deoxidation conditions of chromium steel is produced by plasma melting, Sudostroit. Prom. Ser. Metalloved. Metallurgiya, No. 8, 1988, 43–47.
2. Braun M.P., Microalloying of steel, Naukova Dumka,

Table 3. Effect of the deoxidation conditions on the gas content and the content of nonmetallic inclusions in the investigated steels

Material	Consumption of deoxidation agents, kg/t				Residual gas content, wt.%		Degree of refining of metal, %		Oxide inclusions, vol.%	Total content of nonmetallic inclusions, wt.%
	Preliminary		Final							
	Al	Mn	Al	Zr	[O]	[N]	[O]	[N]		
05Kh1415MZTs	1.0	15	0.5	5	0.0080	0.0130	72	46	0.043	0.0069
	2.0	15	0.5	5	0.0030	0.0120	87	Not determined	0.012	0.0042
	3.0	15	0.5	5	0.0060	0.0160	64	35	0.016	0.0035
05Kh12N2M	1.0	15	0.5	—	0.0180	0.0270	45	35	0.339	0.0200
	2.0	15	0.5	—	0.0140	0.0240	48	30	0.151	0.0150
	2.5	15	0.5	—	0.0160	0.0380	43	38	0.169	0.0190
07Kh12NMFBR	1.0	15	0.5	—	0.0055	0.0078	51	63	0.058	0.0100
	2.0	15	0.5	—	0.0052	0.0190	62	46	0.058	0.0149
	3.0	15	0.5	—	0.0078	0.0080	57	58	0.055	0.0084

Kiev, 1988.
3. Smirnov N.A. and Kudrin V.A., Refining of steel by blowing with powders in the furnace and the ladle, Metallurgiya, Moscow, 1986.
4. Povolotskii D.Ya., Deoxidation of steel, Metallurgiya, Moscow, 1972.
5. Kulikov I.S., Deoxidation of metals, Metallurgiya, Moscow, 1975.
6. Vagner K., Thermodynamics of alloys, Metallurgiya, Moscow, 1957.
7. Averin V.V., et al., Theoretical fundamentals of electric steel melting processes, Metallurgiya, Moscow, 1979.
8. Grigoryan V.A., et al., Physical–chemical fundamentals of deoxidation of steel, Metallurgiya, Moscow, 1979.
9. Samarin A.M., Physical–chemical fundamentals of deoxidation of steel, Academy of Sciences of the USSR, Moscow, 1956.
10. Latash Yu.V., et al., Spets. Elektrometallurgiya, 1987, No. 63, 66–70.
11. Latash Yu.V., et al.,ibid,1989, No. 68, 77–84.
12. Danilevskii S.K. and Svede-Shved N.I., High-temperature thermocouples, Moscow, Metallurgiya, 1979.
13. Burnashev V.R, et al., Quality of deformed Cr steels produced by plasma melting, Proc. Kramatorsk, 2002 390–393.

Advances in Electrometallurgy 2010 ***8*** *(2) 120–127*
Translated from Sovremennaya Elektrometallurgiya 2010 ***8*** *(2) 34–39*

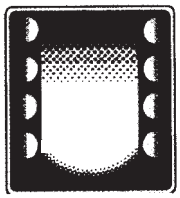

VACUUM INDUCTION MELTING

Intensification of molten metal flows in the liquid pool in induction heating

A.S. Pis'mennyi, V.M. Baglai, A.A. Pis'mennyi and S.V. Rymar

E.O. Paton Electric Welding Institute, Kiev

The conditions of intensification of microflows of molten metal directed to the surface being treated are defined to organize the fluid metallic working tool for treatment of metallic bodies due to a specific arrangement of the inductor as regards the molten metal pool, optimizing of the ratios of the inductor dimensions, heater casing and lining of the operating space of the induction heater by refractory material.

In surfacing of parts of worn components, and also surfacing the surface of the blanks for projecting elements, local remelting of the surface layer of metallic components, the optimum method of the removal of defects or local alloying of the surface layer is, in addition to the electrometallurgical surfacing technologies, the technology based on induction heating [1–8] offering new possibilities in the production and repair of components.

The extensive application of induction heating for these applications has been delayed by the high consumption of electric energy. Therefore, it was important to develop a method with the reduced electric energy consumption. The studies in this direction are also important because of the fact that induction heating is the ecologically efficient method.

One of the methods of reducing the energy consumption in induction heating is the intensification of molten metal flows in the liquid pool because this is accompanied by the increase of the intensity of heat exchange between the already molten metal and the metal to be melted. This shortens the melting time and the applied power. The development of the method of intensification of molten metal flows in the liquid pool is also the subject of the present work.

The E.O. Paton Electric Welding Institute, Kiev has developed a method which creates suitable conditions for intensification of the macroflows of molten metal in the central part of the liquid pool directed to the process the surface of the metallic component in induction heating. This is achieved by optimising the ratio of the dimensions of the induction coil and the body of the heater, lining the induction heater with a refractory material, selection of the shape of the crucible, covering the surface of the metal with the refractory cover and, most importantly, special position of the induction coil in relation to the heated component.

To fulfil this task, investigations were carried out to develop a special method of

calculating the induction coil–heated component system which would make it possible to simulate electromagnetic processes taking place in the system. The method is based on the stationary movement of the liquid along the closed trajectories situated inside the geometrically single-connected region, under the effect of the vortex field of the volume forces [9].

The density of electromagnetic forces, acting on the electrically conducting liquid, contains the vortex and potential components. The ratio between these components in the individual points of the volume of the liquid differs. Only the vortex component of the electromagnetic forces excites the movement of the liquid.

By analogy with certain types of induction melting furnaces ('cold crucibles'), the proposed method uses the principle of transfer of the energy of the alternating electromagnetic field through the metallic wall consisting of the individual parts (sections) electrically insulated from each other [6].

In conventional induction furnaces, the induction coil is placed in the deposition in which it completely or partially affects the pool of molten metal, and the end part of the coil do not project outside the limits of the pool (Fig. 1).

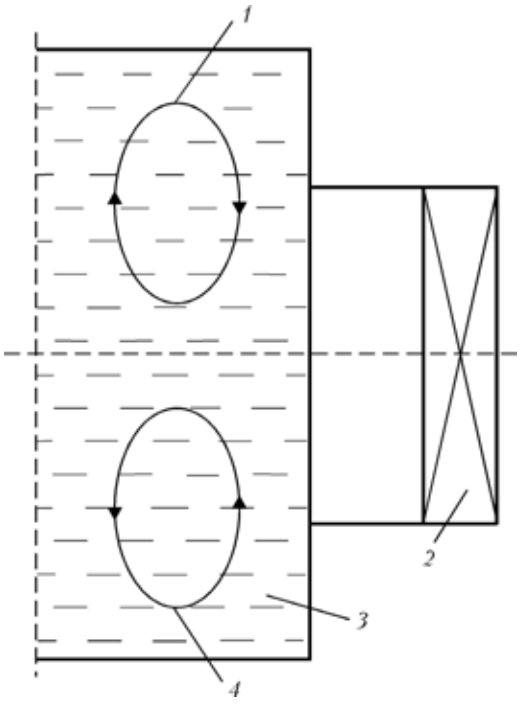

Fig. 1. Diagram of moment of macroflows of liquid metal in induction heating: 1) upper vortex; 2) induction coil; 3) melt; 4) lower vortex.

Figure 1 shows part of the molten metal pool and part of the induction coil, distributed in relation to the vertical axis of symmetry. Two zones of the vortex electromagnetic forces form in the investigated part of the pool. The zones formed closed macro flows of molten metal (upper and lower), moving in the direction of these forces and having the opposite directions [5–7].

The intensity of movement of the macroflows of molten metal depends on the hydraulic resistance and the shape of the crucible. In the absence of mechanical obstacles, the region of the metal, affected by movement, may extend far outside the limits of the zone of vortex forces, causing movement of the flows. For this position of the induction coil on the vertical axis of symmetry the macroflows in the lower part of the pool are directed downwards, and those in the upper part of the pool are directed upwards with the formation of a convex section on the surface of molten metal.

In the case of different intensity of the two vortex zones of the force field, the boundary of the vortex speed is displaced into the side of the zone with the less intensive circulation of molten metal. In the presence of the asymmetric hydraulic boundary conditions, the speed field is also deformed, underlying separating the vortices is displaced in the direction of the vortex with more constricted movement conditions. The volume of the macroflow of molten metal, circulating in the zone with the lower intensity of circulation of the melt or situated in the constricted conditions, decreases, and the volume of the macroflow in the second zone increases (in comparison with the symmetric case).

The asymmetry of the force field may be caused also by the nonuniformity of the gap between the induction coil and the liquid metal pool, the nature of distribution of the density of the macroflow in the induction coil,

the displacement of the crucible in relation to the induction coil, and the shape of the crucible. For example, when using a conical crucible (in a cylindrical induction coil), the maximum magnetic induction is displaced into the region with a smaller gap (a wide part of the crucible). This increases the relative value of the intensity of circulation of the melt and the length of the vortex zone of the force field, acting in the narrow part of the system. On the other hand, the hydraulic conditions are more favourable in the wide part of the crucible. This is confirmed by the experimental data, presented in [3], which indicates that the resultant effect of the conicity of the crucible on the movement of the melt is not strong.

The molten metal flows may be used as the liquid metal working tool for the treatment of metallic components. In this case, the crucible with the orifice in the lower part is placed on the treated component. The macroflows of molten metal in the crucible treat the component, depositing it with metal, melting the metal or welding to it the metal located in the crucible.

To ensure more efficient application of the macroflows of liquid metal formed in the crucible for the treatment of metallic components, it is necessary to intensify the macroflows of molten metal of the liquid pool in the direction of the vertical axis of symmetry of the crucible towards the treated component.

The most intensified movement of the molten metal macroflows is observed in the case in which only one vortex zone of the force field exists in the volume of the melt of one part of the crucible in relation to the vertical axis of symmetry. Consequently, only one macroflow forms. The entire energy of the magnetic field of the induction coil forms a single powerful macroflow, instead of two macroflows, formed in the conventional furnaces.

This movement of the macroflows can be generated in melting on a bottom skull or in the liquid pool during the process of solidification of the ingot in induction furnaces with the cold crucible or in the electromagnetic solidification mould.

The most efficient technological parameters and efficiency update with the induction coil in the position in which the asymmetry of the induction coil–crucible electromagnetic system in the hydrodynamic boundary conditions ensures the suppression of one vortex circuit by another.

This method was developed at the E.O. Paton Electric Welding Institute, Kiev. It is based on the mutual displacements of the induction coil in which both the lower and upper circuits can be suppressed. To intensify the suppression of the upper circuit, the bottom of the crucible can be rounded.

To suppress the upper macroflows of molten metal, the induction coil must be displaced upwards to the distance in which the horizontal axis of symmetry of the induction coil coincides with the upper edge of the molten pool metal (Fig. 2). In this case, the molten metal macroflows in the central part of the pool in the crucible are directed downwards, to the bottom of the crucible. A concave region (not a meniscus-shaped convex region) forms on the surface of molten metal. The convex sections are situated in the vicinity of the crucible walls.

This effect was detected for the first time in the experiments with the displacement of the induction coil in relation to the crucible

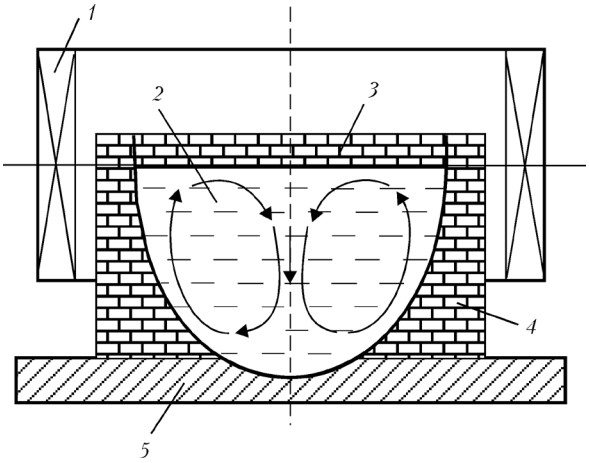

Fig. 2. Diagram of movement of the macroflows of liquid metal in treatment of components: 1) induction coil; 2) the melt; 3) the cover; 4) the crucible; 5) the component.

in the direction of height. To investigate this effect, theory was proposed at a calculation method developed which makes it possible to simulate the distribution of the electromagnetic field of the induction coil on the surface of the melt using the impedance boundary conditions [9].

The experimental results show that the process of the component using the liquid metal flows, directed downwards along the vertical axis of symmetry of the crucible, the most efficient crucible has the form of a cone or a paraboloid of rotation, with the open narrow lower part resting of the component to be treated (Fig. 2).

The investigations of the model of the vortex movement of the liquid metal carried out in [6] yielded important results showing that the tangential electromagnetic forces are of secondary importance for the circulation of the metal in the conventional classic furnaces (less than 3% contribution to the circulation of the melt). The main contribution is provided by the normal forces, determined by the electromagnetic pressure of the field of the induction coil on the metal.

The strength of the radial component of the magnetic field of the induction coil in the classic deposition is equal to 0 in the plane of symmetry of the induction coil along its axis and remains the same on the axis of the induction coil, irrespective of the distance between the observation point and the centre of the induction coil [7].

In any other plane, parallel to the plane of symmetry of the induction coil, the strength of the radial component of the magnetic field increases from 0 to the maximum value in the vicinity of the turns of the induction coil and subsequently decreases with increasing radius of the coil. Therefore, the electromagnetic pressure, determined by the strength of the radial component of the magnetic field, increases from zero at the axis of the crucible with the melt to the maximum at the edge of the crucible, exciting the moment of the melt along the crucible wall downwards, and along the axis of the crucible upwards.

This direction of movement of the melt, used as the working tool for the treatment of the components situated in the lower part of the crucible, is detrimental. To suppress this movement to the maximum extent, it is necessary to combine the surface of the melt with the plane of symmetry of the induction coil along its height.

In the vicinity of this plane, the electromagnetic pressure on the melt is exerted also by the forces are directed from the side surface to the axes of the crucible and associated with the axial component of the strength of the magnetic field. Since the axial component of the strength of the magnetic field and the strength of the electrical field have the highest values, the electromagnetic forces will be of the same magnitude. In particular, these forces caused the formation of the axial flows of the metal in the crucible directed in the upper part of the crucible upwards with the formation of a meniscus, and in the lower part of downwards with the formation of the metal jet essential for the treatment of the component.

It is evident that to suppress the upper vortex in the crucible it is necessary (in addition to the proposed method) to place the crucible in the induction coil in deposition in which the upper surface of the melt is on the level of the plane of symmetry of the induction coil in the direction of its height. It is convenient to restrict mechanically the possibility of movement of the melt in the upper circuit, for example, by placing a restricting wall in the plane of symmetry of the induction coil on the surface of the melt. The wall has the form of a cover preventing lifting of the metal which forms and avoidably as a result of compression of the melt by the forces determined by the effect of the axial component of the strength of the magnetic field.

In addition, to reduce the relative value of the radial component of the magnetic field in the zone of the crucible, it is convenient to use the induction coil with the axial length not smaller than the diameter of the crucible.

To test the specimens of induction heaters, experiments were carried out with a device

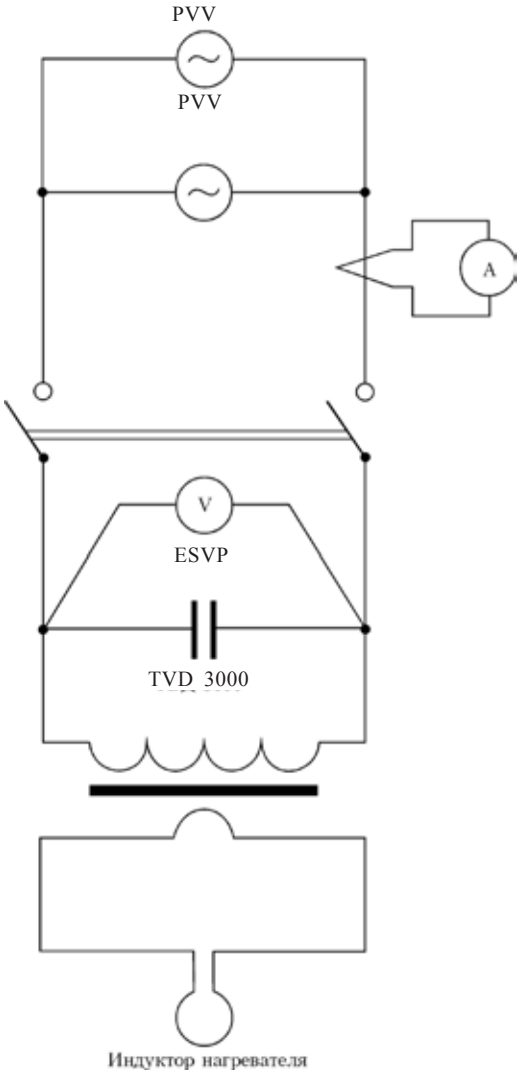

Fig. 3. Power source for the equipment.

which included two frequency converters PVV with a power of up to 100 kW, frequency 8 kHz, a TVD 3000 transformer, used for quenching components in the condensers ESVP 800/1000.

The condensers were connected parallel to the primary winding of the transformer (Fig. 3), and the total capacitance of the condensers was 26.6–29.2 μF. The transformation coefficient was equal to 5, the maximum voltage in the induction coil was 160 V. Equipment A550 was used for moving the heater with the molten metal in relation to the induction coil.

The proposed method of calculating the induction coil was used in designing and

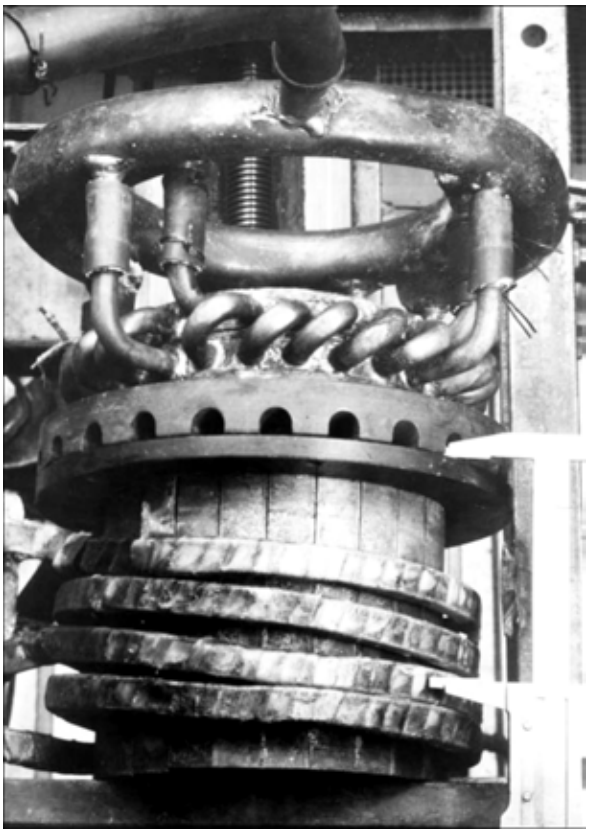

Fig. 4. The cooling part of the induction heater with the induction coil.

producing a two-winding induction coil with the height of (80±5) mm, diameter 190 mm. The conductors were produced from the copper pipes with the cross-section of 10×15 mm (Fig. 4). The windings of the induction coil were connected in parallel and were matched. This design of the induction coil has made it possible to change in a wide range of the weight of the component for melting and the position of the induction coil in relation to the molten metal. The induction coil was used in all tested heaters.

In the improved lined induction heater, the treatment of the horizontal surfaces of the metallic components was carried out by the formation of the vertical macroflows of liquid metal, directed downwards to the treated component along the vertical axis of symmetry of the induction coil. The macroflows formed after melting of the blank.

The possibilities of melting the steel component with the liquid metal macroflows and

Table 1. Main parameters of the process of melting of steel sheets

Sheet thickness, mm	Hole diameter, mm		Parameters of molten metal		Melting productivity, kg/min
	Upper	Lower	Volume, cm^3	Mass, kg	
20	65–56	38–28	45–50	0.35–0.39	1.00–1.95
40	73–65	25–20	80–100	0.625–0.780	0.39–0.42
60	110–93	30–22	240	1.88	0.48–0.38
80	130–125	15	600	4.68	0.335

the melting rate can be estimated on the basis of the penetration data for the sheets of St3sp steel, wt.%: 0.14–0.22 C; 0.15–0.30 Si; 0.40–0.65 Mn; <0.3 Ni; <0.05 S; 0.04 <P; <0.3 Cr; <0.008 N; <0.3 Cu; <0.08 As of different thickness (Table 1) produced in the experiments with melting of the blanks weighing 5.0–5.5 kg (temperature 1420–15 20°C) at the same power of the induction coil in the range (170–180 kW).

The melting time of the steel sheet in relation to the thickness was as follows:

sheet thickness, mm 20, 40, 60, 80
melting time of the sheet, min ..... 0.2–0.3; 1.5–2.0; 4.0–5.0.

The dynamic pressure of the molten metal jet, in relation to the diameter of the penetrated depression or orifice, was 100–1500 N/m^2.

To isolate the molten metal from the cooled walls of the heater and defined the dimensions of the zone of the effect of the liquid metal on the surface of the treated component, the lining was produced using a mixture of magnesite with kaolin and sand (5–10% each), mixed using water glass with water. The mixture was deposited on the melted component and dried using the induction heater. The dimensions of the lining were smaller than the dimensions of the heater and, consequently, after introducing the blank with the lining into the heater, it was possible to place dry sand in the gap between the wall of the heater and the coating ensuring the reliable thin wall lining. This lining did not fracture during long-term holding of the molten steel in it. The cracks, formed in the lining, have no effect on the technological process, and the dry sand prevented the risk of escape of molten metal, ensuring easy removal of the heater from the lining after completing heating.

Fig. 5. A steel sheet 20 mm thick with holes melted by the jet of molten steel, with the blank for melting.

Holes in the form of a funnel (Fig. 5) with the dimensions presented in Table 1 formed in the sheets below the heater. These dimensions can be recommended for melting steel components to a depth of 20, 40, 60 and 80 mm using the macroflow, formed at the frequency of the induction current of 8 kHz. However, it should be mentioned that these data can be regarded as optimum because even they resulted in arrests of the process associated with the switching of the containers, and in the experiments with a sheet 80 mm thick it was not possible to reach the

maximum power.

The experimental results show that the depth of penetration of the component depends only shape and dimensions of the blank, i.e., on the shape and dimensions of the cavity in the lining.

Figure 5 shows the solidified molten metal pool, which may be used as an example of melting the given elements on the sheet.

If the size of the orifice in the lining (refractory material) is not sufficiently large, the macroflow of molten metal maybe restricted under the heater (Fig. 6a), and if the size of the orifice is as required, but the rising macroflows of liquid metal freely leave the funnel in the treated component (Fig. 6b). This increases the depth of the funnel with other conditions being equal.

The large increase of the intensity of the macroflows of liquid metal as a result of the application of the lining was utilised in penetrating for the first time the steel sheets with a thickness of 60 and 80 mm. In melting the sheet with a thickness of 60 mm, the specific consumption of electric energy was 4 kW h per kilogram of molten steel. However, it is not possible to compare this value with a specific consumption of energy when using the heaters without the lining since the large number of experiments carried out to melt the sheet with a thickness of 60 mm using the heater without the lining have not been successful.

The experimental results show that the intensity of the steel jet depends on the position of the induction coil in relation to the surface of the treated component and the blank. For example, in the case of the 80 mm thick sheet, ridges were detected around the funnel under the heater indicating the lifting in relation to the cold steel in the direction of the perimeter of the funnel.

The experiments were carried out at the same current frequency in the induction coil (8 kHz). Therefore, the effect of frequency on the formation of the molten metal macroflows was not evaluated in the experiments. It may be claimed that the decrease of the current frequency increases the pressure of the macroflows and the efficiency of the effect of the current frequency on the treated metal. This is associated with the increase of the strength of the magnetic field of the induction coil and, correspondingly, the pressure on the liquid metal at the same power of the induction coil.

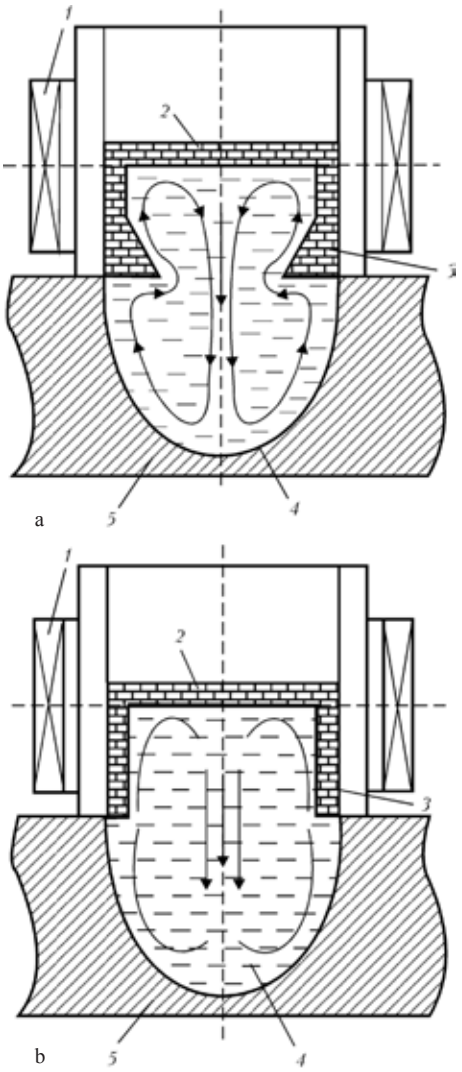

Fig. 6. Diagram of movement of the liquid metal macroflows in the refractory material for the insufficiently large (a) and normal size (b) holes; 1) induction coil, 2) the cover; 3) the crucible; 4) the melt; 5) the component.

The experiments with the investigation of the melting of the steel sheets show the extent of intensification of the macroflows of liquid metal in the given method of induction heating when they are capable of freely melting relatively thick steel sheets. However, this method is no design for producing holes in sheets. The application of the proposed

method of positioning the induction coil in relation to the molten metal pool makes it possible to save electric energy in induction heating of components (by a factor of 1.2–1.4 in comparison with the currently available methods).

It is promising to use the proposed method of induction heating for developing technologies of depositing parts of worn components, projecting elements, local remelting of the surface layer of metallic components in order to eliminate defects or carry out local alloying of the surface layer.

Conclusions

1. Analysis of the electrodynamic processes in the liquid metal, sustained on the horizontal surface of the metallic component in the field of the induction coil, shows the following conditions of the formation in the liquid metal of intensified macroflows of molten metal, directed to the component: the upper surface of the melt should be situated on the level of the plane of symmetry of the induction coil; it is recommended to use the induction coil with the axial length close to the diameter of the coil; it is recommended to prevent the formation of the upper convex meniscus of the metal as a result of the application of the restricting cover.

2. Experiments have confirmed the possibility of formation of molten metal macroflows directed from top to bottom on the vertical axis of symmetry of the induction coil on the treated component in induction heating.

3. The improved lined heater enables the macroflows of molten metal to penetrate freely of the horizontal section of the treated component to a depth of up to 80 mm.

4. The proposed ecologically efficient method of induction heating may be used for developing the technologies of depositing parts of worn components, surfacing the projecting elements, local remelting of the surface layer of metallic components in order to remove defects or carry out local alloying of the surface layer, because the proposed method is characterised by a considerably lower energy consumption in comparison with the currently available induction heating methods.

References

1. Farbman S.A. and Kolobnev I.F., Induction furnaces for melting of metals and alloys, Metallurgiya, Moscow, 1968.
2. Tir L.L., Magnitnaya Gidrodinamika, 1973, No. 3, 144–146.
3. Svilo A.V. and Tir L.L., ibid, 1973, No. 3, 144–146.
4. Fomin N.I., Determination of the parameters of the induction coil-crucible-charge system in the induction furnaces with a cold crucible, i:Investigations inthe area of industrial heating, Tr. VNIIETO,No. 7, Energiya, Moscow, 1975, 65–71.
5. Tir L.L., ibid, No. 7, 1975, 72–77.
6. Tir L.L. and Gubchenko A.P., Induction melting furnaces for the processes with improved accuracy and cleanness, Energoatomizdat, Moscow, 1988.
7. Furui M., et al., ISIJ Intern., 1993, No. 3, 400–404.
8. Gorislavets Yu.M., Induction equipment for the electromagnetic treatment of metals and alloys, Dissertation, Kiev, 1988.
9. Pis'mennyi A.S., Induction heating for welding and related technologies, E.O. Paton Electric Welding Institute, Kiev, Kiev, 2005.

Advances in Electrometallurgy 2010 **8** *(2) 128–142*
Translated from Sovremennaya Elektrometallurgiya 2010 **8** *(2) 40–51*

GENERAL PROBLEMS OF METALLURGY

Strength and microstructure of brazed joints in ZhS6U alloy, produced using boron- and boron-silicon-containing brazing alloy

A.F. Belyanin, V.V. Kurenkova, I.S. Malashenko, V.V. Grabin, V.V. Trokhimchenko and L.V. Chervyakova

Pratt and Whitney Paton Centre, E.O. Paton Electric Welding Institute, Kiev

The relationship between the microstructure of the metal of brazed joints and physical–mechanical properties of joints of alloy ZhS6U, produced using complex boron- and silicon-containing brazing alloys, in which 60 mass % of powder of alloy Rene-142 was used as a filler. It is shown that the adding of 2.4–3.0 wt% of silicon to the basic brazing alloy Ni–Co–Cr–Al–2.5 % B + Rene-142 causes changes in the morphology and amount of precipitated carbide–boride phases. The results of high-temperature brazing of cast plates of ZhS6U alloy are given, the structure of brazed joints, their strength and ductile characteristics at temperature 20°C are determined. The quality of brazed joints is 0.85…1.00 of the strength of the basic alloy. Special attention is paid to the effect of gaps on the results of mechanical tests of brazed joints of alloy ZhS6U in tensile loading.

The ZhS6U alloy is one of the most widely used creep-resisting cast nickel alloys in industry. Applications include the working and guide blades, and also the section blades of the nozzle system of the aviation turbines and energy-force equipment for different applications.

The increase of the gas temperature at entry into the turbine and the need to increase the period between repairs in service results in gradual failure of the components of the section as a result of the occurrence of structural changes in the basic material [1], formation of thermal fatigue cracks, corrosion damage, etc.

To increase the service life of the components, it is necessary to use the methods of restoration repair, carried out by brazing, since argon-arc welding of the low weldability ZhS6U alloy is difficult as a result of the cracking of welded joints caused by the high level of alloying of the alloy, in particular with aluminium and titanium.

In addition to other cast alloys, alloyed with chromium, molybdenum, tantalum, tungsten, rhenium, etc, this alloy is very difficult to weld by argon-shielded arc welding as a result of the formation of hot cracks in the heat affected zone (HAZ) and the welded joint during cooling caused by the precipitation of a large amount of the hardening γ'-phase [2, 3].

The upper limit of the working temperatures of the creep-resisting alloys (CRA) is

1050–1100°C. The softening of CRA is caused in particular by the decrease of the volume fraction of the secondary precipitates of the γ'-phase which is a result of the increase of the solubility of these precipitates in the γ-Ni-matrix and also coarsening of the particles of the γ'-phase.

The ZhS6U alloy belongs in the group of alloys with high creep strength, containing 9.5–11.0 wt.% of tungsten. Tungsten is characterised by the nonuniform distribution in the grain, the concentration of tungsten at the dendrite axis is 1.2–1.5 times higher than in the interaxial areas, molybdenum is distributed mainly at the grain boundaries and the boundaries of the primary γ'-phase.

The total amount of Al + Ti, which determine the high creep strength of the alloy, is 7.1–8.9 wt.%. The cast ZhS6U alloy has a coarse-grained heterophase structure, including the high-alloyed matrix γ-solution, the γ'-phase (boundary and hardening), the carbide and boride phases. This alloy is characterised by differences in the morphology of the hardening phase at the dendrite axis and in the interaxial regions. The volume fraction of the γ'-phase in the centre of the grain is usually 60%, with the grains of the phase being cubic. The interaxial hardening phase is spherical and the size is 2–6 times greater.

The blades of aviation engines are subjected to the effect of temperature and forces during service, and the ZhS6U alloy is subjected directly to high temperature creep. After long-term operation (5000 h) the structure of the metal of the output blade (the hot zone) remains heterophase, consisting of the (γ+γ'), carbide and boride phases [4]. Disintegration of the boundary carbide phases and the formation of continuous carbide chains has been observed.

After 4800 cycles the volume fraction of the γ'-phase rapidly decreases with increase of the size of the phase. Tungsten, being the element having the strongest effect on the creep strength of the ZhS6U alloy and the stability of the γ'-phase at the dendrite axes, takes active part during service in the reactions of carbide- and boride-formation of the compounds Me_6C and Me_5B_3.

The Me_6C particles precipitate at the primary carbides MeC as a result of breakdown of these carbides, so that the tungsten content of the γ- and γ'-phases decreases. This effect is most evident in the areas with the potentially highest service damage of the material – at the grain boundaries and intragranular precipitates MeC. The structural changes in the commercial alloy after high-temperature testing result in extensive softening [4, 5].

The nickel cast creep-resisting alloys, with different alloying systems, the variation of the morphology of the hardening phases, the degree of dispersion, and the condition of the intergranular boundaries in heat treatment differ. According to [2], the ZhS6U alloy with the equiaxed structure shows during homogenising at a temperature of 1210°C followed by cooling changes in the morphology and dispersion of the precipitates of the γ'-phase. This should increase the physical–mechanical properties of the metal.

However, this is accompanied by the formation in the structure of the alloy of the carbides with the unfavourable plate-shaped morphology Me_6C which reduce the plasticity of the metal. At the same time, in the ZhS6K alloy with a low degree of alloying, homogenising at high temperature does not lead to the formation of new phases, and the dual carbide of the type Me_6C forms in the alloy only after ageing for more than 300 h at 900°C [2, 5].

The heat treatment reduces the level of dendritic liquation in the alloy and leads to the more uniform distribution of tungsten in the dendrite axes and in intergranular spaces [5]. This is accompanied by a decrease of the degree of nonuniformity of the distribution of tungsten.

According to [6], standard heat treatment of ZhS6U alloy consists of annealing for 4 hours at a temperature of (1210±10)°C. The structure of the metal of the castings is improved by hot isostatic pressing (HIP). The strength of the ZhS6U alloy, processed by HIP is 930–950 to 1060 MPa. The plasticity (relative elongation) of the metal after HIP

is in the range 4–8%.

The decrease of the cooling rate of the blanks (together with the furnace) in the range (1200–1210) ±10°C prevents the formation of cracks, and a small increase of the size of the hardening phase increases the plasticity of the alloy. Further ageing at 900–950°C (2 h) leads to the formation of the structure with the favourable regular distribution of the particles of the γ'-phase with the size of 0.1–0.2 mm along the dendrite axes. The structure, formed by this mechanism, ensures the combination of the high long-term strength and satisfactory plasticity of the ZhS6U alloy with a minimum notch sensitivity [4, 7].

Regarding high temperature brazing has the most rational method of preparing components of low weldability ZhS6U alloy, it is necessary to take into account the combination of the brazing conditions and subsequent heat treatment with the conditions of reconditioning treatment of the alloy after service.

As a result of the high parameters of the strength of the joints, brazing is regarded as an alternative to the method of argon-arc welding of joining and restoration of the components of nickel creep resisting alloys.

Foreign scientists propose a method of reconditioning components by high temperature brazing [8–10] using an intermediate liquid interlayers. This method is interpreted as the process of diffusion brazing. The main aim of the method reduces amorphised foils as the brazing alloy is the formation of the microstructure and mechanical properties of the brazed joint is equivalent to those of the brazed alloy as a result of its long-term isothermal holding.

However, there are a number of factors restricting the application of this method in repair brazing. It is primarily the long-term temperature effect on the component which may impair the functional properties of the metal of the base and, in addition to this, amorphisation asked the method of producing brazing alloys in the form of strips restrict the possibilities of using multicomponent brazing alloy systems.

In brazing with the intermediate solid-liquid interlayer it is necessary to control efficiently the temperature of the isothermal process, the thickness of the interlayer (the width of the gap) and the composition of the brazing mixture. These factors and the interphase interaction of the weld metal and the brazed material influence the rate of isothermal crystallisation in the formation of the brazed joint in the cast nickel alloys, in particular IN-738LC and IN-718 [8-10].

The possibilities of high temperature brazing asked the method of reconditioning the components of gas turbine engines have been realised in the brazing with composite brazing alloys which makes it possible to modify the chemical composition and physical-mechanical characteristics of the produced brazed joints to get closer to those of the creep resisting alloys to be repaired. The technological special features of isothermal brazing in vacuum of creep resisting alloys of different alloying systems have been investigated in [11–14].

In this work, the brazing alloy was represented by a composition consisting of 20-melting brazing alloys - boron-containing Ni-9% Cu-14% Cr–3.5% Al–2.5% B, the silicon-containing brazing alloy with the eutectic composition Ni–12% Si (HC12), and the filler is in the form of powders of alloys Rene-142, ZhS6U and ZhS32. The binder was in the form of the imported material or the dissolution of acrylic resin in commercial acetone.

René-142 alloy is characterised by the most rational alloying system, wt.%: 6.2–6.5 Ta, 2.6–3.0 Re, 1.3–1.7 Hf, resulting in the satisfactory strengths, creep strength and heat resistance of the brazed joint. Hafnium and tantalum restrict the diffusion processes in the Ni–Cr–Cu–W–Mo–Ti–Al creep resisting systems and increase the energy of atomic bonds. They are uniformly distributed between the matrix, the ‘-phase and carbide phases. Hafnium and tantalum are included in the composition of the MeC primary carbides of the most stable modification and do not form eutectic ‘frames’ nor continuous carbide networks [15].

In this work, investigations were carried out into the possibilities of using boron-

and boron-silicon-containing brazing alloys for the repair brazing of the ZhS6U-carbon casting alloy. The results are presented of determination of the physical–mechanical properties of the brazed joints in this alloy, and the special features of repair brazing of components produced from this alloy are investigated.

Experimental data

Prior to testing the brazed joints, the mechanical properties of the ZhS6U brazed alloy were determined. The initial sheets with a thickness of 6.2 mm, produced by investment casting, were characterised by the equiaxed structure. The tensile test at 20°C was carried out on flat specimens with the cross-section of 1.7×3.0 mm, with the gauge length of (10+0.5) mm. The design special features of the specimen were described in [11].

The blanks for brazing and specimens MI-96 of the parent metal were heat-treated in vacuum. Table 1 and Fig. 1 shows the characteristics of the ZhS6U alloy used for the preparation of packets of nozzle blades for D18T engines. The sheets were homogenised at 1220°C (the temperature of complete dissolution of the γ'-phase in the solid solution) and the pressure of residual gases of $(5...7)\cdot10^{-3}$ Pa for 10 to h. Rapid cooling (approximately 20°/min) resulted in the formation of the supersaturated solution is and with the primary particles of the γ'-phase, precipitated in the matrix in cooling of the specimens with the furnace.

Annealing of the metal prior to brazing resulted in the following required service properties (Table 1): σ_T = 850 MPa, σ_B = 962 MPa, ε_T = 2.5...8.2%. According to [6], intermediate heating at 11 60°C increases the plasticity of the ZhS6U alloy after ageing (Fig. 1). The results show a decrease of the yield limit and ultimate strength with the increase of the relative elongation to 8.2%. Annealing in vacuum at 1160°C (2 h) and subsequent ageing at 900°C (4 h) increase the strength and relative elongation of the metal to ε = 7.80...8.71% at 20°C.

According to the data presented in Table 1, the ZhS6U alloy is characterised by a scatter of the strength characteristics. This is typical of the casting alloys. The highest values of σ_T and σ_B were recorded as a result of ageing of the blanks at 900°C (4 hours) after high-temperature homogenising at 1210–1200°C. The maximum yield limit of the alloy was

Table 1. Properties of the parent metal (in the tensile test) of ZhS6U alloy after different heat treatments

Heat treatment regime	Specimen No.	$\sigma_{0.2}$, MPa	σ_B, MPa	δ, %
Initial	U29	808.7	872.0	3.0
	U30	826.5	875.0	3.4
1220°C, 1 h	U1	853.0	936.4	8.2
	U3	848.2	991.6	2.5
1220°C 1 h + 1160°C, 2 h + 900°C 3 h	U2	702.0	860.6	8.75
	U6	782.0	942.0	7.80
1210°C. 1 h + 900°C, 4 h	U4	925.0	970.0	2.8
	U5	943.3	1016.6	3.0
1220°C, 1 h + 900°C, 4 h	U31	878.5	961.0	6.3
	U32	929.0	1039.0	7.3
1220°C, 1 h + 1050°C, 4 h + 900°C, 4 h	U33	899.0	940.0	0.8
	U34	909.3	955.3	2.3

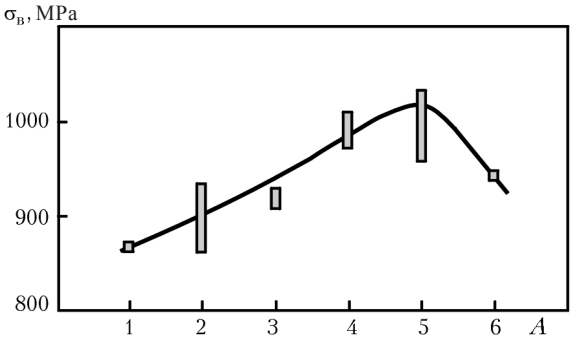

Fig. 1. Ultimate strength of the specimens of ZhS6U alloy after different types of heat treatment: 1) after casting; 2) 12 20°C (1h) +11 60°C (2h) +900°C (3h); 3) 1220°C (1h); 4) 1210°C (1 h) +900°C (4 h); 5) 12 20°C (1 h) +900°C (4 h); 6) 1220°C (1h) + 1050°C (4 h) +900°C (4 h); A – heat treatment variant.

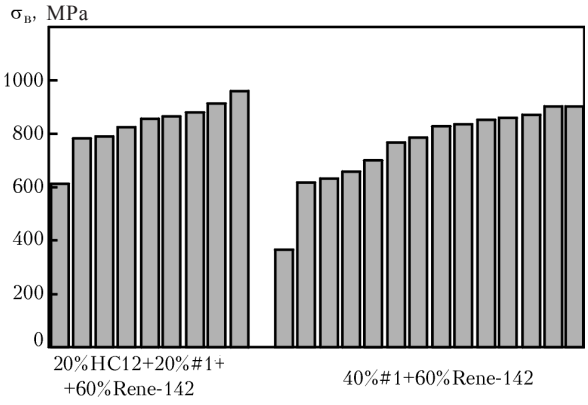

Fig. 2. The strength of brazed joints in ZhS6U alloy produced by resistance brazing at 1220–1225°C (20... 15 min) in a vacuum of $8 \cdot 10^{-3}$ Pa using boron-containing brazing alloys with the addition of silicon in the form of a brazing alloy of the Ni–12% Si system, and without the addition.

930...940 MPa at a relatively elongation of 3...7%. The higher plasticity (ε = 7.8...8.7%) of the ZhS6U alloy was recorded after one of the intermediate stages of heat treatment – vacuum annealing at 1160°C, 2 h. This temperature has been accepted as the stage of thermal fixation of the cast cusps of the aviation gas turbine engine produced from VZhL12U alloy. Correspondingly, the yield limit values were lower, the maximum up to 782 MPa (Table 1).

Detailed analysis of the properties of the alloys is essential for predicting the properties of the brazed joints in ZhS6U alloy, produced using the brazing alloys Ni–Co–Cr–Al–2.5% B (No. 1)+60% Rene-142 and No. 1+20% HC12+60% Rene-142. In [11–14] it was shown that the mechanical properties of the joints to end of the properties of the brazed alloys, thermal stability of these alloys, the level of alloying, carbon content and the method of production of the alloy.

Figure 2 shows the mechanical properties of the brazed joints in ZhS6U alloy after two-stage vacuum annealing at 1160°C (2h) +1050°C (2 h). The joints were prepared for brazing using the following procedure. The sheets with the ground ends were placed freely on a ceramic plate. A bead of the brazing alloy was produced on the joint line.

The brazed joint are produced by resistance brazing at 1220–12 25°C for 20–15 min in a vacuum of $8 \cdot 10^{-3}$ Pa using a boron-containing brazing alloy with the addition of silicon in the form of a powder of the Ni–12% Si alloy and without it.

Relatively high values of B were obtained for the brazed joints for both types of brazing alloys. The higher and more stable strength level was recorded when using the brazing alloy No. 1+20% HC12+ René-142.

The Q factor of the brazed joint was 0.9-1.0. The RMS deviation of the values of σ_B for the specimens of the brazed joints, produced using the boron-silicon-containing brazing alloy, was 81.4 MPa, and that of the boron-containing alloy 102.0 MPa. This

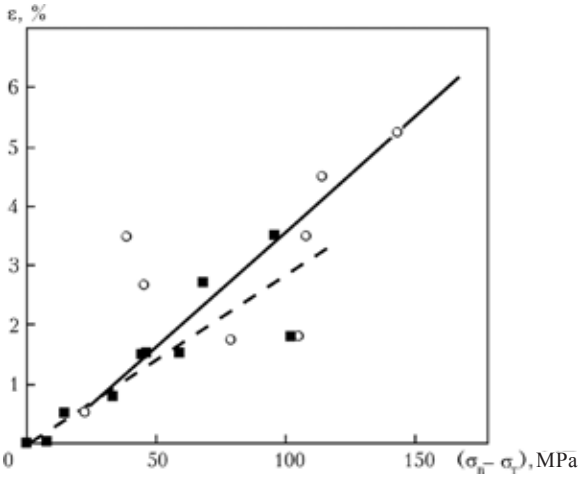

Fig. 3. Relationship of the relative elongation and the level of strain hardening of the brazed joints in ZhS6U alloy, produced using the brazing alloys of the type#1+ René-142 with the addition of 20% HC12 (○) and without the addition (■).

indicates the high reproducibility of the brazing results when using the brazing alloy with two depressants – silicon and boron.

The application of the complex boron- and silicon-containing brazing alloys results in high plasticity of the brazed joints in loading of these joints (Fig. 3). A proportional relationship was found between the relative elongation and the difference between the ultimate strength than the yield limit of the brazed joints.

The short-term strength of the ZhS6U alloy at room temperature reached 920–970 MPa at a relative elongation of 3–6%. These data are in agreement with the results obtained for the ZhS6U alloy, heat-treated by the complete brazing cycle (Table 1). However, in this case the ductility of the alloy exceeded 7.80–8.75%. The relative elongation of the specimens of the brazed joint equalled 1.8...5.2%, which is similar to the certificate data for the ZhS6U alloy [6].

The peak on the statistical curve of ultimate strength (Fig. 4) confirms the Q factor and stability of the brazing process. More than 87% of the specimens of the brazed joints shows the values σ_B of 800–975 MPa. Almost all specimens were plastically deformed to fracture at 20°C. The diagram indicates the capacity of the brazed joints to withstand certain degrees of plastic deformation in tensile loading: the curves show the large difference (up to 100 MPa) between the values of σ_B and $\sigma_{0.2}$ of the tested joints. The broadened maximum of the curve of the yield limit $\sigma_{0.2}$ indicates the presence of technological deviations in brazing of the specimens.

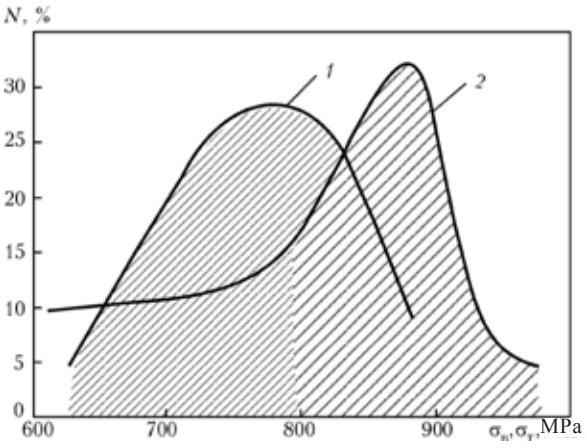

Fig. 4. Statistical curve of distribution of the values of T (1) and B (2) of the brazed joints, produced by brazing the ZhS6U alloy in vacuum at 1220–1225°C (20...15 min) after heat treatment (T_{test} = 20°C); N is the number of specimens.

Metallography

The satisfactory mechanical properties of the brazed joint in the case that alloy are determined by the structure of the brazed joints (Fig. 5). The application of the composite boron-containing brazing alloy #1 (NiCoCrAl–2.5% B) +Rene-142 produce brazed joints of satisfactory quality (Fig. 5a, c, e).

The interaction of the brazing alloy with the base is detected at a depth of up to 300-500 μm indicating the high reactivity of this brazing alloy with the mean boron content, equal to 1 wt.% (Fig. 5a, c, e).

Boron as the element with a minimum atomic radius, characterised by a high diffusion rate, migrates through the joint into the brazed metal during formation of the brazed joint and subsequent heat treatment and forms boride phases at the fusion line and the grain boundaries of the brazed metal which greatly reduce the creep resistance of the component under stress.

The developed nature of the zone of the thermal effect indicates the high rate of diffusion processes taking place at the joint-brazed metal interface in the brazing alloys with both one depressant (boron) and with two (boron and silicon). This leads to an increase of the heterophase nature of the investigated zone and the volume fraction of the secondary phases (Fig. 6, Table 2).

The phase composition of the diffusion zone indicates that heat treatment applied when using the brazing alloy with a single depressant (boron) results in active diffusion of boron into the base with the formation of mono-carboborides (Ti, Nb) (C, B) (Table 2) along the fusion line at a depth of up to 300 μm. These phases can be both globular or of arbitrary shape. Plate-shaped chromium carboborides of the type Me $(Cr, W, Mo)_{23}$

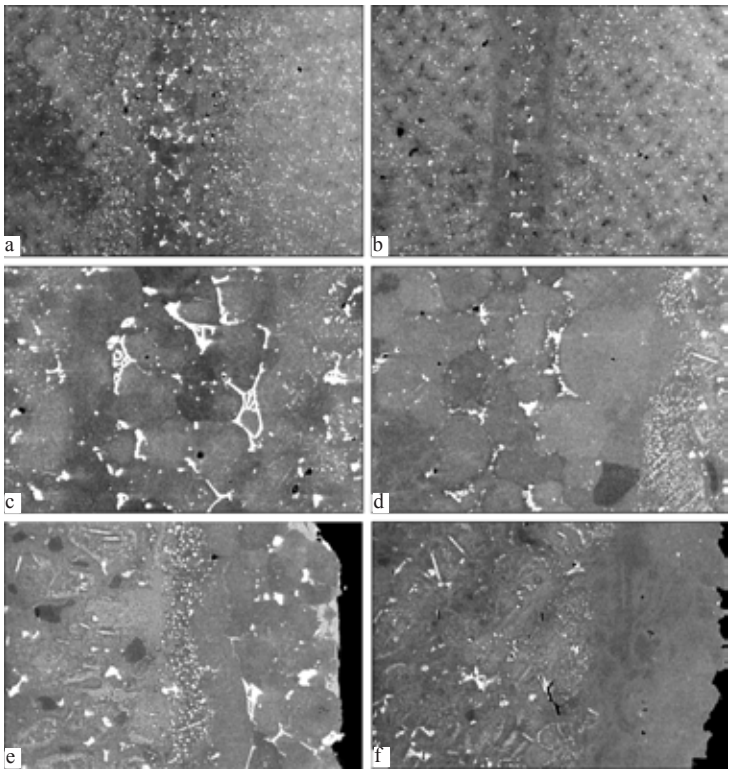

Fig. 5. The microstructure of the specimens of brazed joints in ZhS6U alloy, produced at a temperature of 1220°C (20 min) using the boron-containing brazing alloy #1+ René-142 (a, c, e) and also boron- and boron-and silicon-containing brazing alloy #1 +20% HC12+ René-142 (b, d, f); a, b) × 450); c, d) × 200; e, f) failure of the brazed joint under uniaxial tensile loading, × 200.

$(C, B)_6$ were found at the grain boundaries.

Silicon in the composite brazing alloy restricts the diffusion of boron into the base [16], as indicated by the width of the diffusion zone (up to 100 μm) and its minimum heterophase nature. Silicon 'keeps' boron in the brazed joint and prevents erosion of the brazed base, embrittlement of its boundaries during loading and thermal cycling.

The modification of the boron-containing brazing alloy #1+Rene-142 with the HC12 (Ni–12% Si) brazing alloy message possible

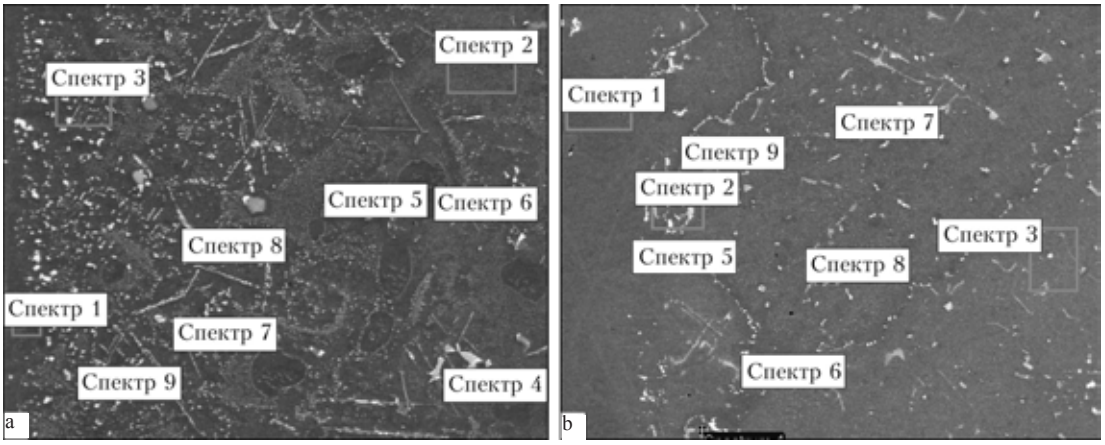

Fig. 6. Sections of x-ray spectrum microanalysis of the diffusion zones in the brazed joints produced at 1220°C (15 min) and subjected to complete heat treatment using to systems of brazing alloys (× 200) (Table 2): a) #1+60% René-12; b) #1+20% HC12+60% René-142.

Table 2. Mass fraction of the components in the structural constituents of the diffusion zone of the brazed joints, produced with composite brazing alloys with and without the addition of HC12

Spectrum No.	C*	Al	Ti	Cr	Co	Ni	Nb	Mo	Hf	Ta	Si	W	Re
						#1+60% Rene-142 (Fig. 6a)							
	0.85	5.30	1.01	9.20	11.08	64.08	0.66	1.06	—	1.18	—	5.07	0.52
2	1.03	5.40	2.49	8.22	10.13	64.42	0.30	1.24	—	—	—	5.95	0.81
3	0.99	5.32	2.08	9.39	11.11	61.1	0.34	1.22	—	—	—	7.29	0.21
	13.50	0.10	23.47	1.36	—	3.3	15.87	4.30	0.30	—	—	35.69	2.12
	16.27	—	25.49	0.61	—	2.42	26.9	4.36	0.73	—	—	24.50	0.96
6	1.69	6.77	3.64	3.49	7.86	70.12	1.11	0.85	0.56	—	—	3.29	0.62
7	13.37	0.1	22.17	2.84	0.96	4.96	12.66	3.67	0.93	—	—	36.55	1.78
	1.96	2.05	2.19	13.78	4.78	25.71	0.33	7.22	1.36	—	—	37.77	2.84
9	2.32	0.11	3.44	20.36	3.32	7.72	1.85	8.28	1.18	—	—	47.82	3.59
						#1 + 20%HC12+60% Rene-142 (Fig. 6b)							
	1.17	4.52	0.72	7.94	9.77	66.12	0.32	0.85	—	1.52	1.3	4.42	1.35
2	3.21	3.42	3.75	6.67	8.58	53.21	1.45	1.01	0.61	6.62	—	9.79	1.67
3	1.57	4.46	2.59	8.58	9.84	59.27	0.80	1.29	—	—	—	11.04	1.28
4	14.03	—	23.89	1.07	1.05	6.17	15.61	1.99	0.89	11.27	—	23.3	0.70
	9.25	0.53	21.02	0.85	0.97	10.09	12.08	1.56	0.96	25.33	1.6	15.73	—
6	14.28	—	25.26	0.77	0.46	4.49	17.80	3.75	—	4.74	—	28.44	—
7	12.75	0.35	19.07	4.23	1.55	11.50	12.01	4.11	—	—	—	35.08	1.50
	17.17	—	28.61	0.62	—	3.13	23.20	2.29	—	—	—	27.26	—
	8.57	2.09	10.63	4.13	3.98	33.71	7.51	2.12	0.47	7.13	—	19.65	—

*Quanlitative determination of carbon

not only to introduce the additional depressant but also dilutes the high-alloy melt of the brazing alloy with a nickel. In this case, the boron content decreases to 0.5 wt.%. The solidification range of the brazing alloy becomes smaller, the fluidity of the alloy increases; shrinkage in solidification of the joint becomes smaller. This is determined by the properties of the Ni–12% Si eutectic component characterised by a low susceptibility of liquation, formation of shrinkage pores and solidification cracks [17].

The brazed joint is, formed using boron- and boron-silicon-containing brazing alloy #1+20% HC12+ René-142, are characterised by high density and absence of defects. They have a cellular structure with the size of the equiaxed crystals of up to 50 μm (Fig. 5b, d, f). The eutectic formations, represented by carboboride quasi-eutectics based on Cr were not found (Fig. 7, Table 3). The volume fraction of the secondary phases in the weld metal after all types of heat treatment for the boron- and boron-silicon-containing brazing alloys did not exceed 5–7%. The secondary phases where are presented mainly by the discrete carbide phases MeC (based on tantalum, hafnium), Me6C carbides and single island-like complex with alloyed eutectic precipitates based on the Ni_nHf_m intermetallic phases (Table 3, Fig.7).

The brazed joints, produced using the boron-containing brazing alloy #1+60% Rene-142, were characterised by a large number of secondary carboboride formations, are presented mainly by the quasi-binary eutectics of the type $\gamma+Me_{23}$ $(C, B)_6$, formed on the basis of the CrB borides. These eutectic precipitates are relatively stable. In the presence of a wide gap and a large amount of the melt, they form and remain in the joint after a treatment (Fig. 7a, 8d, Table 3). In

Table 3. Mass fraction of the components in the structural constituents of the metal of the brazed joints. produced with composite brazing alloys with and without the addition of HC12

Spectrum No.	C*	Al	Ti	Cr	Co	Ni	Nb	Mo	Hf	Ta	Si	W	Re
						#1+60% Rene-142 (Fig. 7a)							
1	1.41	4.94	0.72	9.07	11.56	64.94	—	0.34	—	2.83	—	3.00	1.19
2	2.81	5.05	0.56	9.36	10.40	62.56	—	0.50	—	2.57	—	4.54	1.66
3	1.15	1.79	1.34	7.45	13.97	59.79	0.93	0.60	5.73	4.81	—	0.99	1.44
4	2.17	1.54	1.25	7.80	13.82	58.78	0.40	0.44	6.24	4.84	—	1.05	1.67
5	1.15	4.45	1.41	6.55	10.21	66.24	0.37	0.56	2.19	4.19	—	2.68	–
6	3.46	—	—	55.43	4.60	5.03	2.29	7.00	—	—	—	22.18	–
7	3.17	—	0.43	25.34	3.94	6.39	0.47	12.38	—	3.00	—	39.36	5.52
8	11.89	—	7.33	0.96	2.20	8.70	4.89	1.03	10.28	50.93	—	1.79	–
9	11.84		7.45.	1.42	1.51	6.50	3.51	0.45	13.09	52.32	—	1.91	–
						#1+20% HC12+60% Rene-142 (Fig. 7b)							
1	0.99	4.39	—	7.63	9.85	65.50	0.66	0.74	—	2.51	1.37	4.90	1.45
2	0.65	4.61	0.42	7.53	9.66	65.26	0.38	1.03	0.39	2.48	1.18	4.93	1.47
3	0.73	4.57	1.07	7.53	10.13	63.69	0.14	1.17	0.28	1.42	0.55	7.61	1.11
4	1.92	0.70	0.83	5.04	11.19	61.49	0.15	—	10.46	6.81	—	1.43	–
5	3.43	—	—	28.73	3.40	9.18	0.95	13.50	0.55	3.60	—	23.17	13.48
6	2.02	0.63	0.98	5.35	11.63	63.49	0.35	—	8.67	5.55	0.52	0.82	–
7	2.96	—	—	30.57	3.43	6.43	0.55	14.40	—	3.09	—	25.23	13.34

*Quanlitative determination of carbon

addition to the γ(Ni) + CrB eutectic, weld metal also contained interdendritic precipitates of the complexly alloyed eutectics based on γ(Ni) + Ni_3B (Fig. 7a, Table 3). The volume content of the secondary phases in the joints in the ZhS6U alloy when using the boron-containing brazing alloy #1+ René-142 after brazing reached 40%, and after complete heat treatment 9–21 wt.%, depending on the width of the gap (Fig. 5, 7, 8).

The degree of heterophase appearance of the structure of the welded joints, produced using the basic brazing alloy 40%#1+60% René-142, and the complex brazing alloy 20%#1+20% HC12+60% René-142, was determined on the basis of the microhardness of the brazed joint and the diffusion zone measured in the condition after brazing and heat treatment.

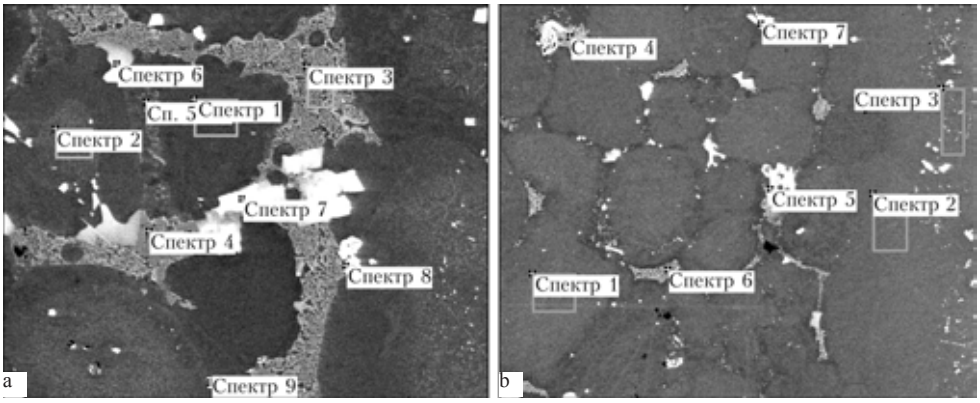

Fig. 7. Sections of x-ray spectrum microanalysis of the metal of the brazed joints produced at 1220°C (15 min) and subjected to complete heat treatment using to systems of brazing alloys (×200) (Table 3): a) #1+60% René-12; b) #1+20% HC12+60% René-142.

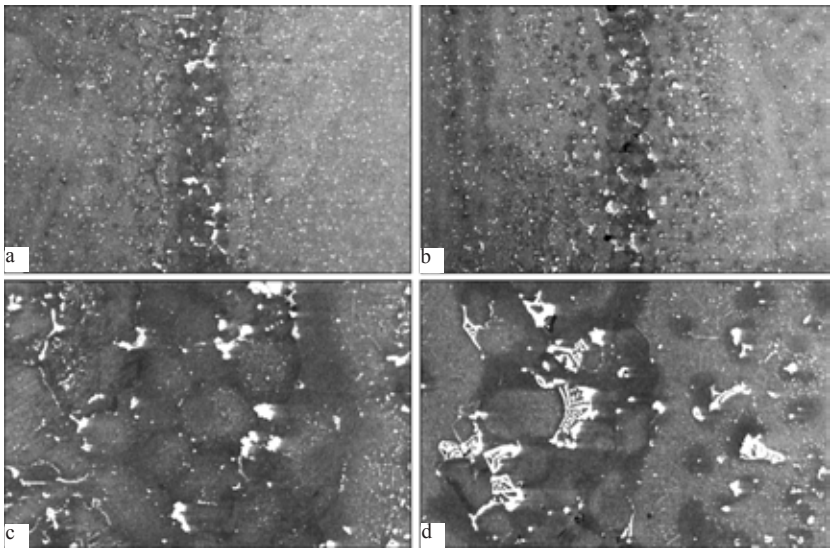

Fig. 8. Microstructure of the specimens of the brazed joints in ZhS6U alloy with a fixed gap for long-term strength testing, produced at 1220°C (20 min) using boron- and silicon-containing brazing alloys #1+20% HC12+ René-142 (a, c) and boron-containing brazing alloy #1+ René-142 (b, d): a, b) × 50; c, d) × 200.

The reduction of the heterophase nature of the structure and the increase of homogeneity, recorded when using the silicon- and boron-containing brazing alloy has been confirmed. The matrix solution of the brazed joint with silicon which contained discrete precipitates of the carbide phases of the type MeC and Me6C had a microhardness of 4200 MPa (Fig. 8). After finishing heat treatment, the microhardness of the matrix of the welded joint decreased and became equal in all the areas of the brazed joint.

The complex brazing alloy 20%#1+20% HC12+60% René-12 made it possible to produce in the ZhS6U alloy joints in gaps with the width of 100–800 μm whose structure underwent the dispersion hardening as a result of the γ'-phase (Fig. 9). The results show approximately the same volume fraction (54–59%) of the hardening phase in all the zones of the brazed joint, including the weld metal, the diffusion zone and the base. The size of the particles of the ‘-phase in the dendrite axes of the metal of the brazed joint (brazing alloy 20%#1+20% HC12+60% René-142) was 0.2–0.7 μm, and the shape of the particles changed from spherical to cuboidal during heat treatment.

The brazed joints produced with the boron-containing brazing alloy shows a large scatter of the microhardness values corresponding to the existence of a large variety of the structural components in the metal of the brazed joint. The microhardness of the fusion line and the diffusion zone in the brazed alloy increased as a result of the penetration of the alloying components of the joint into the base and the formation of a developed diffusion zone at a depth of up to 300 μm and greater.

The secondary phases in the brazed joint remained also after heat treatment, their size increased and they coalesced. The scatter of the microhardness values of the metal of the brazed joints, produced with the brazing alloy type #1+60% René-142 indicates the heterophase structure of the joint.

The matrix solution of the brazed joints, produced using the boron-containing brazing alloy, content, after two-stage and meaning, complexly alloyed eutectics (HV = 8480 MPa), MeC carbides (HV = 22,150 MPa), Me_6C (HV = 18 785 MPa), $Me_{23}C_6$ (HV = 13 180 MPa) which reduce the strength of the brazed joint in welding as a result of decohesion on the interfaces of the particles of the second phase and the matrix [9].

The results show this uniform distribution of the particles of the γ'-phase (with the volume fraction of 38–45%) in the metal of

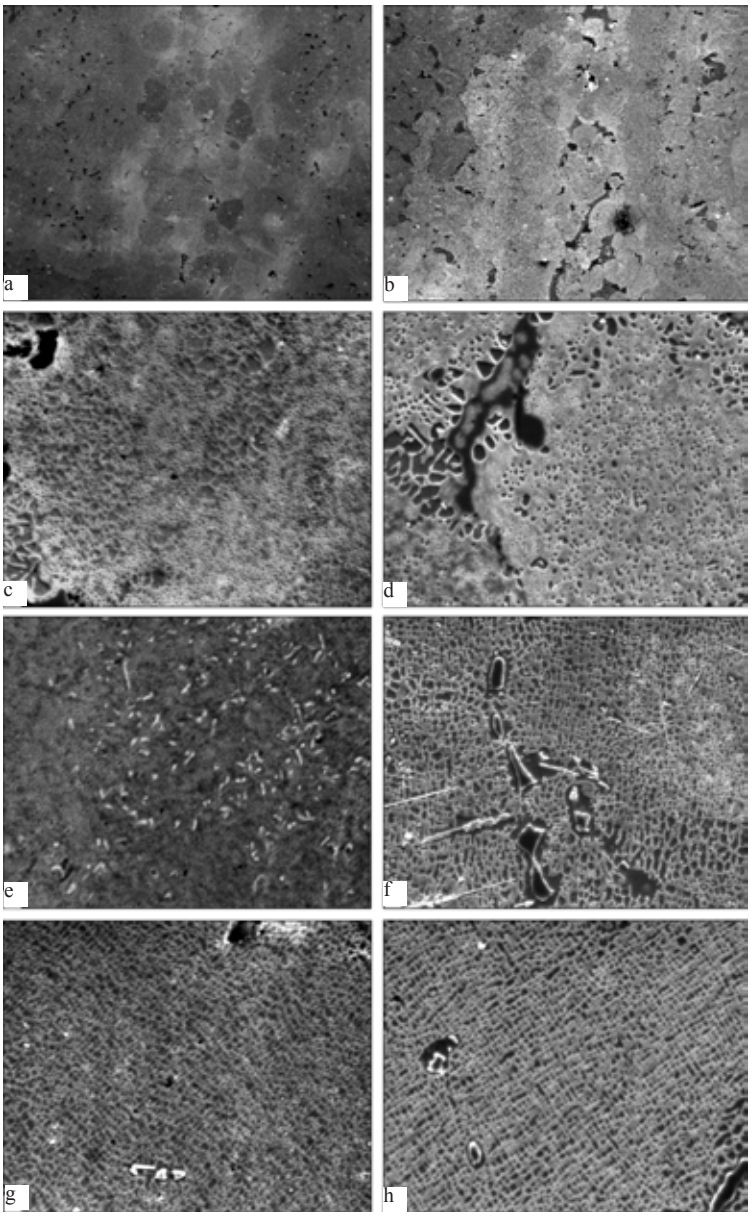

Fig. 9. (γ– γ') Microstructure of the metal of the main zones of the brazed joint, produced using the #1+ René-142 brazing alloy with the addition of 20% HC12 (a, c, e, g) and without the addition (b, d, f, h): c, d) the joint; e, f) the diffusion zone; g, h) the parent alloy; a, b) the general view of the joint after etching (a, b – × 100); (c, d – × 1500).

the brazed joint, in comparison with 59% in the silicon-containing brazing alloy.

In addition to the main hardening phase, the diffusion zone of the basic brazing alloy shows the precipitation of acicular carbide phases of the Me_6C type having a negative effect on the plastic properties of the joint (Fig. 9f). These phases are relatively stable and are also found at high temperatures having a notch effect in loading.

The estimates of the parameters of the structural mismatch a for the solidified metal of the brazed joints produced with the two types of brazing alloys show that when using the brazing alloy at 20%#1+20% HC12+60% René-40 there is a slight dispersion hardening of the matrix after solidification (Δa = ($a\gamma$–$a\gamma$')/$a\gamma$ = 0.09242%), after heat treatment value a increases and approaches the mismatch of the creep-resisting alloys (Δa = 0.263773%). The application of the boron- and silicon-containing brazing alloys ensures the

required creep strength of the brazed joint as a result of the precipitation in the matrix of the brazed joint of the regular dispersed γ'-phase with the volume density of 58–67, size 0.2–0.7 μm (Fig. 9c) [1].

When using the 40%#1+60% René-142 composite brazing alloy, the degree of dispersion hardening of the matrix of the brazed joint (after solidification) is lower as a result of the negative value of Δa (–0.0624%). After heat treatment and equalisation of the structure of the brazed joint, the value Δa (–0.00041%) slightly increases but there is no extensive hardening because of the high liquation heterogeneity in the brazed joint and the irregular precipitation of the hardening phase at the dendrite axes (Fig. 9d).

Long-term strength of brazed joints – important service characteristic

The effect of high temperature and applied loading during testing and leads to the evolution of the initial microstructure of the alloy, especially the metal of the brazed joint, alloyed with boron and silicon (Fig. 10, 11). The brazed joints in the ZhS6U alloy, produced using the brazing alloys 40% type # 1+60% René-142 with and with the addition of 50–20% HC12 and annealed at 1160°C (2 h)+1050°C (2 h) were tested for long-term

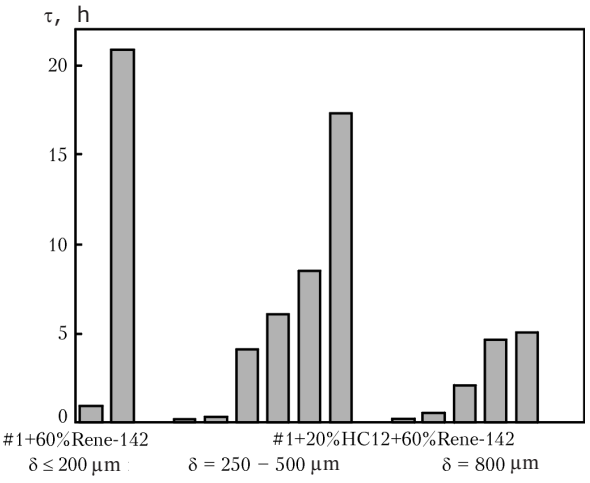

Fig. 10. Endurance of the brazed joints in ZhS6U alloy at a temperature of 900°C and a stress of 195 MPa after heat treatment (1160°C, 2 h +1050°C, 2 h), at different widths of the gap.

strength at a stress of 196 MPa and a temperature of 900°C. The long-term strength of the brazed joints, produced in the gaps 250–800 μm wide, reached 1.5–27.0 h (Fig. 10, 11). The joints failed mostly through the weld metal, the elongation was 2.0...5.7%.

The results of the tests of the specimens of the brazed joints to determine the longevity of the joints shows that the brazed joints, produced using the boron-containing brazing alloy 40%#1+60% René-142 were characterised by extensive structural changes, in particular, the melting of the eutectic component of the weld metal at a high temperature and active diffusion of boron into the brazed metal (Fig. 11). After 55 min of testing for the long-term strength, the depth of penetration of boron was 1–2 mm on each side (Fig. 11a).

The structure of the weld metal and of the diffusion zone produced using the brazing alloys with silicon did not show any extensive changes, the size of the brazed joint did not change, and the diffusion of silicon into the base after 16 h longer at a temperature of 900°C did not exceed 50 μm.

Thus, the application of the boron-and silicon-containing complex brazing alloy not only makes it possible to maintain the stability of the structure of the brazed joint and of the joint as a whole, but also ensure the acceptable longevity of the brazed joints with the width of the gap of 200–800 μm.

In brazing of the ZhS6U alloy, extensive softening at high temperature was recorded in the specimens of the brazed joint produced using the brazing alloy without HC12. Dispersion of the particles of the carboboride phase when adding silicon into the basic brazing alloy increased the strength of the brazed joints in short-term tests in air at 950–1000°C (Table 4). This is almost 1.5 times lower than the short-term strength of the brazed joints in the ZhS26NK alloy [11]. Thus, it has been confirmed that the properties of the brazed joints are determined by the properties of the brazed alloy and its chemical composition.

The process of repair brazing, developed on the working blades of the ZhS26NK alloy, has been applied in the reconditioning

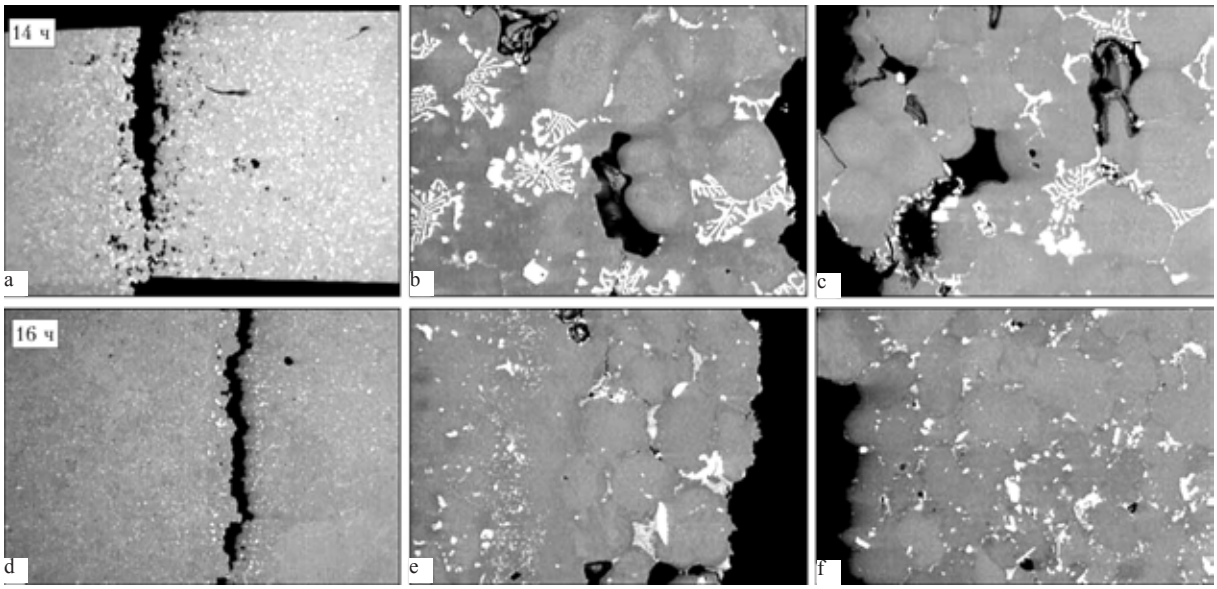

Fig. 11. High-temperature failure in the process of testing for longevity at 900°C of the metal of the brazed joints in ZhS6U alloy, produced using the standard #1+60% René-142 (a–c) and the complex brazing alloys #1+20% HC12+60% René-142 (d–f); × 25.

of the guide blades made of ZhS6U alloy at the Progress company. Gaps in a modelling blade were filled by brazing at 12 20°C (20 min) using 40%#1+60% René-142 brazing alloy with the additions of 20 and 25% HC-two (Fig. 12). Analysis of the microstructure has confirmed the high quality of the brazed joint – minimum porosity, complete filling of the gap, low reactivity of the brazing alloy (Fig. 13).

The structure of the brazed joints in the ZhS6U alloy, produced using the silicon-containing brazing alloy, is identical with the joints obtained previously in the blades of the ZhS26NK alloy [14]. The difference was found only at the fusion line between the base material and the joint. This is associated with differences in the carbon content in the brazed alloys (in ZhS6U up to 0.16% C). The ZhS6U alloy is characterised by the formation of a developed as on the mutual diffusion up to 200 μm wide.

The 20%#1+20% HC12+60% René-142 complex brazing alloy was used in the repair of a segment of a nozzle system produced from ZhS6U alloy for D18T engine. Thermal fatigue cracks were detected in service in a shelf and in a blade (in dye pen-

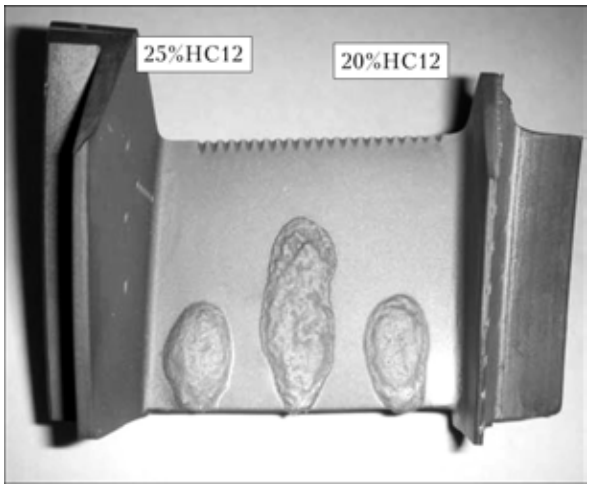

Fig. 12. External appearance of the guide blades made of ZhS6U alloy with processing gaps, brazed with composite brazing alloys of the #1+ (20… 25) % HC12–60% René-142.

Table 4. Short-term strength of the brazed joints in ZhS6U alloy at a temperature of 950°C

Specimen No.	Brazing alloy	σ_B, MPa	ε, %
U1		306.4	0.45
U2	#1+15% HC12+60% Rene-142	218.5	0.10
U3		218.0	0.10
U4	#1+20% HC12+60% Rene-142	264.8	0.21

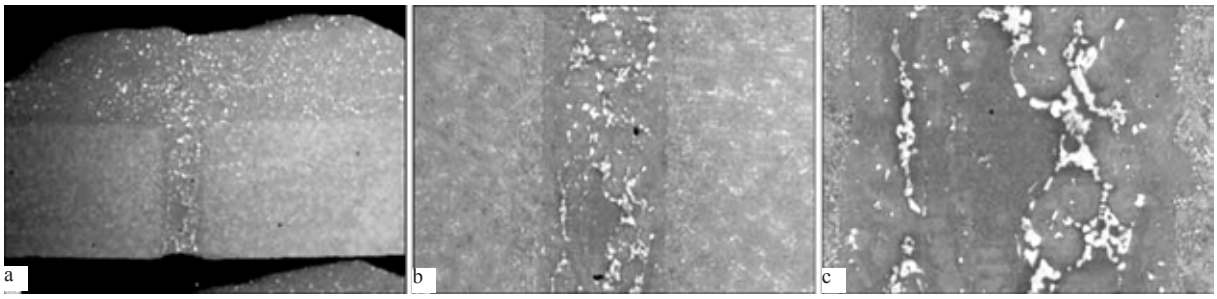

Fig. 13. Microstructure of the brazed joint (gap 350 μm), produced using the #1+20% HC 12-60% René-142 brazing alloy at 1220°C (20 min) after heat treatment: a) cross-section of the body of the blade; × 100) fragment of the joint on the side of the spine, × 50; c) the structure of the brazed joint, × 100.

etrant inspection). After cleaning the surface, the component was annealed in vacuum at 1210°C and subjected to repair brazing. To improve the efficiency of brazing the cracks, situated in different planes, the defects were coated with a powder brazing alloy and saturated with the solution of acrylic resin in acetone. After brazing, it occurred component was characterised by a satisfactory quality, as confirmed by the results of dye penetrant defectoscopy (Fig. 14).

Conclusions

1. The brazed joints in ZhS6U alloy, formed using the brazing alloy with (15–20) wt.% XE12 showed high stability of the strength characteristics in the tensile test. The Q factor of the brazed joints at 20°C was 0.87–1.00 the relative elongation of the brazed joints in ZhS6U alloy, produced using the boron- and silicon-containing brazing alloy, after heat treatment reached 1.5–5.5%, whereas in brazing with the brazing alloys without silicon in the elongation didn't exceed 3%.

2. As a result of additional alloying of the boron-containing brazing alloy with the eutectic component Ni–12% Si the quality of the brazed joints was high. The high level of the physical–mechanical characteristics of the brazed joints in ZhS6U alloy was the result of the formation of a regular ($\gamma+\gamma'$) structure of the weld metal with the volume fraction of the hardening phase of 57–60%, and dispersion and suppression of the formation of the carboboride phases, suppression of the formation of carboboride eutectics in the brazed metal in the diffusion zone, and the restriction of the penetration of boron into the brazed metal. Failure of the brazed

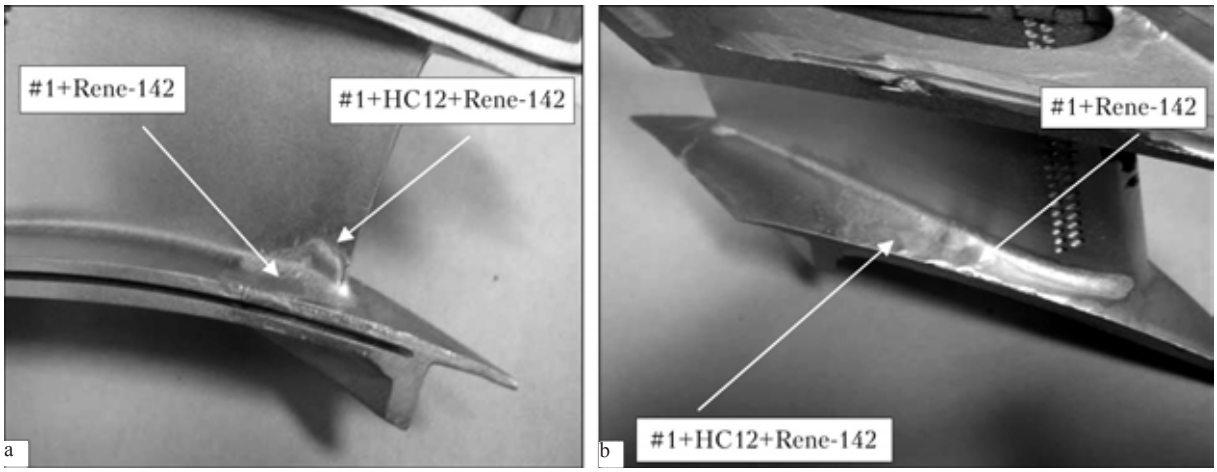

Fig. 14. Sections of repair brazing at the outlet edge (a), on the shelf (b) of a blade made of ZhS6U alloy in a segment of the nozzle system of D80T engine.

joints in loading place mainly in the in the diffusion zone or through the parent metal.

3. It has been shown possible to produce in the and all the little and one figure alloys and alloy brazed joints in capillary and processing gaps up to 200–900 μm wide, and the width of the gap has no effect on the evolution of the structure of the brazed joint and the penetration of boron silicon into the brazed base in high-temperature tests.

4. A technology was developed for repair brazing of single blades of guide segments of the nozzle system of D18T engine using the complex boron- and silicon-containing brazing alloys, applied in practice at the Pratt and Whitney Paton Innovation Centre.

References

1. Kablov E.N., Cast creep-resisting alloys, Nauka, Moscow, 2006.
2. Paton B.E., et al., Creep strength of cast nickel alloys and oxidation protection, Naukova Dumka, Kiev, 1967.
3. Lashko N.F., et al., In: structural and creep-resisting materials for new technology, Nauka, Moscow, 1978.
4. Nemirovskii Yu.R., et al., Fiz. Met.Metalloved., 1990, No. 11, 160–163.
5. Polyanskii V.M., et al., Metalloved. Term. Obrab. Met., 2004, No. 9, 32–34.
6. Sigachev A.N. and Chigrinskaya S.A., Aviats. prom., 1991, No. 11, 14–16.
7. Shalin R.E., et la., Single crystals of nickel creep resisting alloys, Mashinostroenie, Moscow, 1997.
8. Arafin M.A., et al., Mater. Sci. Eng., A, 2007, **447**, No. 1/2, 125–133.
9. Ohsasa K., et al., J. Phase Equilibria, 1999, No. 20, No. 3, 199–206.
10. Chaturvedi M.S., et al., Afnaces in Technol.: Materials and Materials Proc., 2004, **2**, No. 6, 206–213.
11. Kurenkova V.V., et al., Sovremen. Elektrometall., 2006, No. 3, 30–40.
12. Malashenko I.S., et al., Sovremen. Elektrometall., 2007, No. 1, 25–32.
13. Kurenkova V.V., et al., Sovremen. Elektrometall., 2007, No. 2, 23–34.
14. Kurenkova V.V., et al., Sovremen. Elektrometall., 2008, No. 1, 26–35.
15. Musienko V.T., et al., Aviats. Promst., 1986, No. 6, 48–49.
16. Kurenkova V.V., et al., Avt Svarka, 2009, No. 6, 60–27.
17. Khorunov V.F., Fundamentals of the brazing of thin wall structures made of high-alloy steels, Naukova Dumka, Kiev, 2008.

Advances in Electrometallurgy 2010 **8** *(2) 143–148*
Translated from Sovremennaya Elektrometallurgiya 2010 **8** *(2) 52–56*

SPECTRO xSORT - a manual x-ray fluorescence spectrometer for fast and accurate analysis of metals on components

M.M. Livitskii and Ya.P. Grytskiv

SPECRO Analytical Instruments GmbH in Ukraine, Kiev
E.O. Paton Electric Welding Institute, Kiev

The technical capabilities of a portable X-ray fluorescent spectrometer SPECTROxSORT for analysis of the chemical composition of alloys based on iron, titanium and copper are investigated. The results of analysis of the chemical composition of alloys, obtained using spectrometer SPECTROxSORT, are compared with data of testing these specimens, carried out in laboratory equipment of the E.O.Paton Electric Welding Institute. The feasibility of application of the portable spectrometer for sorting and preliminary analysis of metals on products is shown.

The devices with the SPECTRO mark are regarded throughout the world as the standard of mobile and portable tools for analysis of metals. No other company has comparable know-how and such extensive and thorough experience in this region. From the moment of foundation of the company in 1979, the main product of the company were the mobile and small analytical spectrometers for the analysis of the chemical composition of metallic components without taking laboratory samples. The devices include SPECTRPORT I, SPECTROPORT II, SPECTROPORT F, SPECTROTEST and SPECTROTEST JR, modifications L, M, F, used widely in industry, SPECTROSORT^{CCD} and, finally, special light models SPECTRO iSORT and SPECTROTEST.

The powerful laboratory x-ray spectrometers also represent the important range of products of analytical equipment of SPECTRO company.

The latest model SPECTRO xSORT by SPECTRO A.I. is a compact energy-dispensing x-ray fluorescence spectrometer for the continuous and long-term analysis and sorting of metals on components. The device uses effective innovation components for excitation and detection. In addition to other high-quality modules, these two rises are present the basis for ensuring the unique accuracy, speed and safety of the system, combining the possibilities of analysis of the metal of the component with the requirements on the quality of measurements in the laboratory conditions.

The devices fitted with a miniature low-power x-ray tube whose design is very similar to the models of the tubes used in SPECTRO devices of a higher grade. This guarantees the stability of the power of ionising excitation. The specially developed technology of detection, based on SDD, ensures that the analytical signals can be processed at a rate 10 times higher and, consequently, this results in unique analytical flexibility.

The portable SPECTRO xSORT device produces the measurement results for up to

41 elements, close to the laboratory results (from magnesium to thorium), in a single measurement cycle which lasts only 2s. Only 10 s is required for sorting various alloys of light metals aluminium and magnesium. In analysis, even like metals, such as magnesium, silicon, aluminium, phosphorus, are measured in air without the application of complex technologies of evacuation of the measurement zone or helium blowing. The greatly simplifies the design of the device and facilitates the analysis process.

The lower limits of detection of the elements based on iron, produced on the prepared standard specimens with the measurement cycle of 10 s, are as follows, wt.%: 1.80% of aluminium, 0.03 Cd, 0.01 Co, 0.01 Cr, 0.01 Cu, 0.03 Mn, 0.01 Mo, 0.01 Nb, 0.02 Ni, 0.0 9P, 0.03 Pb, 0.06 Sb, 0.50 Si, 0.04 Sn, 0.02 Ti, 0.01 V, 0.06 W, 0.01 Zn, 0.01 Zr.

The specially prepared, certified specimens of Cr18Ni10Ti high-alloy austenitic steel and AK12MMgN (AL30) high strength cast piston aluminium alloy were used for testing the analytical possibilities of the SPECTRO xSORT spectrometer. The results of the tests are presented in Table 1 in which the measured values of the alloying chemical elements and impurities in the alloys were obtained at the simultaneous determination and averaging five parallel experiments with the calculation of the RMS error of measurements.

The results, shown in Table 1, indicate satisfactory convergence of the results of analysis of the alloys obtained in SPECTRO xSORT equipment with the certified values of the concentration of the chemical elements, obtained on the laboratory spectrometers with a high accuracy grade.

SPECTRO xSORT is a compact device. Its weight does not exceed 1.5 kg, the overall dimensions 333×84×314 mm. The accumulator and the personal computer are assembled with the measuring device in a single reliable plastic casing protecting the elements of the structure against impacts and vibration. The lithium-ion accumulator battery ensures continuous operation of the device for no less than 3 h. The required power in the measurements is 15 W, in the expectation regime 6 W. The charging device is used for operation directly from the alternating mains of 100-240 V without any restriction on time.

Table 1. Results of certification tests of SPECTRO xSORT in the company SPECTRO F.I, wt.%

Chemical element	Measured mean concentration	RMS measurement error	Certified concentration
Cr18Ni10Ti high-alloy austenitic steel (GOST 5632-72). 2 s			
Ti	0.63	0.02	0.63
V	0.12	0.02	0.13
Cr	17.64	0.10	17.45
Mn	1.38	0.05	1.52
Fe	69.6	0.2	69.4
Ni	9.5	0.1	9.42
Cu	0.24	0.03	0.30
Nb	0.04	0.01	0.04
Mo	0.35	0.01	0.36
AK12MMgN (AL30) cast aluminium alloy (DSTU 2839-93). 10 s			
A	85.9	0.2	84.8
Si	11.5	0.2	11.4
Ti	0.070	0.002	0.057
V	0.023	0.002	0.020
Cr	0.036	0.004	0.031
Mn	0.035	0.002	0.033
Fe	0.484	0.005	0.47
Ni	0.931	0.003	0.97
Cu	1.033	0.006	0.94
Zn	0.020	0.002	0.033
Zr	0.007	0.001	0.008
Pb	0.023	0.003	0.027

The protective casing makes the SPECTRO xSORT device not sensitive to the effect of climatic conditions. For the ferry displacement of the operator with a device in the complicated reduction conditions, the device is placed in a case. A box is used for transport over large distances and for storage.

It is important to mention the automatic screen, opening the measurement window in front of the sample for the duration of analysis. One of its functions is the protection of the measurement zone containing the devices

(the source of primary x-ray radiation – x-ray tube and a detector) against contamination and damage, the second function is the use of the surface as the reference specimen for calibration of the measuring device after every analysis of the sample with the screen closed.

The system of diagnostics of the efficiency of the device after each measurement of the sample measures the x-ray spectrum from the screen, and this is followed by comparison and correction of the spectrum with respect to the sample of the spectrum stored in the memory of the ICAL intellectual calibration logics. Possible deviations of the measurement system, obtained in this manner, are rapidly detected and corrected. Therefore, calibration of the device is always possible, and the results of analysis of the sample are very accurate.

To prevent the damage to the detector with the screen open, a protective film 75 μm is used in the measurements. The film is placed in the measuring window between the sheets of the adapter and the screen. If the device is used mainly for analysis of light alloys with the measurement of the content of magnesium, aluminium, silicon, it is recommended to use a thin protective film 4 μm thick.

The standard input window of the SPECTRO xSORT adapter is calculated for analysis of the components with the diameter of the surface of 8 mm and more, whereas special adapters are used for smaller dimensions or the distorted surface of the specimens.

Special attention in the design of SPECTRO xSORT is given to ensuring the most efficient protection of the operator against x-ray radiation. Using two light diodes, installed in the side wall of the device, the operator and other participants of tests can visually determine when the x-ray tube is active and measurements are being taken.

Further two light diodes, reflecting the state of the device and the measurement status, are located directly below the panel of the computer which is usually centre point of attention of the operator. In addition to this, there is a special protective module which prevents random uncontrollable starting of the measurements. At the beginning of analysis, SPECTRO xSORT determines in a fraction of a second whether the specimen is situated in front of the measurement window. In the specimen does not cover the window, the screenis closed immediately and the measurement is interrupted.

The operation of the SPECTRO xSORT device is control by the measurements than that in situated on the handle, and the personal computer, installed in the back wall. The computer is controlled with a stylus or a finger through a sensitive screen.

To facilitate reading, the screen is positioned under the angle of 45°. If it is required to analyse a large number of specimens in the laboratory conditions, the device can be placed in the stationary position on a special support. The computer can be easily disconnected from the device and using Bluetooth technology, it remains connected with it.

The connection of the personal computer with the external devices, such as printer or other computer, can be established using a built-in USB port, and also W LAM or Bluetooth connection. The data from the computer can also be transferred to other computers using a memory card. TheSPECTRO xSORT may also be fitted with an ingot printer with accumulator power supply and wireless connection for printing the results in the analysis area.

The program software SPECTRO XRF Analyzer CE is based on the Windows Mobile operating system and characterised by a simple operating interface in the space device with a large number of possible application configurations. The analysis screen provides the operator with all the required operation and can be used to display measurement results in different forms. The rapid sorting regime in which all the tested specimens are compared with the initial measures specimen, is available in addition to the analysis regime. The results of the measurements are stored and can be later displayed on a screen, a printer, and after transfer to an external computer they can be processed using the Result Manager software included in the system.

The system for detailed monitoring of the device, including ICAL calibration with the functions of diagnostics of apparatus and program facilities, guarantees that the equipment is ready for measurements.

The SPECTRO xSORT has been demonstrated in many engineering companies and firms of the mining-metallurgical complex of Ukraine were it received positive responses of the experts of the following companies: Turboatom, Khar'kov; Kotloturboprom, Khar'kov; NKMS, Kramatorsk; KZMO, Konstantinovka; Dneprospetsstal', Zaporozh'e; Motor Sich, Zaporozh'e; Ordzhonikidze GOK; Marganetsk GOK; Marganetsk Ore Repair Plant; TsGOK, Krivoi Rog; InGOK, Krivoi Rog; Acelor Mittal, Krivoi Rog; REGOM, Krivoi Rog; Aleksandriiskii Ore Repair Plant.

The analytical testing laboratory of the Department of physical-chemical investigations of the E.O. Paton Electric Welding Institute, Kiev, carried out detailed tests of the device, including the analysis of specimens of low- and-alloy steels, and also titanium, copper-nickel and copper-zinc alloys.

Table 2 compares the results of analysis of low-alloy steels, obtained in the SPECTRO xSORT equipment, with the results of analysis of the specimens carried out at the laboratory of the E.O. Paton Electric Welding Institute, Kiev, using the vacuum optical emission spectrometers (certified by Derzhmetrteststandart), using certified standard specimens.

Table 3 compares the results of the analysis of high-alloy steels, obtained in the SPECTRO xSORT equipment, with the results of analysis of the specimens carried out in the laboratory of the E.O. Paton Electric Welding Institute, Kiev.

Table 4 compares the results of analysis of titanium alloys, carried out in SPECTRO xSORT equipment, with the results of tests of the specimens in the laboratory of the E.O. Paton Electric Welding Institute, Kiev.

Tables 5 and 6 compare the results of analysis of copper-based alloys, carried out inSPECTRO xSORT equipment, with the results of tests of the specimens conducted

Table 2. The results of comparative analysis of low-alloy steels, wt.%

Analysi methods	Sample code	Mn	Cr	Ni	Mo	W	V	Nb	Cu
xSORT emission spectrometer	Compo-nent	0.47	0.90	2.91	0.04	—	-	-	0.25
		0.43	0.86	2.85	0.03	-	-	-	0.20
xSORT emission spectrometer	Sheet	0.86	0.04	0.06	0.04	<0.010	<0.020	0.028	<0.010
		0.88	0.05	0.023	0.028	<0.017	<0.018	0.029	<0.013
xSORT emission spectrometer	Kh-G2VM	1.88	1.72	0.17	0.52	0.80	0.13	-	-
		1.86	1.66	0.19	0.60	1.05	0.18	-	-
xSORT emission spectrometer	KhVG	0.94	1.20	0.20	<0.1	1.06	<0.10	-	-
		0.82	1.10	0.18	0.017	1.23	0.025	-	-
xSORT emission spectrometer	Kh2N2M	0.46	2.04	2.05	0.36	-	-	-	0.29
		0.53	2.01	1.94	0.34	-	0.038	-	0.29
xSORT emission spectrometer	Kh4VMF	0.35	3.66	0.25	1.20	1.00	0.74	-	0.14
		0.27	3.32	0.26	1.31	0.99	0.75	-	0.18
xSORT emission spectrometer	Kh4VM6	0.30	3.60	0.20	1.48	0.96	0.90	-	-
		0.22	3.30	0.20	1.43	1.01	0.93	-	-
xSORT emission spectrometer	R3AM3	0.39	3.60	0.21	2.90	2.70	2.00	0.110	-
		0.20	3.40	0.21	2.70	2.60	2.30	0.120	0.14
xSORT emission spectrometer	Kh5MF	0.41	4.90	0.18	1.30	-	0.45	-	0.15
		0.32	4.70	0.17	1.40	-	0.41	-	0.08

Table 3. Results of comparative analysis of high-alloy steels, wt.%

Analysi methods	Sample code	Mn	Cr	Ni	Mo	W	V	Cu	
xSORT emission spectrometer	Cr3Ni9	0.28	2.7	9.6	-	-	0.40	-	-
		0.23	2.65	9.0	-	-	0.37	0.17	-
xSORT emission spectrometer	Kh11NV	-	11.8	1.7	0.50	1.85	0.30	-	-
		0.20	10.7	2.1	0.45	1.70	0.25	-	0.11
xSORT emission spectrometer	Kh12MF	0.27	13.3	0.28	0.52	-	0.34	-	0.02
		0.19	12.8	0.19	0.50	-	0.37	-	0.07
xSORT emission spectrometer	40Kh13	0.68	14.0	0.35	<0.10	-	<0.10	-	0.08
		0.68	14.9	0.33	0.026	-	0.064	-	0.15
xSORT emission spectrometer	St.363	0.42	12.95	0.19	0.38	-	0.31	-	-
		0.43	13.8	0.20	0.35	-	0.36	-	0.08
xSORT emission spectrometer	Cr16Ni3	0.90	15.5	3.4	1.80	-	-	1.30	<0.10
		0.91	16.0	3.0	1.67	-	-	1.34	0.058
xSORT emission spectrometer	KhN35VT	0.45	14.5	34.5	-	2.8	-	-	3.2
		0.24	12.9	35.0	-	2.87	-	-	2.9

Table 4. Results of comparative analysis of titanium alloys, wt.%

Analysi methodss	Sample code	Al	Mn	Zr	Si	Fe	V	Mo
xSORT emission spectrometer	301	0.71	2.31	0.095	0.056	0.53	-	-
		-	2.06	0.035	-	0.55	-	-
xSORT emission spectrometer	305	6.74	0.20	0.34	0.40	0.092	-	-
		-	0.21	0.34	-	0.14	-	-
xSORT emission spectrometer	311	2.21	-	-	0.064	0.14	5.59	5.85
		-	-	0.35	-	0.11	4.92	6.60
xSORT emission spectrometer	312	3.09	-	0.12	0.078	0.24	3.56	4.46
		-	-	0.089	-	0.35	3.54	4.65
xSORT emission spectrometer	313	3.90	-	0.29	0.14	0.34	1.55	2.90
		-	-	0.26	-	0.34	1.46	3.03
xSORT emission spectrometer	314	5.30	-	0.31	0.10	-	3.92	-
		-	-	0.26	-	0.12	3.80	0.15
xSORT emission spectrometer	315	7.49	-	0.043	0.21	0.41	0.91	1.78
		-	-	<0.003	-	0.46	0.76	2.05

Comment. Titanium is the base of alloys

Table 5. Results of comparative analysis of copper-nickel alloys

Analysis methods	Sample code	Ni	Fe	Mn	Zn	Si	Pb
xSORT emission spectrometer	6024	29.4	0.63	0.96	0.33	0.09	0.010
		30.3	0.55	0.91	0.15	-	0.019
xSORT emission spectrometer	6071	29.4	0.99	0.48	0.19	0.23	0.020
		31.1	0.58	0.89	0.19	-	<0.018

Comment. Copper is the base of alloys

at the E.O. Paton Electric Welding Institute, Kiev.

The test results indicate that the results of analysis, carried out using theSPECTRO xSORT equipment, are in excellent agreement with the laboratory analysis results. This analyser may prove to be an irreplaceable tool for the sorting and preliminary analysis of alloys in cases in which it is not possible to take samples and supply them to a laboratory.

It is important to mention the possibilities of using the device in the field conditions for survey analysis, for example, ore minerals, individual components of the slag waste.

More detailed information on this and other

Table 6. Results of comparative analysis of copper–zinc alloys

Analysis methods	Sample code	Zn	Cu	Pb
xSORT emission spectrometer	B1A	45.0	55.0	
		44.4	55.6	
xSORT emission spectrometer	B2A	39.8	60.2	—
		39.3	60.7	—
xSORT emission spectrometer	B3A	35.8	64.2	—
		35.6	64.4	—
xSORT emission spectrometer	B4A	31.0	69.0	—
		31.4	68.5	—
xSORT emission spectrometer	B5A	25.0	75.0	—
		23.6	70.6	—
xSORT emission spectrometer	B6A	20.2	79.8	—
		19.2	74.1	—
xSORT emission spectrometer	B7A	15.0	85.0	—
		14.1	79.8	—
xSORT emission spectrometer	B8A	10.4	89.6	—
		10.8	88.9	—
xSORT emission spectrometer	B9A	5.0	95.0	—
		5.7	94.0	—
xSORT emission spectrometer	B18A	**Balance**	58.6	0.97
		40.0	58.9	1.04
xSORT emission spectrometer	B20A	**Balance**	57.5	5.40
		35.6	58.5	5.48

devices can be obtained from the representatives of the company Spectro Analytical Instruments GmbH, in Ukraine.

Advances in Electrometallurgy 2010 **8** *(2) 149–153*
Translated from Sovremennaya Elektrometallurgiya 2010 **8** *(2) 57–60*

INFORMATION

A high-voltage power source for electron beam heating

V.V. Martynov, Yu.P. Monzheran, A.G. Mozharovskii, B.B. Lebedev, G.E. Smityukh, N.V. Chaika and A.M. Ivanov

Institute of Electrodynamics, National Academy of Sciences of Ukraine, Kiev
Antares International Company, Kiev

The main results of development and tests of a high-voltage source of the power supplies for electron beam guns of technological installations are given.

When using in advanced electrical technologies, based on the application of electron beam, plasma, arc, laser and other methods of processing materials, it is necessary to develop specialised electric power sources. In addition to the conventional requirements on the regulation and stabilisation of output voltage or current, these systems are also subject to specific requirements, reflecting the properties of electrical technology equipment (the need to ensure continuous processes during the formation of the breakdown in the vacuum chamber or in the electron beam gun, leading to short circuits of the output of the high-voltage source; maintenance of the glow discharge regime without transition to arc discharge; restriction of the level of output current under dynamic disruptions in welding, etc). The electric power source should ensure efficient operation of equipment in the conditions from idle running to short-circuiting and should have high dynamic characteristics.

The application of the systems of power electronics, working with the industrial mains frequency, for electrical engineering applications that make it possible to realise all advantages of the new technological processes and restricts their productivity.

The power of advanced electron beam guns axis hundreds of kilowatts at the voltage in the load of several tens of kilovolt. A special feature of the operation of the electron beam gun is the presence of periodic breakdowns and, consequently, when using high powers it is necessary to minimise the energy reserves in the electric power system and rapidly the street the level of output high-voltage current.

These requirements contradict the parameters of the quality of electrical energy and in particular as regards the level of pulsations of output voltage, which is traditionally ensured by the application of energy-consuming electrical filters.

In these devices, breakdowns in the circuit of the gun result in instantaneous discharge of the capacitance of the filter and this is one of the reasons for the formation of discharge supercurrents which are many times higher

than the working current and lead to the formation of defects in the component and on the cathode surface. The presence of a high impact and is in the output circuit of the hour sources improve the conditions of transfer of the short-term pulsed breakdowns to long-term arc breakdowns and this increases the frequency of the arc discharges. In addition, in a breakdown, the voltage may change at a high rate leading to the formation of pulsed displacement currents, causing breakdown and even failure of the electronic sections.

These requirements on the quality of electrical energy in the presence of nonstationary breakdowns between the electrodes of the gun are satisfied by the Dzhen 30-15 specialised high-voltage power source designed for supplying power to the electron beam guns with a 'cold cathode' [1]. The power source was developed at the Institute of Electrodynamics on the basis of the technical projects of experts of the Antares International Organisation.

The conversion of electrical energy in the high-voltage power sources of this type takes place at a frequency of 20 kHz. IGBT transistors are used as switching elements [2]. The application of the module principle made it possible to distribute uniformly the electrical and thermal loads between the sections of the structure and, at the same time, reduce the density of heat generation energy and also simplify the design of the converter. As a result of the synchronous non-sinphase control, the current of the individual modules are displaced with respect to time thus improving the parameters of electrical energy both at the input and output of the power source.

The simultaneous application of synchronous non-sinphase control and high-frequency energy conversion makes it possible, on the one hand, to reduce greatly the output capacitance of the power sources and in some cases to avoid using the condensers of the filters on the high-voltage side, and on the other hand, to increase the speed of processing of the control signals by the power source and ensure optimum transition processes at disruptions in the load.

The main sections of the high-voltage power source are the module inverter and the transformer-rectifier module (TRM). The structural scheme of the high-voltage power source is based on the in-series connection of the power rectifier with the capacitance filter, the module inverter and the TRM.

The module inverter is a multiphase regulated high-frequency inverter with pulsed modulation producing rectangular two-polar voltage pulses at the output. In the TRM, these policies are transformed to the required level by the higher potential windings of the high-frequency transformer and are rectified by a multi-cascade rectifier. To reduce the 'jumps' of the required current for connecting the device to the power remains, the power rectifier is based on the function of the smooth charging of the input capacitance filter.

The regulation and stabilisation of the high-voltage of the power source in the presence of oscillations of the load current and voltage of the mains are ensured by the appropriate changes of the relative intensity of the control pulses by the transistors of the inverter.

The power source is characterised by the illumination of the technical contradiction between the requirement on the high quality of output electrical energy and the amount of stored energy, built up in the output circuits, as a result of producing the high-frequency transducer section of the device in the form of a multiphase circuit in which the inverter part has the form of a group of half-breach inverters with current-restricting choke coils at the output.

When disconnecting the inverter, the energy, stored in the choke coils, returns to the condensers of the filter of the power rectifier, bypassing the primary circuit of the TRM. Consequently, it is possible to disconnect rapidly high-voltage from the load and restrict instantaneously the current at any overloading.

The high-voltage power source can operate in one of the two stabilisation regimes: output voltage of output current. Stabilisation of output voltage is the main operating regime of the control system in which the output current changes in the range 0–15 A.

When detecting a arc discharge or formation of the conditions which may be interpreted as the beginning of another discharge, the control system switches over to the current restriction regime. Consequently, in the case of breakdown in the electron beam gun it is possible to prevent the development of an arc discharge.

If the load current does not decrease over some period of time, the control system disconnects the power source for the time from 0.2 to 100 ms and subsequently returns it to the main working regime.

Interaction of the discharge reduces the load current, and the control system again returns the power source to the main working regime – stabilisation of output voltage. This algorithm ensures the stable operation of the high-voltage power source in the presence of breakdowns in the electron beam gun.

TRM is used for the effective transfer of energy to the out circuit of the power source and galvanic uncoupling on the level of 50 kV of the high-voltage and low-voltage circuits. The small size of the transformer-rectifier module, and the high electrical strength of its high-voltage insulation and the effective removal of heat from the heat generating elements are ensured by the application of the special design of the TRM and a liquid synthetic dielectric.

The TRM is characterised by high efficiency, and satisfies the requirements on the quality of output energy in load at disruptions, and is resistant to switching overvoltage and breakdown.

The Dzhen 30-15 power source for electron beam heating fulfils the following functions:

– stabilisation of output voltage (using the multi-circuit system with feedbacks with respect to the current in the inverter module, load current, output voltage, etc);

– maximum current protection (restriction of current through switching elements of the inverter on the permissible level);

– automatic restarting – interruption of the output current of the inverter for a specific period of time, sufficient for disrupting the arc discharge in the cases in which there are breakdowns short-circuiting longer than the given value.

The high-voltage power source uses microprocessor controlled with advanced digital signal processors, realising the flexible algorithm of control of the source in different operating conditions. Consequently, the operation of the power source can be matched with the central computer controlled ensuring the continuity of the technological process.

The Dzhen 30-15 high-voltage power sources are compact, simple design, and can be placed together with the electron beam equipment, this has a positive effect on the quality of transition processes at breakdown in the gun and makes it possible to reduce the expenditure in the construction of electron beam equipment.

Main technical characteristics of Dzhen 30-15 power source

Output voltage, kV0	30
Maximum output current,	A15
Level of restriction of the output current	130% of the maximum value

In the tests, investigations were carried out into the dynamic characteristics of the new high-voltage power source in the conditions of high voltage breakdown [3] using the circuit shown in Fig. 1 and an auxiliary device – the equivalent of discharge load for simulating high voltage breakdown. In the device, the air discharged *D* with the ballast resistor Rintegral are connected in series. The discharger has the configuration of the electrodes of the

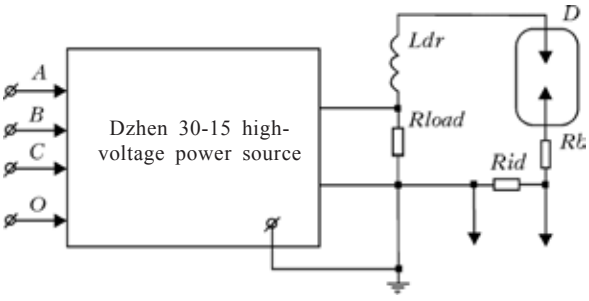

Fig. 1. Diagram of the investigations of the effect of high voltage breakdowns on the dynamic characteristics of the electric power source using the three-phase alternating-current mains.

mid-plane type and the regulated distance between them in the range 5–35 mm. Ballast resistance *Rb* has the form of a set of resistors. To measure the breakdown current *Id* a resistor *Rid* = 0.1 ohm is connected in series with the equivalent of the discharge load. The output of the source is connected with the higher potential electrode of the discharger through the high-voltage cable of the type KVEL-60, and a high voltage induction coil with the inductance *Ldr*. Some of the tests were carried out at the resistance of the load *Rload*, connected directly to the output of the high-voltage source.

When simulating the breakdowns in the load of the high-voltage source, the distance between the electrodes of the discharger *D* was set to ensure that the breakdown takes place at the given output voltage of DZhen 30–15 equipment. The measured current and voltage were recorded with a GDS-806S digital memory oscilloscope. The nature of the dynamic processes at the output of the high-voltage power source in the two variants of the high-voltage breakdown in accordance with Fig. 1 is shown in Fig. 2.

Figure 2*a* shows transition processes at the output of the power source *Uh* (upper curve) and current Ih through the discharger *D* in the idling regime of the power source (*Rload* =∞). At the initial moment of time *t* = 0 the output voltage *Uh* smoothly increases to the steady value and this is followed by the formation of a corona discharge (characteristic surges appear at the tip of the curve *Uh*) which at the moment of time *t* = 220 μs changes to an arc discharge, and a breakdown takes place in the discharger *D*.

The output voltage decreases to 0. The short pulse of the discharge current *Ih* in the initial breakdowns stage (Fig. 2a) is determined by the discharge of the parasitic capacitances of the high-voltage circuit of the power source, the high-voltage choke coil *Ldr* and the test circuit.

The voltage at the output remains equal to 0, and the discharge current *Ih* smoothly increases to the previously selected restriction current and subsequently rapidly decreases during a break. The surges of the discharge current amplitude in this period are associated with the switching frequency of the transistors of the inverters. The breakdown process is completed, the discharge current In decreases to 0, the output voltage increases, and the power source continues operation.

Figure 2b shows the transition processes during operation of the power source in the working current regime. In the initial condition, in the period from 0 to 1 ms, the power source works in the regime of stabilisation of output voltage *Uh* (upper curve), and the output current *In* (the lower curve in inverse polarity) is equal to the current through the resistor *Rload*. At time *t* = 1 ms a breakdown starts to take place, the load

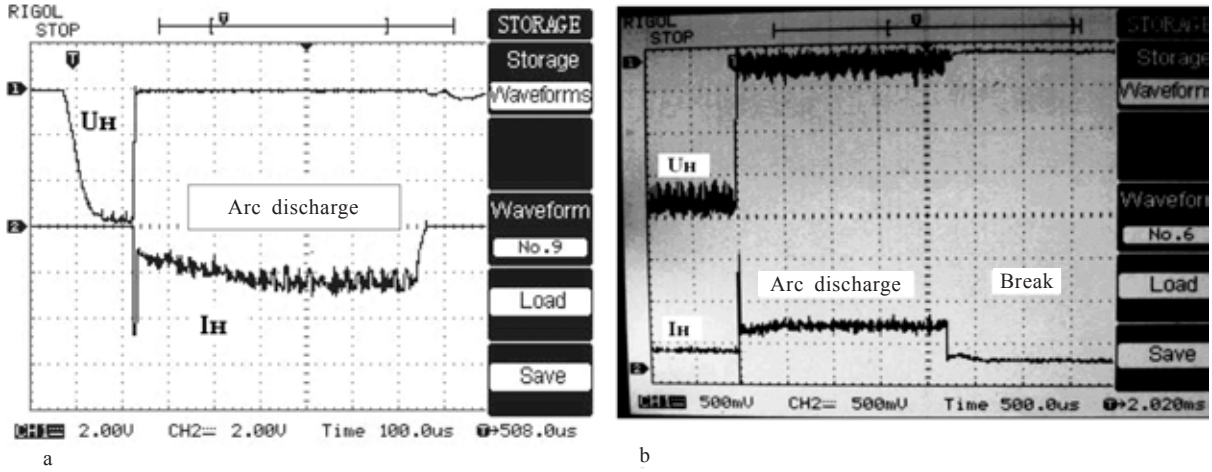

Fig. 2. Breakdowns in the circuit in Fig. 1 in operation of the source in the idling regime (a) and in the regime of the working load currents (b).

resistance *Rload* is shunted by the circuit of the short-circuited discharger *D* and the connected ballast resistor *Rb*. The current In is equal to the sum of the currents through the resistors *Rload* and *Rb*. The voltage *Uh* decreases and a short pulse of the discharge current of the parasitic capacitances appears in the output current. When this pulse is completed, the stage of stabilisation of the current in the arc gap of the discharger starts in the power source, followed by transfer to the current-free break.

Thus, the control system of the Dzhen 30-15 power source at breakdowns in the load changes to the regime of automatic secondary connection characterised by the forced restriction of the output current thus preventing the transfer of the spark discharge to an arc discharge. After some time, the control system switches of the power source, maintains the given time break for complete interaction of the arc discharge and this was followed by automatic reconnection of the power source. This regime is cyclically repeated.

The results of the tests show that the control system together with the module inverter ensures regulation and stabilisation of the arc voltage was smooth transfer to the steady value. The experiments have also confirmed that the methods of high-frequency conversion of electrical energy and active restriction of the lord current during breakdown, realised in the Dzhen 30-15 power source, increase the productivity and quality of the technological process.

References

1. Martynov V.V. and Komarov N.S., Equipment for electric power supply for electron beam systems, Patent 29547, Ukraine, MPC V 23 K 15/00, H02M 7/515, 15.11. 200.
2. Lipkivskii K.O., et al., Progress in and development of semiconductor-transformer switches for powering electrical engineering equipment, Proc., Institute of Electrodynamics, Kiev, 2009, No. 23, 72–82.
3. Shidlovskaya N.A. and Martynov V.V., Tekh. Elektrodinamika, 2010, No. 1, 73–79.